An Investigation of Bovine Lumbar Vertebral Body Stiffness with Experimental Measurement and Finite Element Modelling

by
Michael Morrison Sanders
B.Sc., University of Victoria, 1992

A Thesis Submitted in Partial Fulfillment of the
Requirements for the Degree of

MASTER OF APPLIED SCIENCE

in the Department of Mechanical Engineering

We accept this thesis as conforming
to the required standard

[redacted]

Dr. S. Dost, Supervisor (Department of Mechanical Engineering)

[redacted]

Dr. M. Nahon, Departmental Member (Department of Mechanical Engineering)

[redacted]

Dr. R. Podhorodeski, Departmental Member (Department of Mechanical Engineering)

[redacted]

Dr. R. Vahldieck, Outside Member (Department of Electrical and Computer Engineering)

[redacted]

Dr. T. R. Overton, Additional Member (Department of Mechanical Engineering)

[redacted]

Dr. Y. Altintas, External Examiner (Department of Mechanical Engineering, U.B.C.)

Supervisor: Dr. Sadik Dost

Abstract

Geometrical and structural properties of bovine vertebral bodies were measured from laboratory specimens and used to develop finite element method (FEM) models. The material properties (i.e. moduli) in the models were taken from recent published reports. To validate the models, compression tests were performed on bone specimens using an MTS testing machine, and stiffness was compared to that produced from the models.

For one out of the three vertebral bodies tested, the FEM model predicted a stiffness within the range measured. But by using parameters slightly lower than the mean, two of the three models produced stiffness comparable to the experimental. Though accurate measurement of geometry was shown to improve stiffness predictions, the cortical shell thickness was the most sensitive input parameter affecting stiffness. The models indicated that most of the vertebral body stiffness is due to the cortical shell. But the shell thickness was troublesome to measure in the laboratory. With more efficient and accurate measurement of geometry and bone density (as obtained with Quantitative Computed Tomography, QCT), such FEM models may accurately predict strength and stiffness of human bone in the future.

Examiners:

Dr. S. Dost, Supervisor (Department of Mechanical Engineering)

Dr. M. Nahon, Departmental Member (Department of Mechanical Engineering)

Dr. R. Podhorodeski, Departmental Member (Department of Mechanical Engineering)

Dr. R. Vahldieck, Outside Member (Department of Electrical and Computer Engineering)

Dr. T. R. Overton, Additional Member (Mechanical Engineering)

Dr. Y. Altintas, External Examiner (Department of Mechanical Engineering, U.B.C.)

Table of Contents

List of Figures

List of Tables

Acknowledgments

Thanks to Mr. D. McKercher, Mr. M. Ly, and Dr. G. W. Vickers for their time and use of equipment, to Dr. J. Scriniger for his assistance with the x-rays, and to Mrs. M. O'Flynn for her careful proofreading. Thanks most weightily to my supervisor Dr. S. Dost for his patience and support, and to my mentor Dr. T. R. Overton for his guidance and help in forming the shape of this research. The work was funded by NSERC, and the support has been much appreciated.

Dedication

To Donna

1 Introduction

1.1 Problem

Progress in the fields of structural analysis and medical imaging has provided the opportunity for the development of a new diagnostic tool. The Finite Element Method (FEM) has been applied to orthopaedic biomechanics in an effort to better understand the material structure of bone [1]. Quantitative Computed Tomography (QCT) has provided a non-invasive measure of the amount of mineral in bones and has mapped the physical dimensions of the bone itself. When QCT data is input into a FEM bone model, predictions can be reached about the strength and stiffness of a bone.

The development of a QCT driven FEM diagnostic model is a massive undertaking. This thesis provides an initial investigation into FEM modelling of vertebral bodies with input data similar to that provided by QCT. Bovine (cattle) vertebral bodies will be used for the experiments, but as the work is to be applied to human specimens in the future, human models will be reviewed here and their material properties reviewed in Appendix A and C.

1.2 Background

The muscloskeletal system provides movement and structural support for the body. It is not surprising that the medical science concerned with such function, orthopaedics, has used FEM for mechanical analyses of bone, cartilage, and ligaments. FEM has analyzed

load transfer in bones and artificial-joint replacements, structural failure probabilities, and of late analyzed time-dependent mechanical behavior and structural optimization [1],[2].

The method has also been used to analyze disease. Such a disease affecting the mobility and health of elderly women is osteoporosis, which constitutes a decrease in bone mass. (Recent predictions indicate that 54% of 50-year-old women will sustain osteoporosis-related fractures during their remaining lifetimes [3].) Peak bone mass is reached in the middle to late thirties, after which bone mass begins to decline. The bone loss accelerates in women during the decade after menopause. Osteoporotic women have an increased susceptibility to fractures to the hip and vertebrae by slight or even trivial trauma [4]. Because treatment of osteoporosis is less effective after fracture, research is being developed in bone mineral measurement with QCT [5] and stiffness predictions with FEM models [6].

To provide background for the development of a FEM vertebral body model, this section will review spinal FEM modelling, vertebral body compression tests, and some relevant properties of bone. To provide the reader with an understanding of the complex structure and terminology associated with the spine, a detailed anatomy of both bovine and human spines is contained in Appendix A. (Some biological terms used to describe the FEM models below are defined there and in references [7]-[18]).

1.2.1 Spinal FEM Modelling

FEM has been used extensively to model the spine. In the last few years, very large complex models have been built which represent the vertebral column. The Dietrich et al. FEM model [19],[20] represents the entire spine, including most muscles, ligaments, rib-

cage, abdomen, and part of the pelvis. Shirazi-Adl's model of the L1-S1 ligamentous lumbar spine [21]-[24] has the specific geometry of a 65-year-old male obtained from CT scans. Though these models provide a good analysis of the over-all motion of the spine, they cannot provide an accurate description of the stress and displacement within the vertebral body as the models assume the body to be rigid.

The vertebral body is actually a very complex structure (see Appendix A). Essentially, the body is a mass of bone surrounded by a thin shell of dense bone, in a roughly cylindrical shape. The dense outer bone will be referred to as cortical bone. The inner bone is not solid, but forms bony beams, struts, and plates. The individual rods are referred to as trabeculae whereas the entire structure of bony elements and subsequent pores is called trabecular bone. Material testing has shown that both trabecular and cortical bone are viscoelastic, strain rate dependent materials with anisotropic properties [17]. Linde and Hvid [25] found that the stiffness of trabecular bone increased asymptotically, and then reached a constant level after several nondestructive loading cycles. Carter and Hayes [26] have also shown that trabecular bone properties are affected by strain rate.

Though most models cannot incorporate the complex structure and material properties of the vertebral body, there are some spine models capable of measuring its stiffness. They have been built to represent a functional spinal unit, a portion of the human superior and inferior vertebral body with the intervening disk [27]-[48]. In 1973, Belytschko et al. [32],[33] were the first to apply FEM to a spinal unit, a structure assumed to be the fundamental building block of the entire spine. By stacking their previous spinal unit model, Goel et al. [34]-[39] have recently constructed a complex model which includes

muscle forcing. These models assume linear isotropic material properties for the cortical and trabecular bone. A spinal unit model was used to analyze stress distribution in osteoporotic spines, and it was concluded that reduced thickness of the outer bone shell in the vertebrae was a significant factor reducing ultimate compressive strength [40].

These earlier models put more emphasis on the intervertebral disk. However, the later models are very sophisticated and used non-linear analysis: Shirazi-Adl et al. [41] have developed a spinal unit model which includes the entire vertebrae including pedicles and articulations, the ligamentous attachments, and collagen fibre layers in the disk; the spinal unit model of Dietrich et al. [46] incorporates transversely isotropic materials; and that of Ueno and Liu [47] incorporates both transversely isotropic materials and annulus fiber layers. Yet, the results of the different models are highly variable and dependent on the modelling assumptions. Suwito et al. [48] have investigated how geometric and material properties affect the results in an axisymmetric model and have concluded that the Young's modulus of trabecular bone and the intervertebral disk annulus, the height of the disk, and the ratio of the disk nucleus pressure and axial pressure most affect the results.

1.2.2 Review of Human Vertebral Body Models

Only a few FEM models which just represent a vertebral body have been reported. Short [16] modelled human vertebral bodies in two dimensions by using beam elements to represent individual trabeculae with a failure criterion based on inelastic buckling. The geometry of the beams was based upon trabeculae measured from micrographs. Detailed regional differences in the trabeculae were not modelled; instead, a mesh generator was used to introduce randomization into the otherwise standard mesh. The results suggested

that a single trabecular failure would affect the failure of nearby trabeculae, and the extent of failure depended on the duration of loading at a critical level.

The simple vertebral body model designed by Mizrahi et al. [49] used isotropic linear material properties. Values for trabecular bone modulus were varied and the cortical shell was removed to investigate these effects on bending stress in the end-plate. Osteoporotic-like conditions were found to increase the peak stress by 2.5 times.

Hakim and King's [50] vertebral body model was compared to experimental test results from a vertebral body specimen; the two where in close agreement. However, the dimensions of the model and the actual vertebral body did not match, and subjective observations were used to assign trabecular and cortical modulus values. Hence, the model and the vertebral body cannot be directly compared.

For a FEM model to be used as a diagnostic tool, it must incorporate at least two measurements made on the patient. The specific geometry of the patient's vertebral body must be used in the model, as must the density of the trabecular bone mass inside the body. Neither of these properties where included in Hakim and King's [50] model.

Specific patient geometry, such as measured by Alici et al. [51], has been incorporated into vertebral body models. Lavaste et al. [52],[53] devised a method which builds a simple but complete vertebra based on parameters measured from x-rays. However, the material properties used in this model are not based on the patient's bone density.

FEM models which did include trabecular density distribution have been designed through a procedure described by Keyak et al. [54] where the geometry and density measurements for the model were taken from clinical QCT. The technique has been applied by Bozic et al. [55] to the cervical vertebra, and by Faulkner et al. [6] to the

lumbar spine. The patient-specific, non-linear analysis from Faulkner et al. based cortical and trabecular bone material properties on reports by Carter and Hayes [26]. Defining a yield point using a 2% offset on the stress strain curve, vertebral strength was found to be 0.57 ± 0.26 MPa for patients with osteoporosis and 1.46 ± 0.52 MPa for healthy patients. Furthermore, it was found that the strength of vertebrae with the same total bone mineral content could vary by a factor of two due to variation in bone distribution. Since no compression testing comparisons were done in this study, the results may not correspond with reality. As yet, no model has been found which has been sufficiently validated by experimental material tests.

1.2.3 Material Testing of Vertebral Bodies

Compression tests on human vertebral bodies have been conducted for over 100 years [56]. But tests have neither been conducted in great numbers nor with consistent procedures so no standard test procedure has been formulated. As the material which makes up vertebral bodies has complex structure and properties, a standard procedure would be beneficial.

Figure 1-1 shows the ultimate load determined for the 24 human vertebrae from various studies [56]-[61]. The labels on the horizontal axis are the names of the vertebral bodies listed from head to toe (i.e. L1 refers to the first lumbar vertebrae). The plotted points represent averaged measured ultimate load, except for Yamada's [57] data which was grouped into cervical, upper, middle, and lower thoracic, and lumbar regions. Though there is large variation between different studies, much of this variation is due to the age and bone quality of the specimens. Yamada's and Perey's [56] data are categorized by age

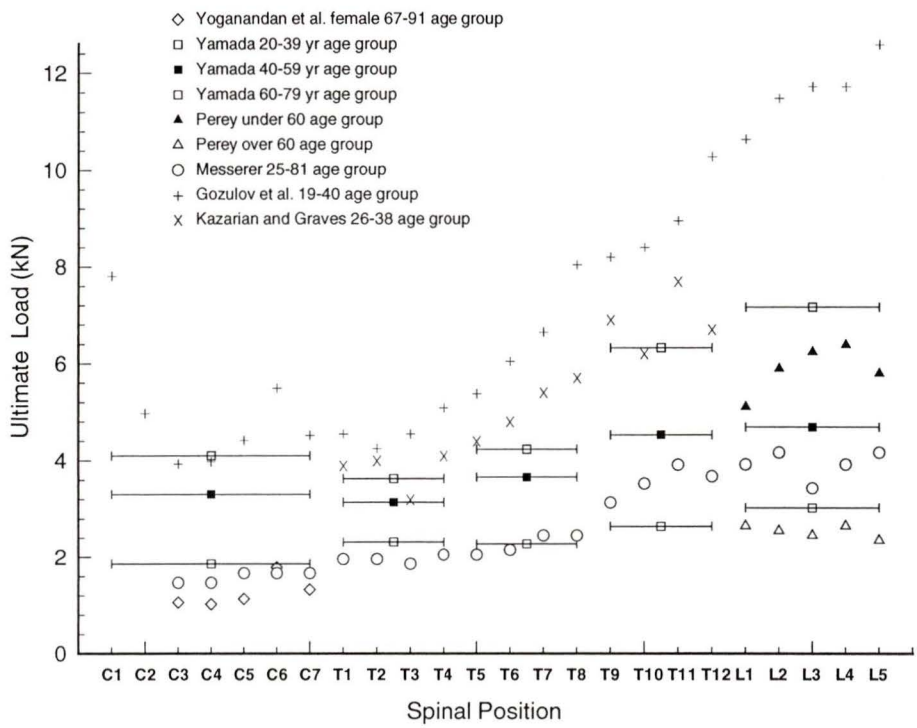

Figure 1-1: Average Ultimate Load of Human Vertebral Bodies as a Function of Spinal Position and Age

and show that strength is lost with age, as expected with lower bone density. Yoganandan et al. [58] used specimens from elderly females, the population most susceptible to osteoporosis, and these vertebrae had the lowest strength. The highest strengths were measured from the two youngest populations (Kazarian and Graves [59]; and Gozulov et al. [60]).

Yet there is unexplained variation between results from these several research groups. Messerer's data [61] includes young specimens which have about the same strength as Yamada's 60-79 age group. Though age can account for much of the variation in strength, other factors such as health and physical fitness level are important. (Bone turnover can be increased by physical activity. The compression forces on the lumbar spine of competitive

powerlifters during lifts were predicted as high as 17 kN, far greater than the average values above [62]). Age and health directly affect the density of bone in the vertebral body. If bone density was measured in all these studies, the variation in ultimate load could have been quantitatively explained by variation in density.

Procedural differences in the vertebral compression tests could also have affected results. Viscoelastic properties ought to be considered when testing vertebral bodies (this is especially true for stiffness measurement). The following should be taken into consideration during compression tests:

- Strain rate
- Preload
- Duration of test and number of test cycles
- End boundary conditions
- Humidity, temperature, and salinity
- Specimen preparation, and time since death.

The properties of bone were not well known when earlier results were taken and the above conditions were not considered.

Other interesting compression testing results have been obtained. It is well known that the strength of vertebral bodies increase with position in the spine [14], which is partly due to the increased cross-sectional area (laterally through the vertebral body) and is logical since the lower spine supports more body weight. Also, Perey found little difference between the stiffness of a vertebra and a functional spinal unit which implies that the intervertebral disk may not supply as much compressional flexibility to the spine as once thought [56].

No compression test was found which used bovine vertebral bodies. Though bovine bone is the easiest and cheapest to acquire, the vertebral bodies are more difficult to test

than human. The highly curved end-plates are inappropriate for compression within flat plates or disks, the typical method employed for human specimens.

1.2.4 Apparent Density of Trabecular Bone

Much of the variation in strength and stiffness of vertebral bodies can be explained by considering the quality of bone inside the vertebral body. This can be achieved quantitatively by QCT (quantitative computed tomography), which provides a means of measuring the mineral content of bone. The average attenuation of x-rays travelling through a volume of bone is determined by CT scans. Scans are also made of potassium dibasic phosphate (K_2HPO_4) samples of various concentration. The two attenuation factors are correlated to obtain a measure of mineral density in the bone.

A simpler and less expensive means of determining bone quality is through the measurement of apparent density, defined as the mass of the trabecular bone material divided by the volume of its structure. The number and size of the trabeculae in a region is related to apparent density. There are relationships between the stiffness and strength of trabecular bone and apparent density.

In fact, the relationships between the material properties of trabecular bone and its density has been actively researched for 28 years. Though various reviews of trabecular bone have been compiled [17], [63]-[68], a more complete list of references regarding correlations between apparent density and material properties is contained in the bibliography [25], [26], [69]-[117]. These references conclude that bone density is linked to strength, Young's modulus, and yield strain [113]. The correlations between Young's modulus and density are significant and power law relationships have been confirmed

through theoretical work [17],[118]. But the correlation coefficients from each study are substantially different. These differences provide evidence that factors other than density contribute to trabecular bone's elastic response, and some of these factors have been discovered through current research.

As trabecular bone is anisotropic, the direction of loading is an important consideration. Hence, any correlation which does not specify the orientation of the trabecular bone cube is inexact. Strain rate is also an important factor, as proved by Galante et al. [73] and Carter and Hayes [26]. Recently, Linde [115] has analyzed the dependence on strain rate more rigorously. Carter and Hayes' work also suggested that bone marrow has no effect on the material properties of trabecular bone, but this point is still under some controversy [66]. Their work compiled data from other studies on human and bovine trabecular and cortical bone, and their relationship between density and modulus was a nonlinear fit which included all the materials. Underlying this relationship are the following assumptions:

i) dense bone material has the same properties whether it is formed in small struts as in trabeculae or in a dense cortical layer, and

ii) bone material is not substantially different between different species or different locations in the body.

The first assumption was originally posed by Wolff [119] in 1892 and has been actively debated since. The latest works by Rice et al. [107] and Rho et al. [116] indicate that the assumption is incorrect. Rice et al. also disproved the second assumption, as they showed that the coefficients of proportionality are different for human and bovine tissue.

Future correlations may incorporate interspecies samples if the following factors are considered:

- accurate representation of trabecular architecture [120]-[124];
- structural anisotropy, possibility through stereology to determine mean intercept length or the fabric tensor [17],[113],[125]; and
- mineralization and collagen fiber orientations [65].

In addition, correlation coefficients may be improved with more sensitive experimental techniques when determining the modulus of the bone samples [64]. Specimen geometry (whether the specimen is a cube, a parallelepiped, or a cylinder of some length to diameter ratio) can greatly affect the results [117], [126]-[127], as can confining the end surfaces or lubricating them [115]. Temperature during testing has also been shown to have a small effect [106].

Though an accurate, reproducible correlation between trabecular bone density and Young's modulus has not been developed, Rice et al. [107] have provided a correlation that can be applied to the data of this study. Rice et al. pooled data from a number of previous experiments. The data was grouped into categories of specimen orientation, tension and compression testing, and species type (bovine and human), which resolves some of the difficulties with previous correlations. Only trabecular bone specimens were considered and the data was adjusted for strain rate using the relationship determined by Carter and Hayes [26]. Though the trabecular bone was not taken from vertebrae, this correlation is likely the most accurate to date for bovine material and will be used in this study.

1.3 Scope of the Present Investigation

This work provides an initial investigation of bovine vertebral bodies. Measurements of structural properties and compression tests are done in the laboratory. The results are then compared to FEM model predictions.

1.3.1 Objectives

The investigation uses the following experimental techniques designed to analyze vertebral body structure and stiffness:

i) external measurement of the shape and dimensions of the vertebral body;

ii) internal measurement of the trabecular bone density, and the cortical bone shell thickness; and

iii) compression tests for the vertebral body to evaluate stiffness.

Three bovine lumbar vertebral bodies are tested. Compression tests and apparent density measurements have not been made on the bovine spine before. The results should provide an interesting comparison to those obtained for humans, which are reviewed in Appendix C. By making such a comparison, these experimental techniques can be verified, providing a background for future work with human specimens.

To further analyze the vertebral bodies, simple FEM models are developed using the geometrical and structural properties measured from the laboratory specimens. These models are used to predict the vertebral body's axial compressional stiffness (which was measured in the compression tests). The material properties (i.e. moduli) used in the model are taken from recent published reports, and the trabecular bone modulus is

determined from its density measured in the laboratory. These models do not predict vertebral body strength, as a failure criterion would be needed. Before such criterions can be considered, the model must represent the elastic response of the bone.

1.3.2 Contributions

The experimental techniques and equipment designed in this work can be applied to human tests in the future. The experimental results obtained from bovine vertebral bodies provide valuable comparisons with human data, and may be used in veterinary medicine as well.

Both the experimental tests and the FEM models demonstrate the important role that cortical shell thickness and modulus play in the stiffness of vertebral bodies. These parameters should be carefully considered in future human investigations.

It is hoped that this work will be applied to human FEM modelling using QCT, or another type of medical imaging. Though the models are based on geometry and bone apparent density (measured invasively in the laboratory), similar data is easily obtained using QCT. The experimental techniques and the simple FEM models described in this work, provide a foundation for future work with models linked to medical imaging. No vertebral body FEM model has been properly validated by stiffness comparisons with experimental compression tests. Such validations must occur before accurate predictions can be made by QCT driven models.

2 Preliminary Experimental Set Up

The material tests investigate the mechanical properties of bovine lumbar vertebral bodies. Stiffness, strength, bone density, and geometry will be assessed. For the mechanical testing data to be meaningful, testing conditions must simulate physiological conditions in the bovine. For the stiffness to be easily compared with the FEM models, a simple test with known boundary conditions and loading should be used. Before commencing with the tests, factors which affect the measurement of bone properties will be addressed, and the availability of equipment determined so the methods can be designed around these constraints.

2.1 Apparatus

Much of the material testing done on bone requires specialized equipment. Table 2-1 lists the apparatus available to these studies. Their use will be described in the following sections.

Table 2-1: Material Testing Apparatus

Equipment Type	Manufacturer and Model
Coordinate Measuring Machine with Touch Probe	Mitutoyo MTI Canada Ltd. DHN710
X-ray Imaging Device	Phillips Radiotherapy Simulator
Computer Driven Data Acquisition System	Video Technology Computers, Inc. LASER™ 286X personal computer running Microsoft Corp. GW-BASIC™ user made programs with Data Translation, Inc. PCLAB™ DT2818 Simultaneous measurement A/D I/O board (12 bit resolution) attached to MTS System Corp. 459.10 Testlink Connector Interface.

Table 2-1: Material Testing Apparatus

Equipment Type	Manufacturer and Model
Servo-Hydraulic Press	MTS System Corp. 810 Material Test System
Load Cell	MTS Force Transducer 661.22C-01 (25000 N maximum load)
Extensometer	MTS 632.12B-20
Band Saw	General MFG. Co. Ltd. Model 590 with 6 teeth per cm blade
9" Circular Sander	Busy Bee Fine Machine Tools Model ST-BDS690
Ultrasonic Cleaner	Struers, Metason 200
Centrifuge	Sorall® Superspeed RC2-B
Compression Test Fixtures	University of Victoria (See Figure 2-1)
Water Jet Spraying Device	University of Victoria, 8 mm (5/16") inner diameter rubber tubing attached to standard water tap. Water passage is reduced to a 2.4 mm (3/32") diameter at the nozzle with a metal reducer.
Mold Release	T.R. Industries, High Temp Mold Release
Fast Setting Expansion Cement	Hartline Products Co., Inc., Rockite®
Top Loading Balance	Mettler Instrument Corp.

As the ends of the vertebral body are not flat, they must be fixed by some means to the loading plate during the compression tests. This can be accomplished by a moldable fixing agent such as a resin or a cement. A compression test fixture was designed to attach to the servo-hydraulic press and hold the ends of the vertebral body with a fixing agent. The fixture shown in Figure 2-1 consists of an aluminum ring and plate which, when combined, form a cup in which the ends of the bone can be affixed with cement. Two fixtures were built to attach to the top and bottom surfaces of the vertebral body during testing. The apparatus must not induce torsion in the vertebra or horizontal misalignment

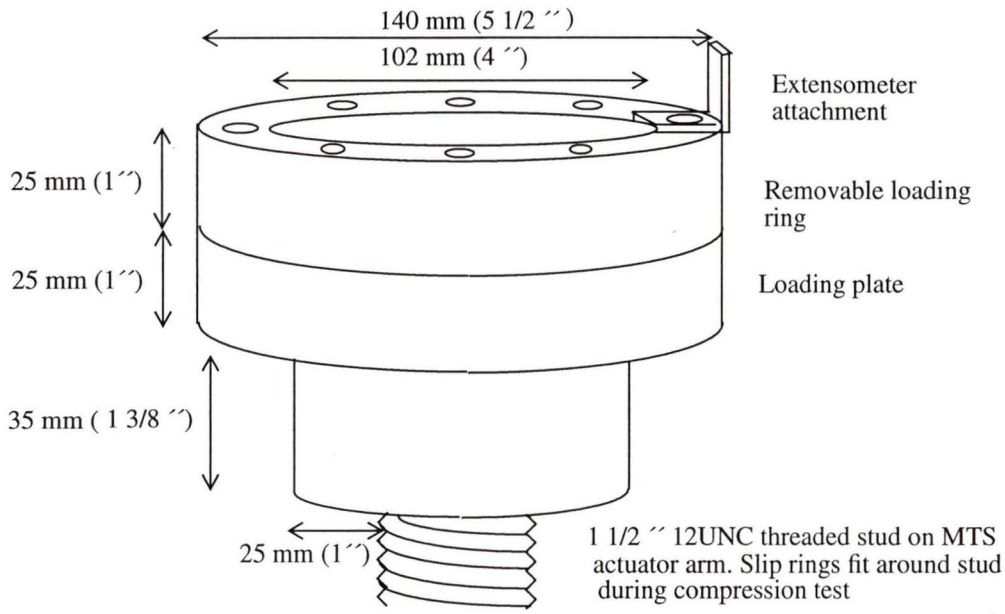

Figure 2-1: Compression Test Fixture

during testing. Misalignment can be avoided by allowing the fixing agent to dry while the vertebral body is in the correct position for loading. One end would be set first, and the second end set while the alignment is adjusted.

2.2 Density Measurements

The density of trabecular bone is used to estimate Young's modulus for the FEM models. Techniques used to determine density must be consistent with those used in other work which correlated apparent density to Young's modulus. This section will examine various techniques for determining density.

Bone mineral content or ash fraction measures the mineral component of the bone only. Such a density is the ratio of the mineral mass to the total volume including the pores. This can be determined in two ways: by baking the specimen in a furnace [128] or

by using medical imaging devices (QCT, single or dual beam photon absorptiometry [65], [98]). These measurements do not include the collagen and water content of bone, but the imaging measurements are useful because they are non-invasive.

In contrast, apparent or structural density is the mass of the bone material (including collagen) divided by the bulk volume of the specimen (including the pores). Measurements have been made with specimens, wet and dry. Wet apparent density will be used in this study for three reasons: Rice et al. [107] used wet apparent density (and their results will be used here), the medical imaging devices are not readily available, and wet apparent density most closely represents the entire structure of live bone in its natural moist state. Though it would be an advantage to use a non-invasive technique, studies have shown a close relationship between bone mineral content and apparent density, indicating that any future model could use either mineral content or apparent density [100].

One other technique used to measure density is ultrasound; this non-invasive technique has been greatly improved over the past year and may be an effective measurement technique in the future.

The determination of apparent density involves three steps: cutting a specimen, removing the bone marrow, and measuring the density. In studies which correlated Young's modulus to density, the cut specimens required precisely flat surfaces for accurate compression tests. As Young's modulus will not be measured, this study need not be as careful in the machining of the specimens (other studies have utilized precision band saws [111] or low speed diamond saws [129] for this purpose).

The removal of bone marrow and other soft tissue from the pores of trabecular bone is

necessary, since marrow has a lower density than bone. Effective bone marrow removal must be balanced against damage caused to the bone during processing. Soft tissue can be removed by boiling the bone in water with an enzymatic detergent [64]. Though this process completely removes the soft tissue, it also causes changes to the surface of the bone, affecting its material properties. Hence, researchers correlating apparent density to modulus do not typically use this technique. For specimens smaller than 10 mm, a water jet can be used to dislodge the soft material. With low water pressure (e.g. that obtained from standard water taps) this technique does not affect the integrity of the bone and keeps the bone wet. It is uncertain whether water jetting completely removes all the bone marrow, so after material testing, the specimens are typically treated with some solvents in a water solution, with and without ultrasonic cleaning [121],[129],[130]. High pressure air jets have also been used [83],[106],[115].

The density is calculated from the dimensions of the specimens (measured with a caliper or micrometer) and the mass of the specimen (measured on a precision balance). Water content of the trabecular bone poses a problem. Though measuring wet bone better reflects its in-vivo properties, it causes the mass measurement to be dependent on time as the water on the bone surface evaporates. This evaporation rate, in turn, is dependent on the humidity and temperature. To obtain accurate results, water must be removed from the pores, and mass quickly measured. Previous studies used time-specified evaporation [115], and centrifuging ([73],[83],[113],[128]) to remove the water. Though all these methods are partially effective in removing water, there is some uncertainty in the results due to this mass measurement.

2.3 A Preliminary Compression Test of a L6 Vertebral Body

As no previous work has tested bovine vertebral bodies in compression, estimates for their compressional properties were needed to design a test with a fixed strain rate. Hence, an L6 vertebral body was compressed in the servo-hydraulic press under manual control (or dial control) of displacement. An epoxy resin was used to fix the vertebral body into an aluminum test fixture. The load and ram displacement were measured when the apparatus was compressed.

The purpose of this test was two fold: first, to determine how difficult the techniques were to perform, and second, to determine "ball park" values for the ultimate load, ultimate contraction, and stiffness of lumbar vertebral bodies. As the stiffness of the epoxy is low, the stiffness of the vertebral body could not be accurately measured and the contraction was likely overestimated. The results are shown in Table 2-2.

Table 2-2: Measured Compressional Properties of the L6 Vertebral Body using Epoxy as a Fixing Agent

Ultimate Load (kN)	Ultimate Percent Contraction	Stiffness (kN/mm)
21	1.8%	24.5

The ultimate load and the percent contraction were used to set the displacement cycles for the L5, L2 and L3 vertebral body tests which will provide the experimental data used in comparison with the computer modelling. By performing this test, the need for a better fixing agent was realized.

2.4 Bone Fixation

Compression testing a structure without flat and parallel end surfaces is difficult. Optimally, the vertebral body be should be rigidly fixed on all parts of its top and bottom surfaces. In practice, a resin or cement is used as a fixing agent. This section will investigate various methods of gripping the vertebral body during the compression test.

Many fixing agents are used for human spine testing. A partial list is given in Table 2-3. Bovine vertebrae have very curved ends compared to human, making the choice of fixing agent more critical. Other fixing agents have been used for long bones with curved ends. For example, canine tibias were tested in compression, fixed with polyester/styrene [136].

Table 2-3: Review of Fixing Agents for Human Spine Compression Testing

Specimen Type	Fixing Agent	Reference
Functional spinal units	Plaster of Paris	[131]
	Dental plaster and screws	[132], [133]
	Bone cement of PMMA (polymethylmethacrylate) and side screws	[134],[30]
	Bone cement only (PMMA)	[135], [136]
	Two component cement (plastic padding) and screws	[137]
Single vertebra	Silastic J-RTV silicone spacers	[16]
	Steel cylinders	[58]
	Partial disk on steel cylinders	[138]
	Dental acrylic	[139]

Many of the fixing agents listed above, such as silicone and plastic padding, have Young's moduli near or below that of trabecular bone. Because silicone deforms during

testing, shearing will occur along the end-plate, increasing the loading complexity. However, this loading more closely represents physiological loading by the disk.

Another approach is to use a very stiff material for fixation which undergoes little deformation during the test. As the load and deformation data is to be compared to a FEM model, this approach is preferred, even though a stiff fixing agent provides a loading different than the physiological situation near the end surface. The cartilage end-plate, the subcondral bone, and the underlying trabecular bone near the end-plate can all be affected; most fractures, in-vivo, occur in this region and previous studies have shown it to be one of the weakest parts of the spine [16], [56], [140], [141].

Four criteria were used to determine a fixing agent. The material must:

- be stiff, i.e. have a Young's modulus near that of cortical bone (~20 GPa).
- be pourable, but set hard within a day so the bone is not exposed for a long time in the laboratory environment.
- be easy to work with and provide reproducible results.
- be inexpensive and readily available.

Table 2-4 lists Young's moduli and setting times for various fixing agents. The measured Young's moduli were determined using cylindrical specimens on a loading platen with a technique similar to that described for the cement samples in Section 3.2 "Compression Testing". These measurements are imprecise: exacting techniques were not used as the purpose was to evaluate the comparative stiffness rather than an absolute standard.

Table 2-4: Possible Fixing Agents

Fixing Agent	Expected Young's Modulus (GPa)	Measured Young's Modulus (GPa)	Setting time
Bone Cement, CMW2, C.M.W. Laboratories Ltd.	~2.8 [142]	---	5 min
Epoxy Resin, Cold Cure, Industrial Formulators of Canada Ltd.	0.88 (tension)[a]	0.9 - 1.0	1 hr 80% cure. 7 days 100%
Epoxy (Cold Cure) reinforced with 70% by vol. Unimin 4060 #30 free silica powder.	---	0.1 - 1.6	~ 18 hr
Plaster of Paris, Poly™ Lepage's Limited	0.9 - 6.9 [143][b]	0.2 - 0.5	~ 20 hr
Fast-setting Concrete, Post-Haste, Target Products Ltd.	---	0.1 - 0.45	~ 24 hr
Fast-setting Expansion Cement, Rockite, Hartline Products Co., Inc.	~30 [c]	20	3 hr

a. Measured by manufacturer.
b. Value depends on water in mix, data not for product tested.
c. Approximated from manufacturers strength measurement (x 1000).

Bone cement, or poly(methacrylate) has most of the characteristics required, yet is expensive and has a low Young's modulus. An inexpensive epoxy was tested as an alternative. Since it also had a low modulus, the epoxy was filled with silica powder to provide stiffening. Unfortunately, either because too much powder was used, or because the epoxy bonded poorly with the silica, the composite lost stiffness. Published reports indicated that plaster of Paris has an acceptable stiffness, yet the product tested in the laboratory had low stiffness and a long setting time, likely due to the amount of water

required in this quality of plaster. A logical step after trying plaster was to try another common building material, namely fast-setting concrete. Again, due to the quality of the product tested, the results were discouraging.

Finally, a high quality fast-setting expansion cement was found with adequate properties. This cement sets within 30 min and within an hour has a strength of 32 MPa (quoted from manufacturer). Laboratory testing indicated a stiffness as required. Though the fast setting time is an advantage, an organized laboratory procedure is required if the vertebral body is to be set into the cement before it hardens. Also, the setting of the cement produces a significant amount of heat which could harm the bone surface.

2.5 Environmental Conditions

Conditions during compression testing must not greatly affect vertebral material properties. Temperature, humidity, and salinity effects are small compared with the variations that will likely occur between different animals, and between different lumbar vertebrae. Hence, this study will conduct the testing at room temperature in an open environment. For a more precise study, the test would have to be carried out under conditions near in-situ (38.6° C, in 0.9% NaCl saline solution).

2.6 Strain Rate and Loading Conditions

As vertebral bodies are composed of viscoelastic materials, consistent loading methods were used throughout the tests. Though a constant strain rate cannot be imposed through out the vertebral body, a constant displacement rate can be specified by the actuator arm on the servo-hydraulic press though the use of a linear variable differential transformer

(LVDT). By compressing the vertebral body many times in succession, an indication of the time dependence on stiffness can be determined. The microprofiler on the servo-hydraulic press was programmed to produce compression cycles of various amplitudes. Thus, during the test the maximum displacement is low until the load-deformation curves are repeatable. Then a ramp-and-hold program on the microprofiler is used to compress the vertebral body to the yield point.

Recording the load and deformation can be done digitally using a computer-based acquisition system. Though the hardware was set up on the MTS machine, custom software needed to be programmed using GW-BASIC. During the test, three channels, load (measured with the force transducer), displacement (measured with the LVDT), and displacement (measured across the test fixtures with the extensometer), will be recorded at 20 or 40 Hz on the personnel computer while the load and deformation will be plotted on the video screen. The program's graphical scaling and error checking are rudimentary.

3 Experimental Methods

As well as measuring load versus deformation for the vertebral bodies, the material tests must provide data for structuring the FEM model. The outer dimensions and shape, along with information on the internal structure of the vertebral body (i.e. apparent density of trabecular bone and thickness of cortical bone shell) will be extracted from the specimens.

To simplify the descriptions of the vertebral body's orientation, the following conventions will be used. The surface of the vertebral body which is closest to the head of the cow when in the animal's body will be referred to as 'top', whereas a surface which is closest to the rear will be 'bottom'. Also, a surface which is closest to the abdomen will be denoted 'front' and the one near the cow's back will be 'back'. 'Lateral' will define a direction either to the left or the right side, relative to the body of the cow. These terms are used to reduce medical jargon.

3.1 Bone Preparation

Though bovine material is widely available, butchers split the animal through the middle of the spinal column, destroying the vertebral bodies. After some searching, an intact bovine lumbar spine was purchased from an animal food processing facility in the Fraser Valley. Unfortunately, no detailed information on the history or health of the animal was available. The lumbar section of the spine, cleaved at both ends, was frozen in a plastic (polyethylene) bag, since freezing reportedly has no effect on the properties of bone. [131], [144].

By cutting the pedicles and disk, the individual vertebral bodies were removed from the spine. Three vertebral bodies were tested: L5 was tested first and L2 and L3 were later tested together. As the vertebral bodies warmed to room temperature, soft tissue was removed using a scalpel. To prevent dehydration, the vertebral bodies were covered with saline-soaked gauze and placed in plastic bags. During the period between dissection and testing, the vertebral bodies were refrigerated.

Before the compression tests, some non-destructive measurements where taken on each vertebral body. Points on the surface of the L5 vertebral body were digitized for use in the FEM models. The vertebral body was supported by screws pressed against its surface (see Figure B-1). The touch probe on the coordinate measuring machine was positioned to measure points on one area of the bone, then repositioned to measure another area. To digitize the entire surface, data had to be referenced to two different origins and the vertebral body had to be removed from the screws, rotated, and repositioned once. To reference all the data sets to a common coordinate system required data processing described in Appendix B. The L2 and L3 vertebral bodies were x-rayed to visualize the internal structure of the trabecular bone. It was hoped that these x-rays would aid in the alignment of the vertebral bodies for the compression test, but an appropriate procedure was not formulated. Height measurements were also taken with a caliper.

3.2 Compression Testing

The compression tests consisted of three steps. The vertebral body was cemented in the test fixtures and test samples of the cement made. Then the vertebral body underwent compression loading cycles. Finally, the cement samples were tested to determine their modulus.

Before the cement was poured into the test fixtures, the aluminum cups were coated with a wax based mold release for easy cement removal. As the concave shape of the bottom vertebral body surface was easier to align than the convex top surface, it was set first with its long axis (top-bottom direction) perpendicular to the plane of the loading plate. A portion of the cement mix was used to fill a cardboard cylinder to form the cement sample. Once the cement was partially hardened, the ends of the cylindrical cement sample were planed with a circular sander. The test fixture / vertebral body assembly was attached to the upper arm of the hydraulic press. The other test fixture, attached to the lower arm, was filled with cement and the vertebral body lowered into the wet cement. Another cylindrical cement sample was made. The assembly was left to harden in the arms of the press for at least one and a half hours before load was applied. The ends of the second cement sample were planed with a sander, and the diameter and height of both cement samples measured (with two opposed diameter measurements on each end, and two or three height measurements). The extensometer was attached to the metal L-bracket on the test fixtures just before compression testing. The procedure took between 3 and 5 hours to complete.

Once the set-up was complete, compression testing began with a number of loading cycles with varying peak displacements. During all the compression cycles, the actuator was moved at 0.0847 mm/sec to its peak displacement and returned. This displacement rate was used to avoid the more pronounced dependence on strain rate at higher rate levels. The first four or five cycles were kept at a low peak displacement level and then the peak displacement was increased. If needed, additional cycles at higher peak displacements were used to fail the vertebral body. Load and displacement across the aluminum cups were recorded using the computer-driven data acquisition system.

Directly after the vertebral body testing, the two cylindrical cement samples were loaded under the same loading rate. The extensometer was attached on the surface at mid-length. The loading plate of the test fixture was used to press against the flat end surface of the cement cylinder.

3.3 Trabecular Density and Cortical Thickness Measurements

The FEM models required a modulus value for trabecular bone, and a thickness for the cortical bone shell. Hence, the intact vertebral bodies were cut into four or five sections across the long axis using a band saw. Calipers were used to measure cortical shell thickness across these sections of L2 and L3. The perimeters of the sections were traced on graph paper so the geometry could be used in the FEM models. Smaller sections were cut across the long axis of L5 to measure the thickness of cortical bone on the end-plates.

Apparent density of trabecular bone was measured to calculate trabecular Young's modulus. Cubes and triangular prisms of trabecular bone were cut from the bone sections

and their edges aligned with wet and dry sand paper (silicon carbide 220 grit). Three to five caliper measurements on each dimension determined volume with a measure of error. Internal soft tissue inside the porous cube/prism was removed by repeating a 10 min water jet and a two hour ultrasonic cleaning in 95% ethanol. The trabecular bone was left in saline to equilibrate overnight. Water was removed by centrifugation at 8000g for 15 min and the cubes/prisms weighed. Most cubes were weighed twice to observe the effect of evaporation during the weighing process. The apparent density was determined by dividing this measured mass by the previously measured volume.

3.4 Calculations for Derived Quantities

Young's modulus for the trabecular cube/prisms was calculated using the empirical correlation given by Rice et al. for longitudinal compression of bovine bone [107]:

$$E = 0.07 + 2.46\rho^2 \tag{3-1}$$

where Young's modulus, E, is in GPa and apparent density, ρ, is in g cm^{-3}. This quadratic prediction model came from a larger model including human and bovine data tested in compression and tension in various bone orientations. The large model explained 78% of the variance in E, with a standard error of the estimate for E as 0.243. Using this equation to predict Young's modulus will produce some uncertainty in the modulus value (though the standard error will be less, at least slightly, to the one for the large model incorporating all the variables).

Young's modulus is also dependent on strain rate: the above equation is normalized to a strain rate of 0.01 s^{-1}. To calculate Young's modulus for the strain rate employed in this

work, the 0.06 power law established by Carter and Hayes [26] was used. The law states that Young's modulus is proportional to the 0.06 power of strain rate. An approximate height of bovine lumbar vertebral bodies is 70 mm. The actuator speed (0.0847 mm/sec) divided by this height approximates a strain rate of 0.0012 s^{-1}. Hence, to correct Equation 3-1 for strain rate, E is multiplied by $(0.0012/\ 0.01)^{0.06} \cong 0.881$.

Vertebral body stiffness was determined from the slope of the load versus deformation curve. A linear regression was fit to the data within a certain load range. Ultimate load was taken at the first point following the elastic region where a tangent to the curve became parallel to the deformation axis.

Cement sample modulus was calculated from the slope (k) of the load versus deformation curve. Load range was determined from the vertebral body tests. Using the gage length (l) and the diameter (d), Young's modulus was calculated as:

$$E = \frac{4kl}{\pi d^2} \tag{3-2}$$

4 Experimental Results

4.1 Measured Geometry

The measured heights and cross-sectional areas of the vertebral bodies are listed in Table 4-1. Each cross-sectional area was measured from a position along the vertebra from the top end. The photographs in Figure 4-1 indicate where those cross-section cuts were made for the L3 vertebral body.

Table 4-1: Measured Vertebral Body Geometry: Height and Cross-Sectional Area

L2		L3		L5	
Position (mm)	Area (mm^2)	Position (mm)	Area (mm^2)	Position (mm)	Area (mm^2)
10.4	1835	7.6	1975	6.8	1337
				14.8	2254
24.4	1211	24.1	1192	24.8	2019
				31.8	1710
40.6	1170	40.6	1271	39.8	1585
				49.8	1621
56.7	1728	58.7	1988	59.8	1944
				67.8	2396
Summed height (mm)	Averaged area (mm^2)	Summed height (mm)	Averaged area (mm^2)	Height (mm)	Averaged area (mm^2)
68	1453	71	1574	76	1881
Height caliper measurement (mm)					
72 ± 2		72 ± 2			

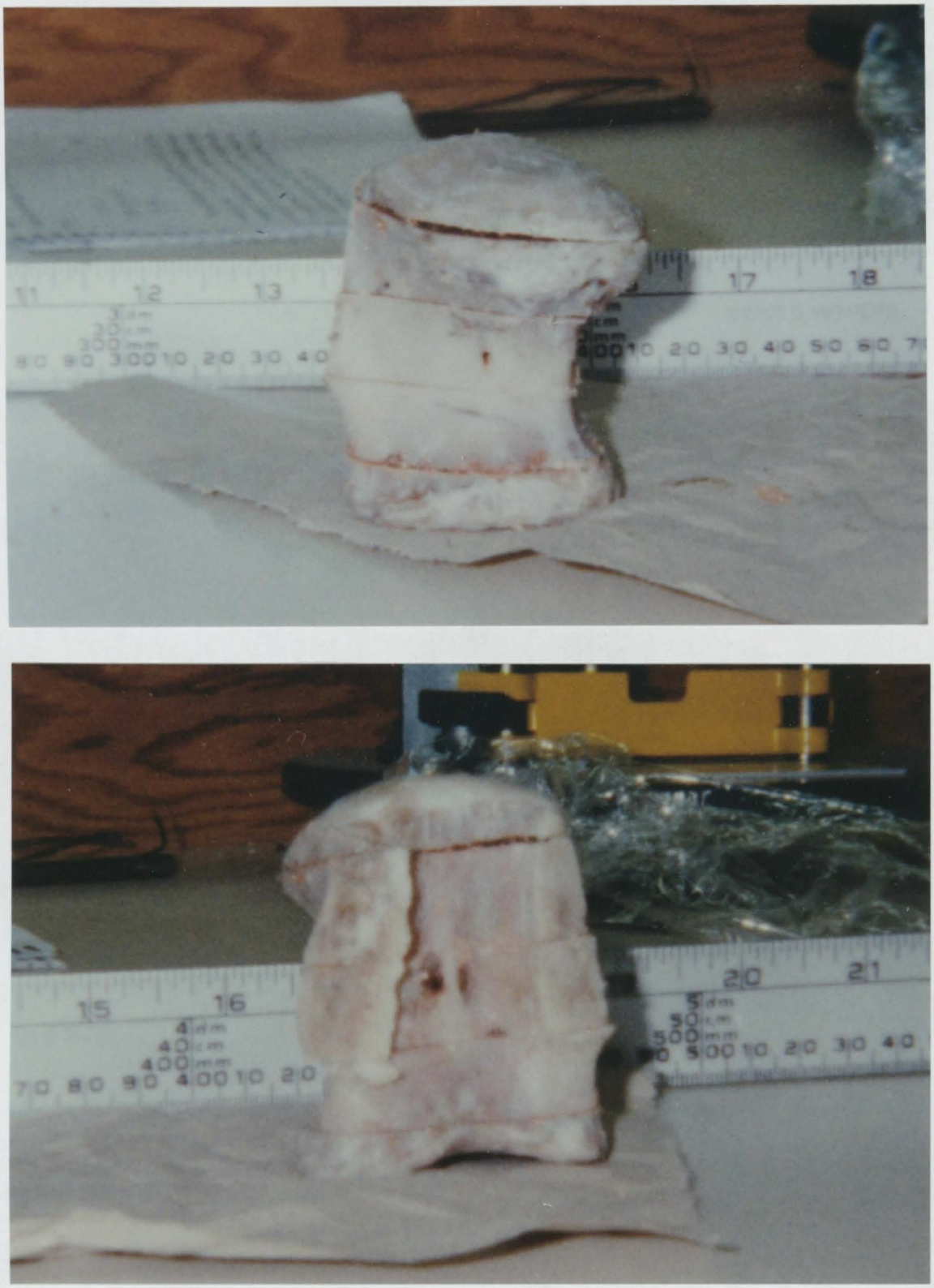

Figure 4-1: Photographs of the L3 Vertebral Body after Cutting into Cross-Sections

The results for L5 were determined from the digitized surface measurements, which were used in the ANSYS® FEM program. Area was determined using the routines in the program. In contrast, the cross-sections of L2 and L3 were traced on graph paper during the sectioning process. Two dimensional coordinate values from the tracings were then used in ANSYS®. The longitudinal positions for L2 and L3 were based on the caliper height measurements on each slice of the vertebrae.

Heights of the intact L2 and L3 vertebrae (also measured with calipers) are listed at the bottom of the table; these correspond to the maximum height on the bodies. A series of measurements were used to determine the error bound, which is high because of the difficulty of measuring the dimensions of a wet, highly curved object. The "summed height" in the table was determined by adding up the individual heights of the sliced sections. This height, when compared to the more accurate intact height below, gives an indication of the accuracy of the position measurement for the cross-sections.

Future calculations require a cross-sectional area representative of the entire vertebra. This "averaged area" was determined by weighting the area to the portion of the length it applies to by the following expression:

$$\sum_{i=1}^{N} A_i \frac{(x_{i+1} - x_i)}{\left(\sum_{j=1}^{N} x_{j+1} - x_j \right)} \tag{4-1}$$

where A_i and x_i are the cross-sectional areas and longitudinal positions in Table 4-1 (x_{N+1} being the summed height) and N is their number (4, 4, and 8 for L2, L3, and L5 respectively). To be consistent, the average L5 cross-section can also be calculated using 4 sections by averaging the first two and using the two others which are close in position to

the L2 and L3 position. The result is then 1819 mm^2, a 3.4% percent difference from the result using all the cross sections for L5.

As in human anatomy, the bovine vertebral bodies become larger as one moves down the spine. Thus, L5 is slightly longer and much broader than L3, and L3 is broader than L2.

Plots of the cross-sections formed in ANSYS® are shown in the next three figures. The number beside each cross-section relates to the order they are found in Table 4-1. Plots for L5 were made with the raw digitized surface data and the surface roughness reflects the data's accuracy. Assuming that the surface is smooth and observing that the surface data points can deviate as much as 5% from an approximate radius, an upper bound on the area's error is 10%. As the surface is irregularly curved, this upper bound is high and the actual error lower. Assuming that the traced data from L2 and L3 may err by about one millimeter normal to the surface, an error approximation of 10% is obtained for L2 and L3. The difference between the area determined from counting the mm^2 boxes on the graph paper, and the area determined in ANSYS® was 2%.

4.2 Cortical Shell Thickness

The thickness of the cortical shell was highly variable in all the vertebrae as indicated in Table 4-2. Mean and standard deviation (in brackets) in the table were determined by a series of approximate measurements. The thickness is categorized by region on the vertebra. Since cortical thickness was measured on the smaller cube/prisms for L5, end-plate thickness was also measured, but the difference between front and lateral position

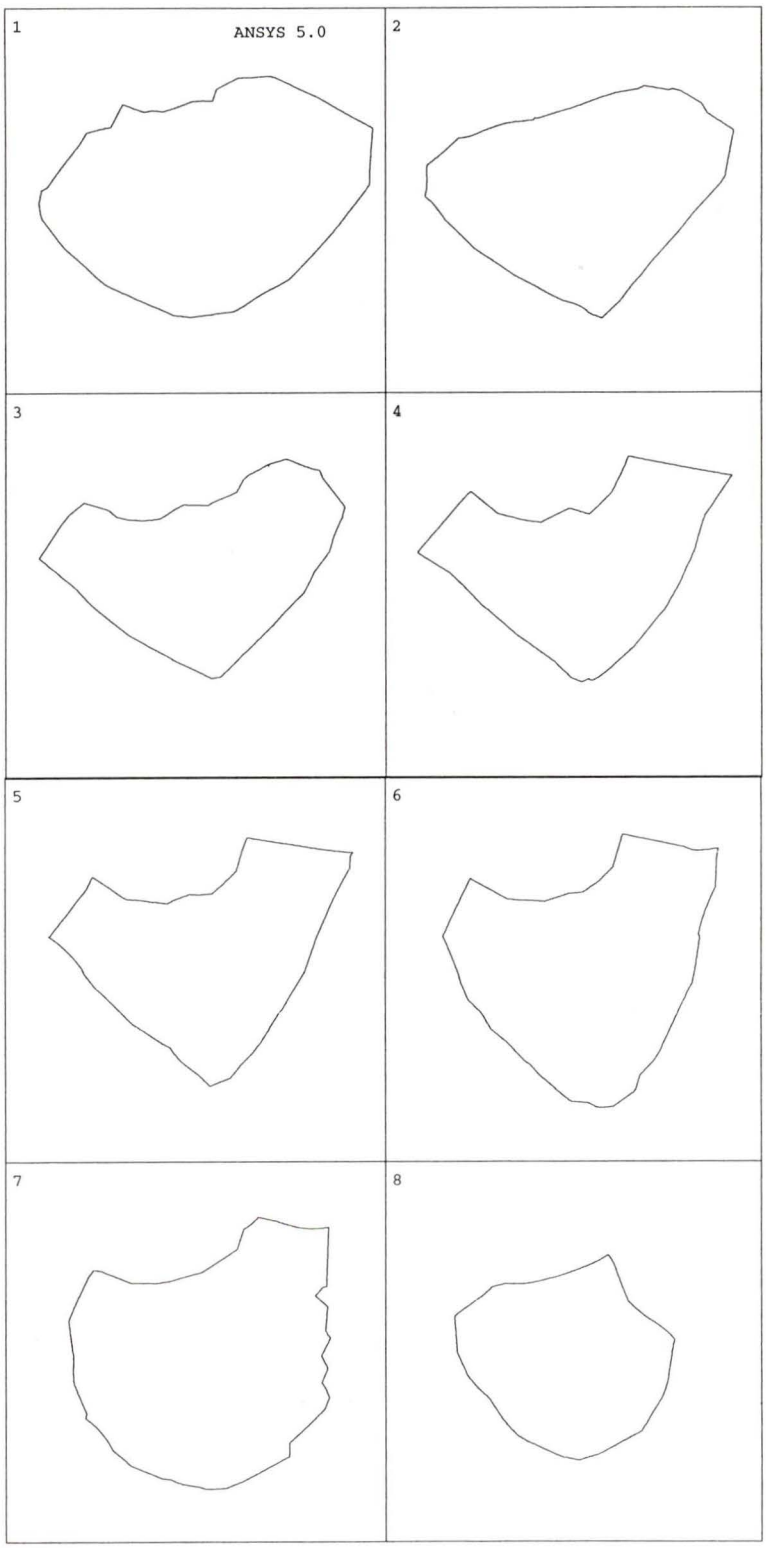

Figure 4-2: L5 Cross-Sections from Digitized Surface Data

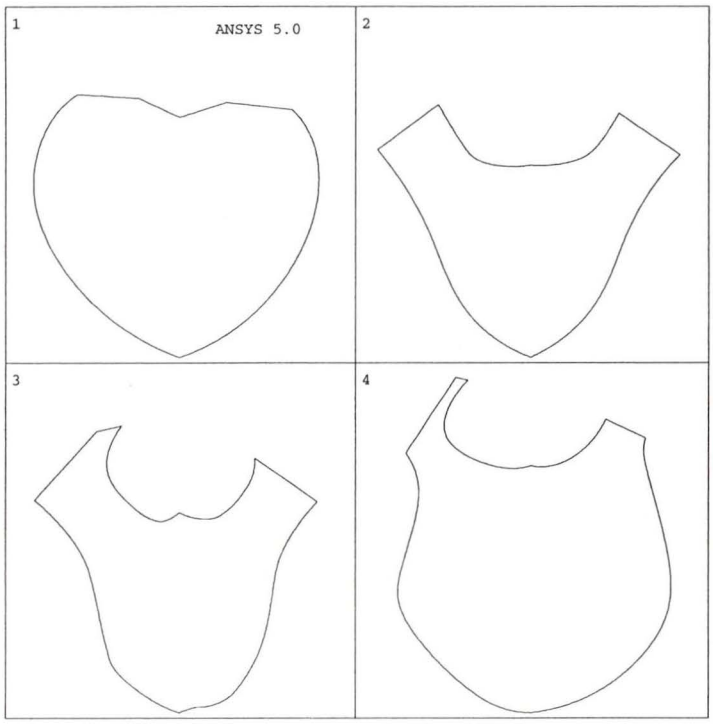

Figure 4-3: L2 Cross-Sections from Tracing Data

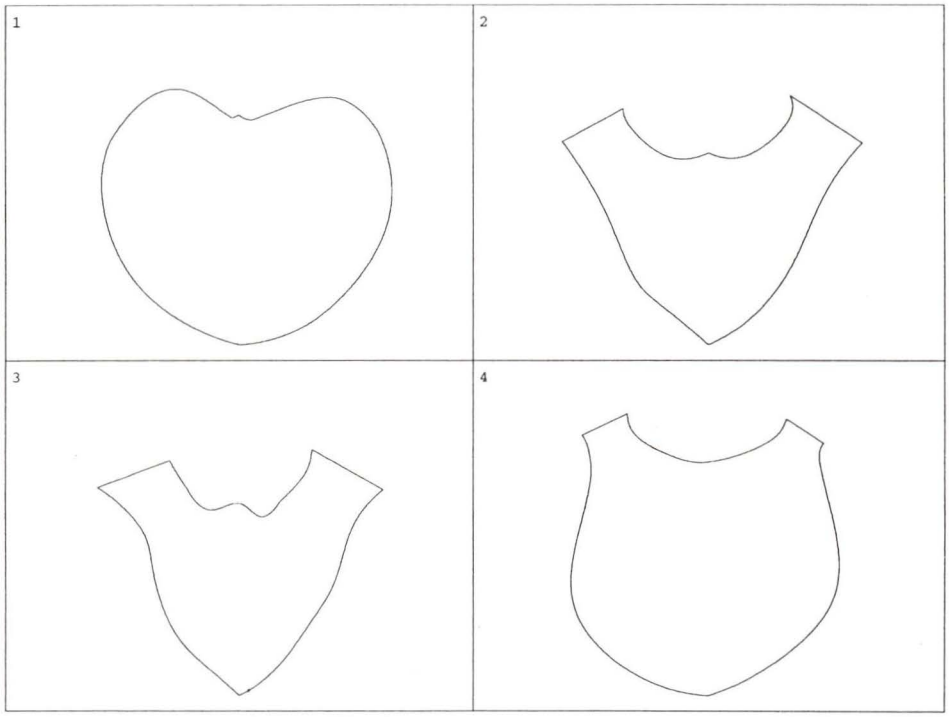

Figure 4-4: L3 Cross-Sections from Tracing Data

Table 4-2: Measured Cortical Shell Thickness*

Vertebral Body	End-plate (mm)	Lateral (mm)	Front (mm)	Back (mm)	Average (mm)	Sample size
L5	3.5 (2.1)	front-lateral 1.5 (.7)		0.9 (.4)	1.23 (.7)	25
L2		1.6 (.3)	1.2 (.5)	0.8 (.2)	1.14 (.5)	17
L3		2.0 (.5)	1.7 (.5)	1.0 (.1)	1.67 (.6)	18

* Standard deviation in brackets.

was not taken into account. The average value calculated for the L5 vertebral body did not include the end-plate measurement.

Statistical z tests were used to determine whether a vertebra or a region on a vertebra was significantly thicker or thinner than another. A 99% confidence level or a significance level of $\alpha = 0.01$ was used. Two assumptions are made in this analysis: the sample's average represents the actual mean of the population, and the measurements are distributed normally. As the size of all the above samples was below ten, these assumptions may not hold perfectly.

Due to the high standard deviations, only one significant difference could be determined between the vertebrae: the L3 back surface is thicker than the L2 back surface. There are significant differences regionally on individual vertebra. The back thickness on L2 is significantly less than the lateral thickness, and in L3 and L5 the back thickness is less than the lateral and front thickness. As the back region of the vertebra is supported by the neural arch, it is not surprising that this region has the lesser thickness.

4.3 Trabecular Density and Modulus

The predictions for Young's modulus through apparent density are given in Table 4-3.

Table 4-3: Sample Statistics for Density and Modulus of Trabecular Bone

	Apparent Density (g cm-3)			Young's Modulus (GPa)		
	L5	L2	L3	L5	L2	L3
Mean	0.711	0.670	0.745	1.176	1.047	1.296
Median	0.708	0.672	0.734	1.150	1.045	1.240
Standard Deviation	0.072	0.061	0.108	0.222	0.187	0.359
Sample Size	23	10	11	23	10	11

A group of specimens, used to measure apparent density from the L3 vertebral body, is shown in the photograph in Figure 4-5. The results from the measurements are shown in the next three figures for the three vertebral bodies. The error bars in these plots denote the experimental error calculated from the combined standard deviations of the volume and weight measurements. The data are plotted from lowest density to highest, making the variation between datum clearer.

The apparent density did not differ substantially between the three vertebra (significance level $\alpha = 0.01$), but there was large variability within each vertebra as indicated by the standard deviation in Table 4-3 and the plots below.

Young's modulus is calculated from the apparent density using Equation 3-1. As the dependence is quadratic, the slight increase in density causes a greater increase in the modulus prediction. Accordingly, the error estimations on the denser cube/prisms correspond to greater error estimations on the modulus.

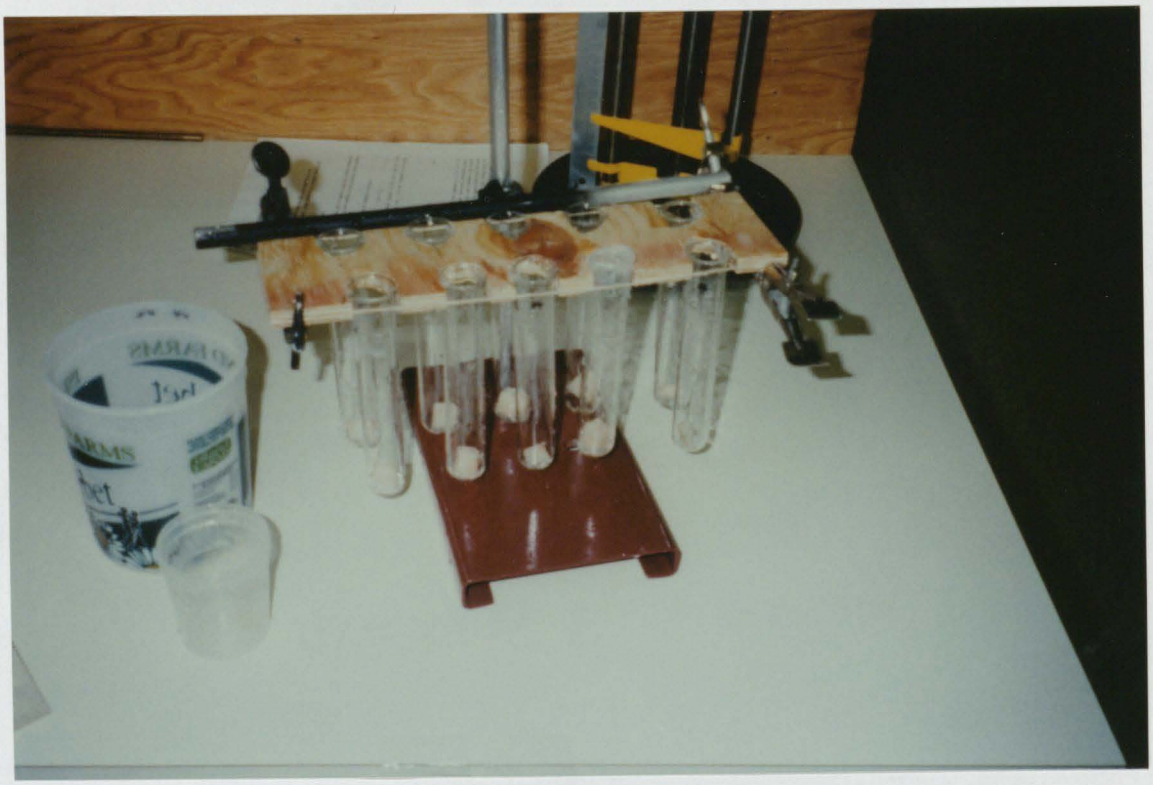

Figure 4-5: Photograph of the L3 Trabecular Bone Specimens used for Apparent Density Measurement

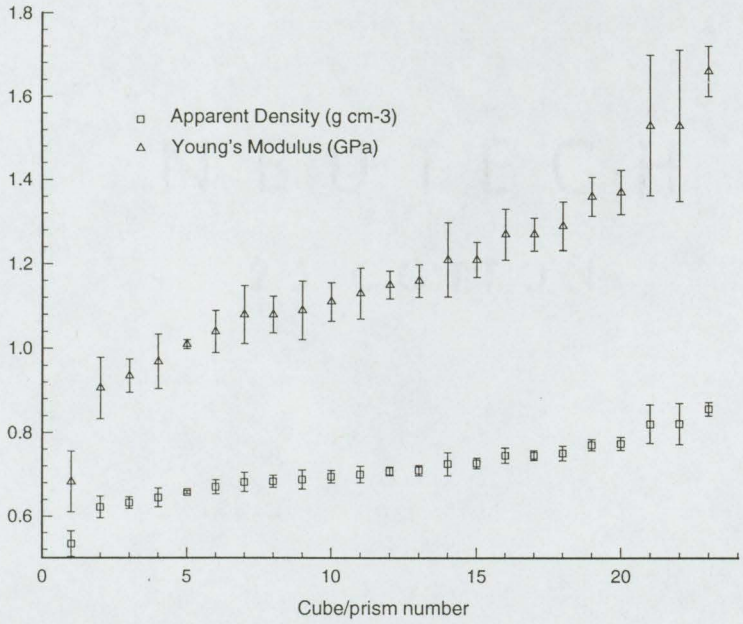

Figure 4-6: L5 Trabecular Apparent Density and Young's Modulus Data

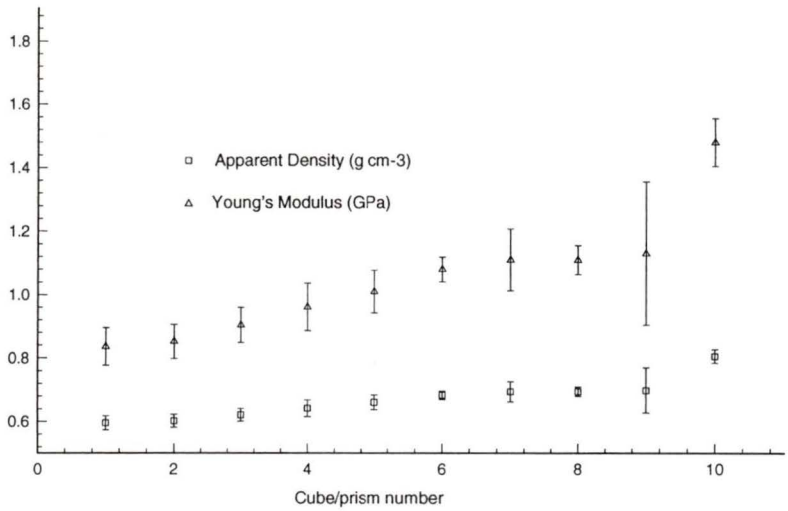

Figure 4-7: L2 Trabecular Apparent Density and Young's Modulus Data

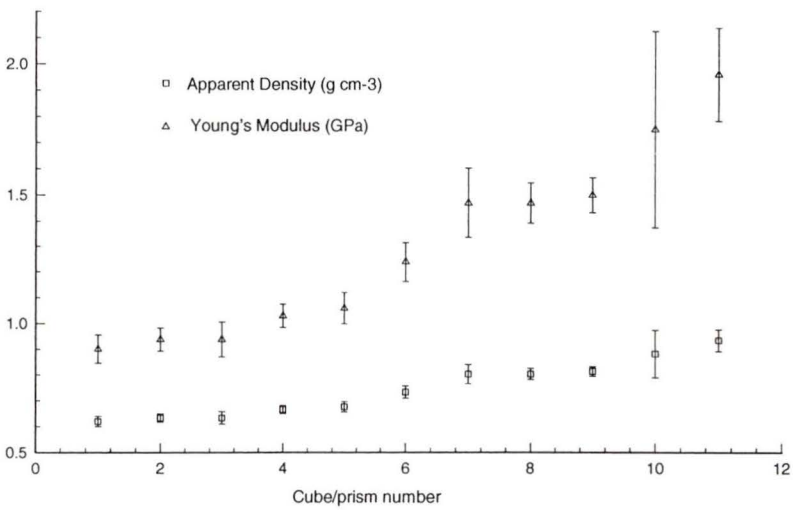

Figure 4-8: L3 Trabecular Apparent Density and Young's Modulus Data

4.4 Compression Testing Data

During the compression tests, stiffness was measured at various loads and cycles. An approximate strength value was also taken for each vertebral body. One observation was made during the tests: blood and marrow was expelled through the back vein canals (see Figure 4-9). Based on this observation the marrow must aid, to some extent, to the stiffness and strength of the vertebral body. The photographs in Figure 4-10 show the L2 and L3 vertebral bodies during the compression tests.

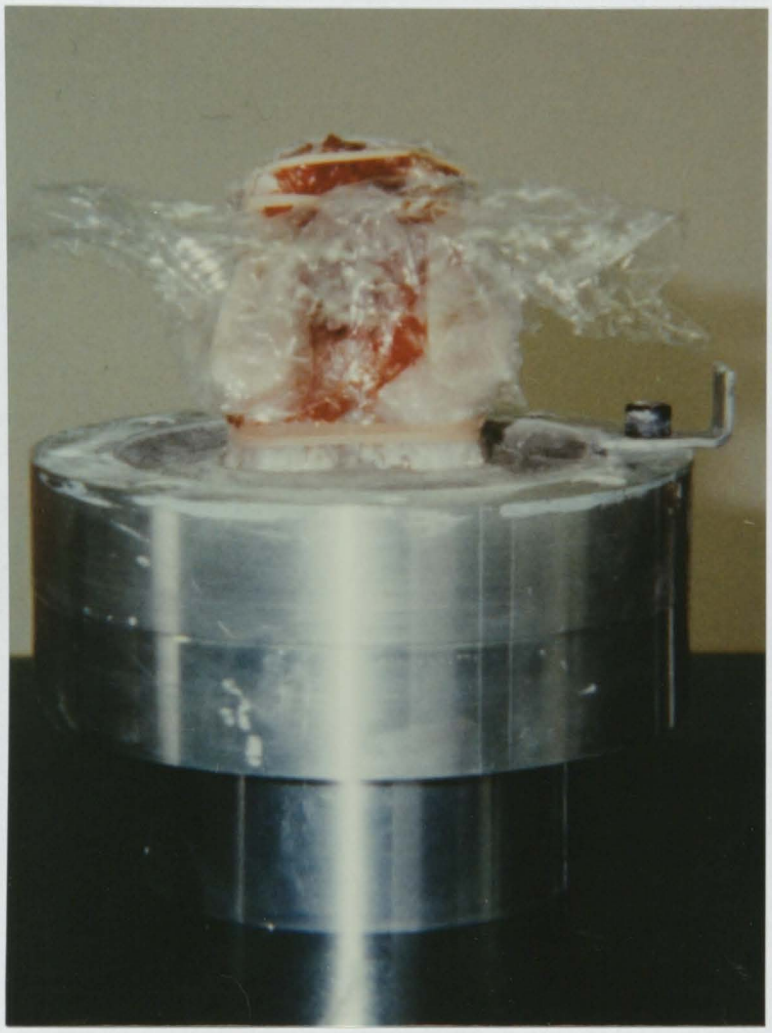

Figure 4-9: Photograph of the Marrow Ejection from the L3 Vertebral Body

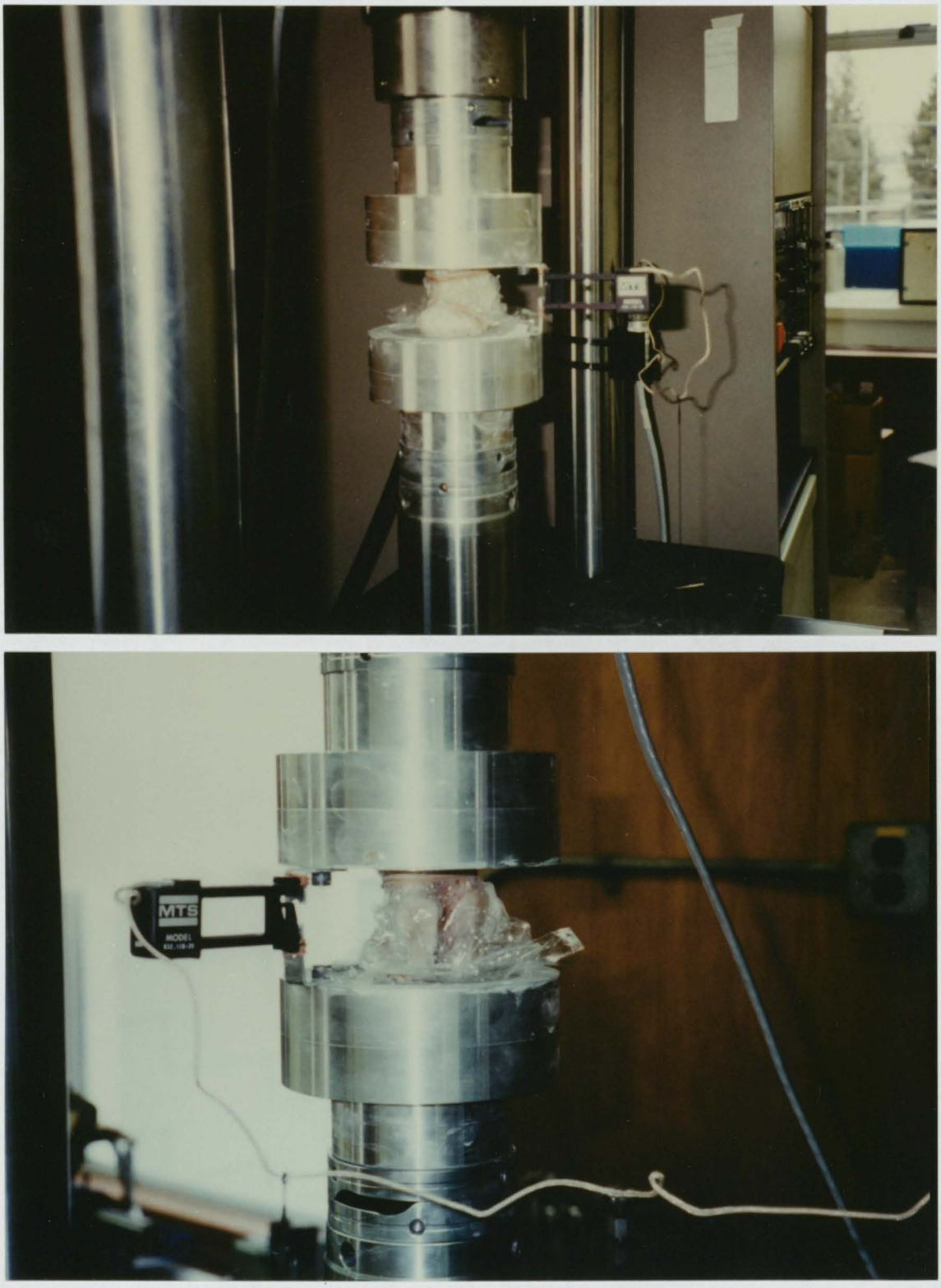

Figure 4-10: Photographs of the (Top) L2 Vertebral Body / Test Fixture Assembly and the (Bottom) L3 Assembly During the Compression Test.

Though the displacement cycles were designed using the results of the test for the L6 vertebral body fixed with epoxy, the maximum displacement in the original cycle was not large enough to fail the vertebral bodies fixed with cement. Hence, different loading cycles were used for each vertebral body. The displacement cycles used are shown graphically in the following sections.

4.4.1 L5 Compression Data

The first nine displacement cycles are shown in Figure 4-11. The original intent was for the first five cycles to determine the stiffness and the sixth to fail the body. After the sixth cycle and no failure, the displacement was returned to zero; and three other higher displacement ramps used.

The load deformation response for the first seven cycles is shown in Figure 4-12. Note the strange flat plateau on the sixth and seventh cycles of the curve. This is not a characteristics of the vertebral body but an error caused by the assumptions made with the L6 vertebral body test. The MTS machine was set for a maximum load just above the recorded ultimate load for L6 (about 22 kN). This was to improve the resolution of the analog to digital conversion. But when a higher load was applied, the result could not be recorded.

A greater load range was set, but the limit of the extensometer range was exceeded without failing the vertebral body. The eighth and ninth cycles show a dramatic change in the stiffness of the vertebral body (Figure 4-13).

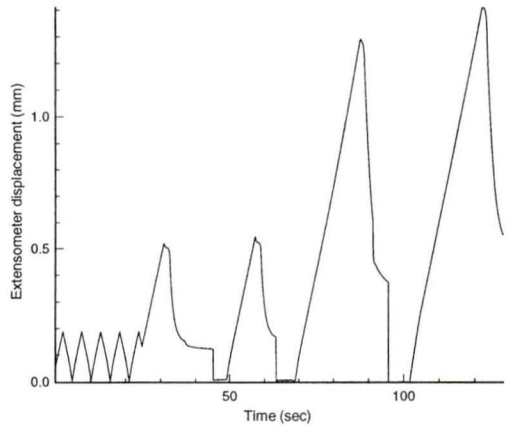

Figure 4-11: L5 Displacement Cycles

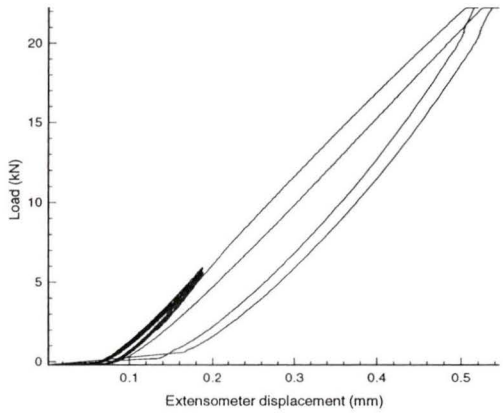

Figure 4-12: L5 Load versus Displacement for Cycles 1-7

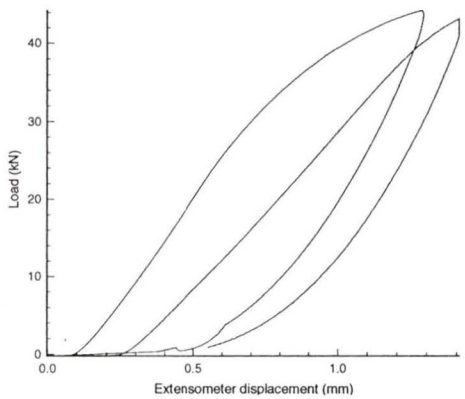

Figure 4-13: L5 Load versus Displacement for Cycles 8-9

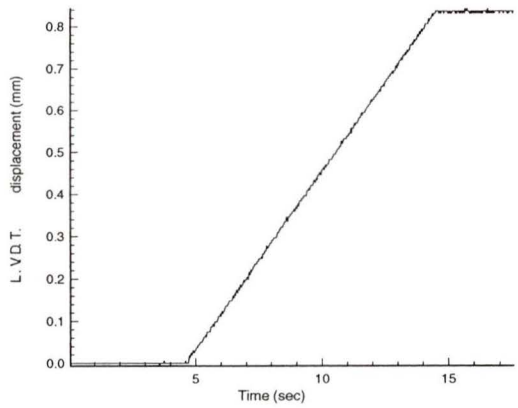

Figure 4-14: L5 Failure Loading from a Prestress

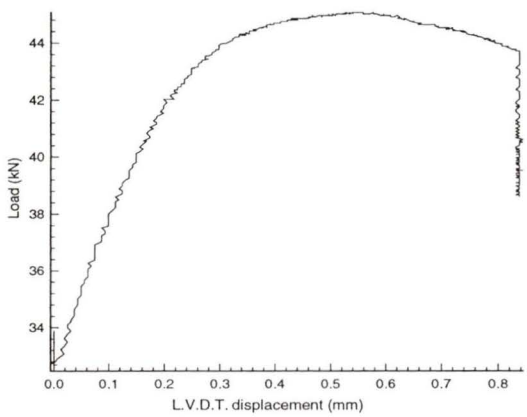

Figure 4-15: L5 Load versus Displacement during Failure

To increase the displacement range, the extensometer was removed. The deformation was recorded with the LVDT and shown in Figures 4-14 and 4-15. An ultimate (maximum) load was achieved. Note the unusual vertical ending to the load deformation curve. During this stage, the displacement is constant, yet the load is continually dropping. Hence, the body is undergoing a relaxation.

4.4.2 L2 Compression Data

During the loading of the L2 vertebral body, the extensometer exceeded its limit twice. As it had to be reset both times, the data was recorded in three sets, with each set referenced to a different zero displacement. Hence, the figures are in three sets of three. Plots of displacement versus time, load versus displacement and load versus time are shown in the following figures for the three data sets.

The first data set consists of cycles one though five, the second, six through seven, and third, eight and nine. The final loading cycle is not shown, though the ultimate load was recorded. The largest loading cycle in the first set shows a strange peak, indicating that the load dropped off with little displacement change. This is in fact a relaxation, as seen in the L5 body. Displacement is not physically increasing, but the electronically recorded zero is being adjusted to compensate for exceeding the limit of the extensometer.

The seventh cycle has a similar anomaly at the highest load which is due to adjusting the load zero. In both the seventh and eighth cycle, the slope of the load deformation curve is S shaped, with the middle displacements causing a higher stiffness than the lower and higher displacements. This is typical of biological materials [57]. But in the eighth and ninth cycle, this trend is less strong with the higher displacements causing a similar stiffness compared to the middle region of the curve.

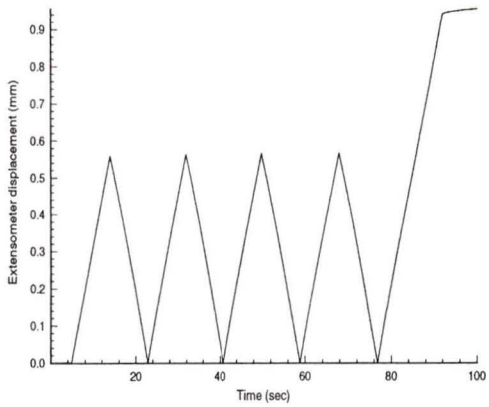

Figure 4-16: L2 Displacement Cycles 1-5

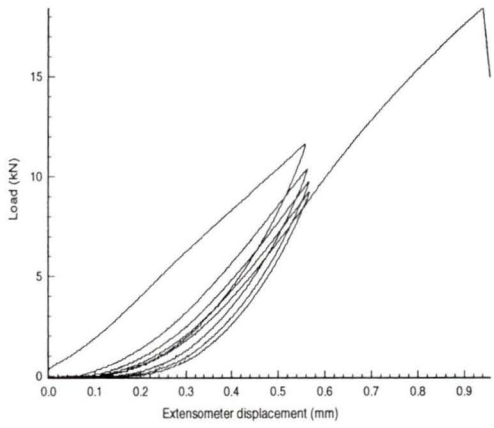

Figure 4-17: L2 Load versus Displacement for Cycles 1-5

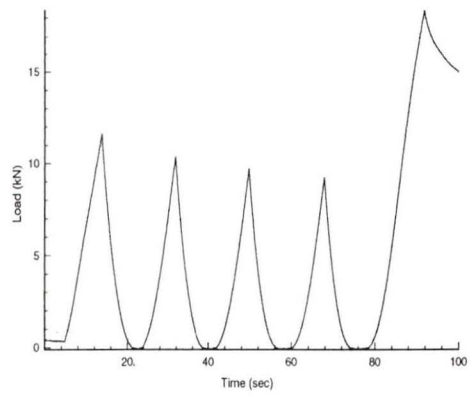

Figure 4-18: L2 Load versus Time for Cycles 1-5

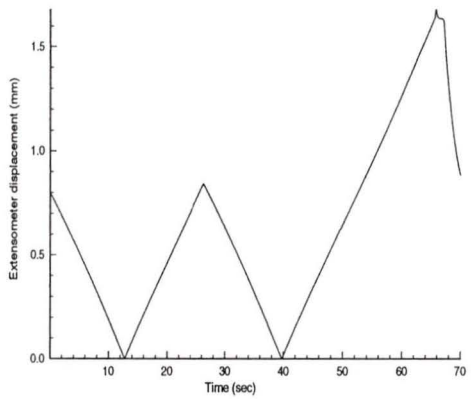

Figure 4-19: L2 Displacement Cycles 6 and 7

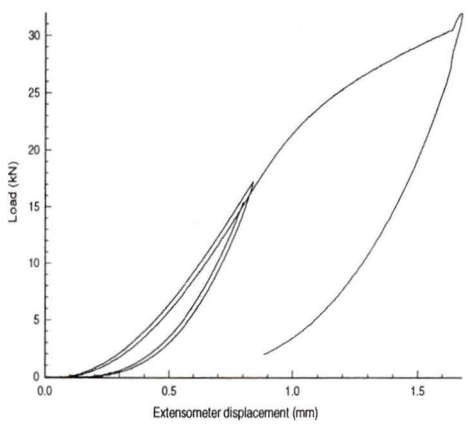

Figure 4-20: L2 Load versus Displacement for Cycles 6 and 7

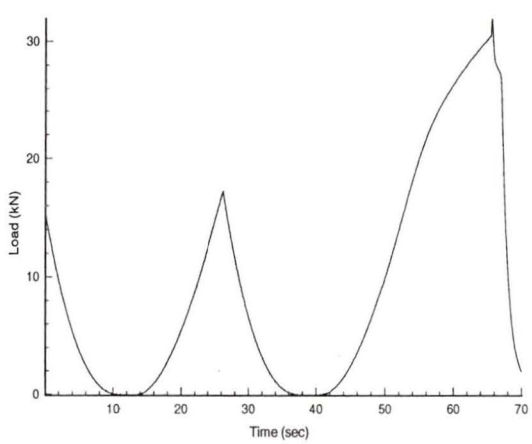

Figure 4-21: L2 Load versus Time for Cycles 6 and 7

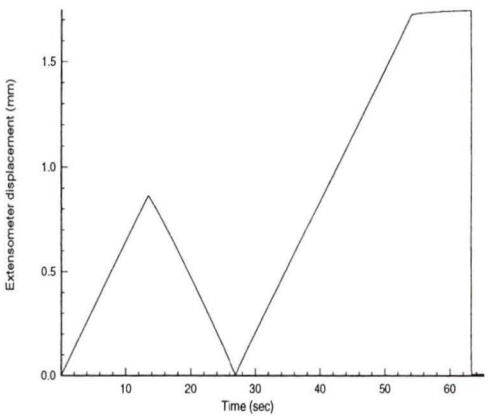

Figure 4-22: L2 Displacement Cycles 8 and 9

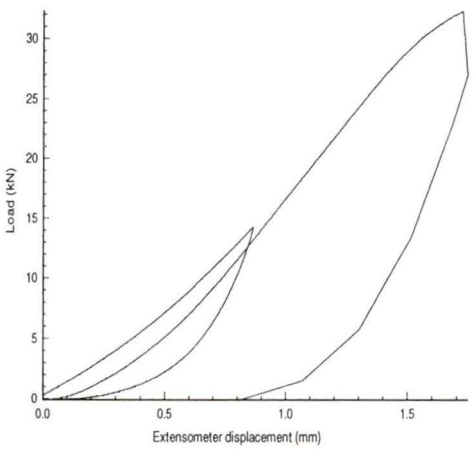

Figure 4-23: L2 Load versus Displacement for Cycles 8 and 9

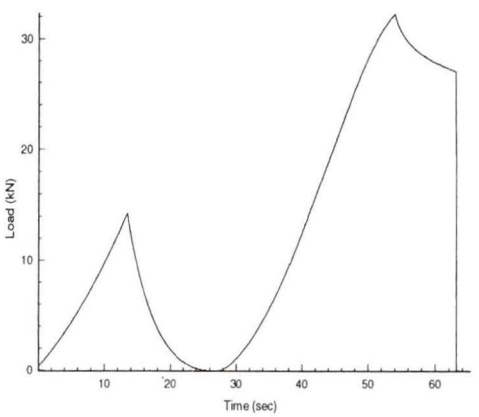

Figure 4-24: L2 Load versus Time for Cycles 8 and 9

4.4.3 L3 Compression Data

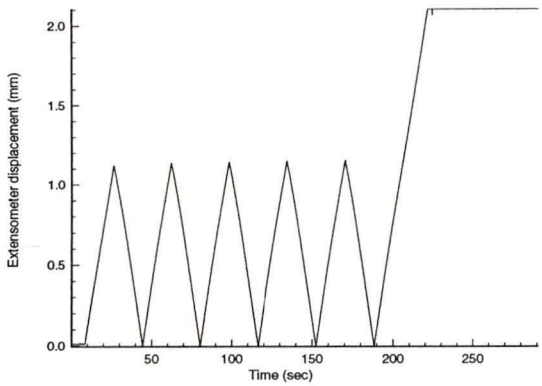

Figure 4-25: L3 Displacement Cycles

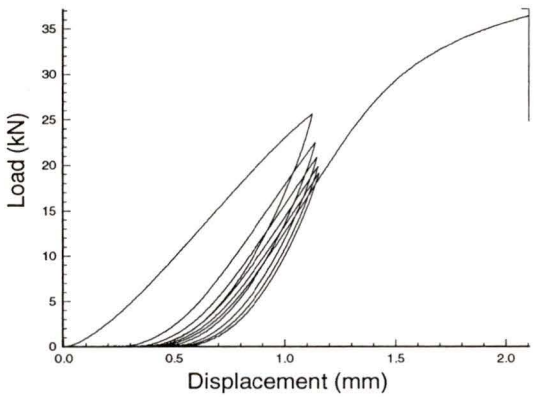

Figure 4-26: L3 Load versus Displacement

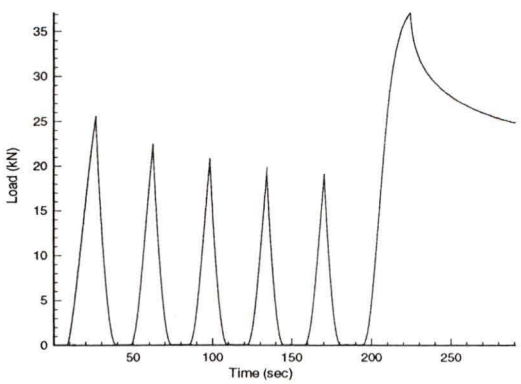

Figure 4-27: L3 Load versus Time

The five loading cycles used for the L3 vertebral body are shown in Figures 4-25 through 4-27. An error is seen at the peak load and displacement. The maximum set displacement was not great enough to fail the vertebral body. The displacement exceeded both the electronic limit and the physical limit of the extensometer. As a consequent, a straight horizontal line can be seen in Figure 4-26 at which point the displacement held constant at its physical limit.

Subsequently, a relaxation occurred where the load decreased during this fixed displacement. Note that L3 was not displaced enough to enable an accurate measurement of ultimate load before the relaxation had substantially altered the body.

4.5 Stiffness

The slope of the displacement versus load curves was determined at 5, 15, and 25 kN load levels and plotted against displacement cycle in the following figures. The general trend was a stiffening of the vertebral body with increased loading until a large load was applied causing a drop in stiffness. L5 was the stiffest vertebral body, with a measured stiffness between 37.5 to 60.9 kN/mm. The stiffness measured at the 5 kN level was generally highest followed by the 15 and 25 kN. The L2 and L3 vertebral bodies had lower stiffness ranges (between 15.2 to 35.3, and 21.1 to 38.4 kN/mm respectively). For these two vertebral bodies, the middle 15 kN load level had the highest stiffness, followed by the 5 kN and then the 25 kN levels.

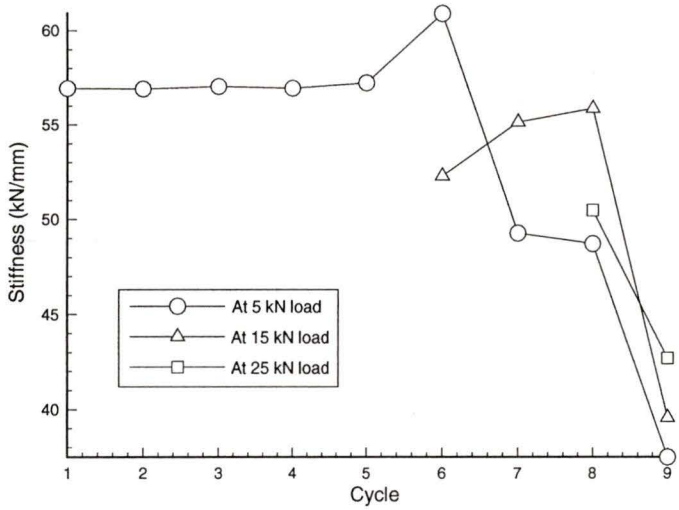

Figure 4-28: L5 Stiffness versus Cycle

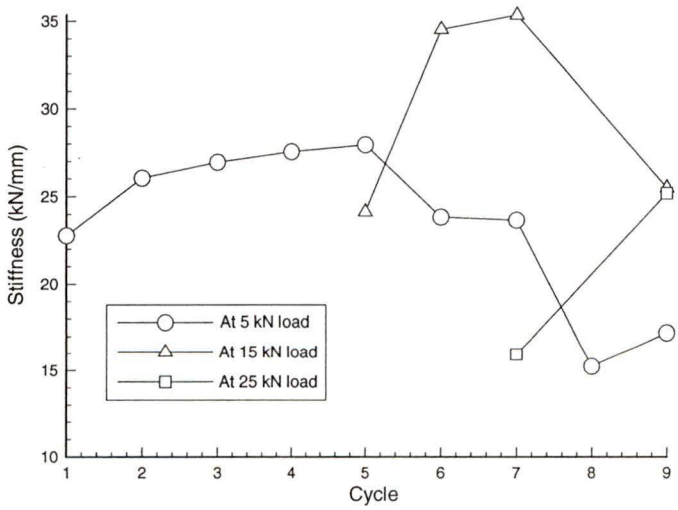

Figure 4-29: L2 Stiffness versus Cycle

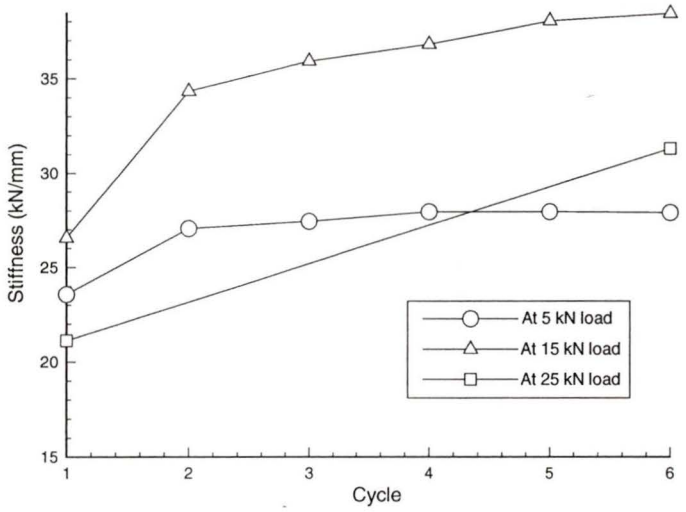

Figure 4-30: L3 Stiffness versus Cycle

4.5.1 Cement Fixation Modulus

In general, the testing of the cement cylindrical samples had a high error. During some of the testing, the extensometer attached to the surface of the cement slipped in position. Though the ends of the cylinders were sanded flat and were relatively parallel, some of the test samples broke in two along the middle of the long loading axis, indicating that the stress on the cylinder was not equal through a cross-section.

Another problem occurred because the cylindrical samples were set to harden in card board molds whereas the cement used with the vertebrae was set in the aluminum test fixture. The cardboard was a much better insulator, keeping more heat in the curing process of the cement when compared to the aluminum container. This influenced the Young's modulus measurements which were made less than two hours after the cement had hardened.

Table 4-4: Young's Modulus for the Cement Samples

Cement Test Sample	Mean Compressive Modulus (GPa)	Standard Deviating for Modulus	Load Range (kN)	Sample Size
L5 #1	7.1	0.4	4-14	13
	8.3	0.3	4-30	2
L5 #2	10.1	0.6	4-16	5
	11.4	0.3	4-37	2
L2 #1	7.2	0.7	4-16	3
L2 #2	20.1	0.8	4-25	1
L3 #1	10.6	0.5	4-25	1
L3 #2	25	1	4-20	1

Though these measurements are not precise, they do provide some information on the loading condition at the surface of the vertebrae. Table 4-4 lists the measured moduli for the two cement samples for each vertebrae. The sample size indicates the number of displacement cycles used for a particular vertebrae. The standard deviation is calculated from the error approximation made during the area measurement and from the standard deviations for the displacement versus load slopes. If only one slope was measured, the standard deviation was calculated from the least squares fit to the line.

The reproducibility of the cement's stiffness was evidently poor, with a range of values between 7.1 and 25 GPa. Assuming that these results are correct, the average modulus (12 GPa) is below the 20 GPa set as a criteria for the cement (see page 21).

How this affects the measured stiffness of the vertebral bodies is not easily determined. Material at the bone/cement interface may undergo different stress

depending on its lateral position. The curved surface of the end-plate further complicates the loading. As an approximation, consider the loading system equated to three springs compressed in series. Also assume that the modulus of the concrete can be related to its stiffness by multiplying by the cross-sectional area of the vertebral body contacted to it, and dividing by the cement's height (~25.4 mm). Then the stiffness of the vertebral body can be corrected by the following formula:

$$K_c = \frac{K_m}{1 - 25.4K_m\left(\frac{1}{E_1A_1} + \frac{1}{E_2A_2}\right)} \tag{4-2}$$

where K_c and K_m are the corrected and measured stiffness, E_1 and E_2 are the cement compressive moduli from Table 4-4, and A_1 and A_2 the bottom and top vertebral body cross-sections in Table 4-1 (except A_2 for L5 which is the average of the two most upper areas). A plot of these relationships for each vertebrae in the domain measured is shown in Figure 4-31. The range of the corrected stiffness is 42-74 kN/mm for L5, 16-39 kN/mm for L2, and 22-41 kN/mm for L3. The correction affects the higher stiffness values to a greater degree than the lower. A more accurate correction will be considered in Section 5 "Model Stiffness Predictions".

4.6 Strength

Ultimate strengths have been included in this study for completeness, but these results are questionable. There is no fixed cross-section on a vertebral body and dividing the ultimate load by some particular cross-section does not give a good indication of the material level stress at failure. Yet, researchers have used the area of the end-plate to calculate a stress

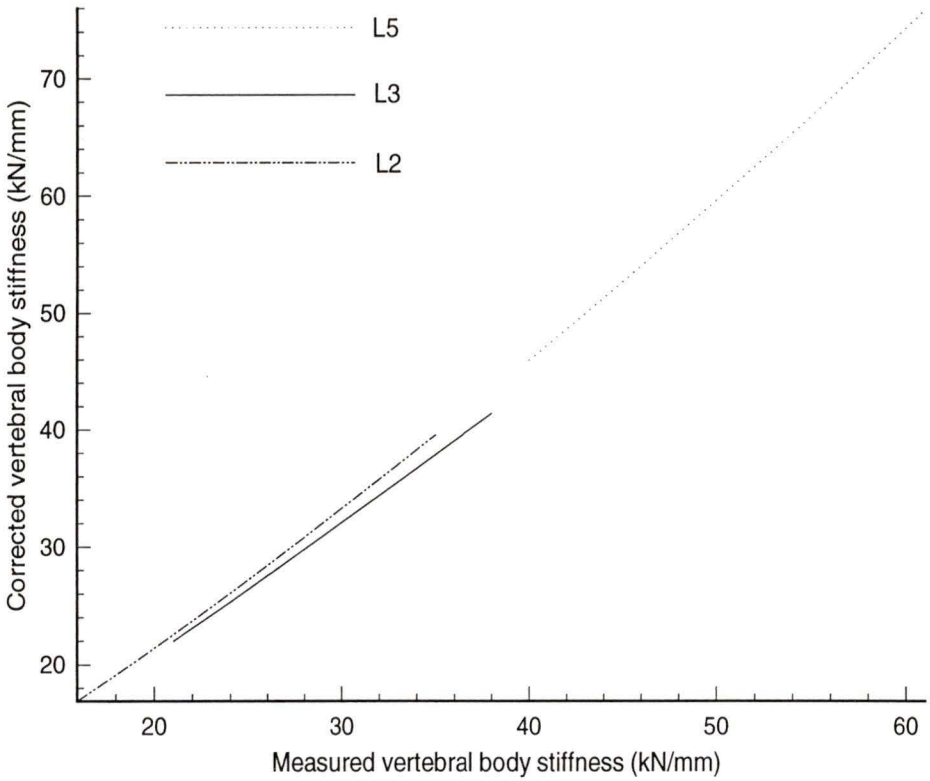

Figure 4-31: Stiffness Correction Due to Cement Fixations

value. A more accurate method would be to use an average area as defined in Section 4.1 "Measured Geometry". The bottom area, which represents the end-plate area, and the average area will both be used in Table 4-5. The ultimate strength calculated from the average area varies less between the vertebral bodies than the strength calculated using the bottom area.

The displacement cycle used during compression testing made measuring ultimate load difficult. The displacement rate was constant throughout a compression cycle, except when the vertebra was to be failed. Then it would be compressed at a constant rate until a certain displacement was reached and the ram would hold at that point. As was seen in the

load and displacement data in Section 4.4 "Compression Testing Data", this holding position was typically below the level required to break the specimen. During the holding position, the vertebral bodies went through a relaxation. Therefore, the values shown in Table 4-5 do not accurately represent the ultimate load at 0.0847 mm/sec. This is especially true in the case of the L3 vertebral body. As seen in Table 4-5, the vertebral bodies had increased ultimate load with position along the spine (i.e. L5 had the greatest ultimate load, and L2 had the lowest).

Table 4-5: Measured Vertebral Body Ultimate Load and Ultimate Strength

Vertebral Body	Ultimate Load (kN)	Bottom Cross-Section		Average Cross-Section	
		Area (mm^2)	Ultimate Strength (MPa)	Area (mm^2)	Ultimate Strength (MPa)
L2	34	1728	19.7	1453	23.4
L3	37	1988	18.6	1574	23.5
L5	45	2396	18.8	1881	23.9

4.7 Vertebral Body Strength Predictions Based on Trabecular Bone Strength

In section 4.3, empirical relationships from Rice et al. [107] were used to predict the modulus of trabecular bone from apparent density; Rice et al. also derived empirical relationships for trabecular bone strength. Assuming that the failure of the vertebral bodies is due to the failure of trabecular bone, there should be a close correlation between vertebral strength and trabecular bone strength.

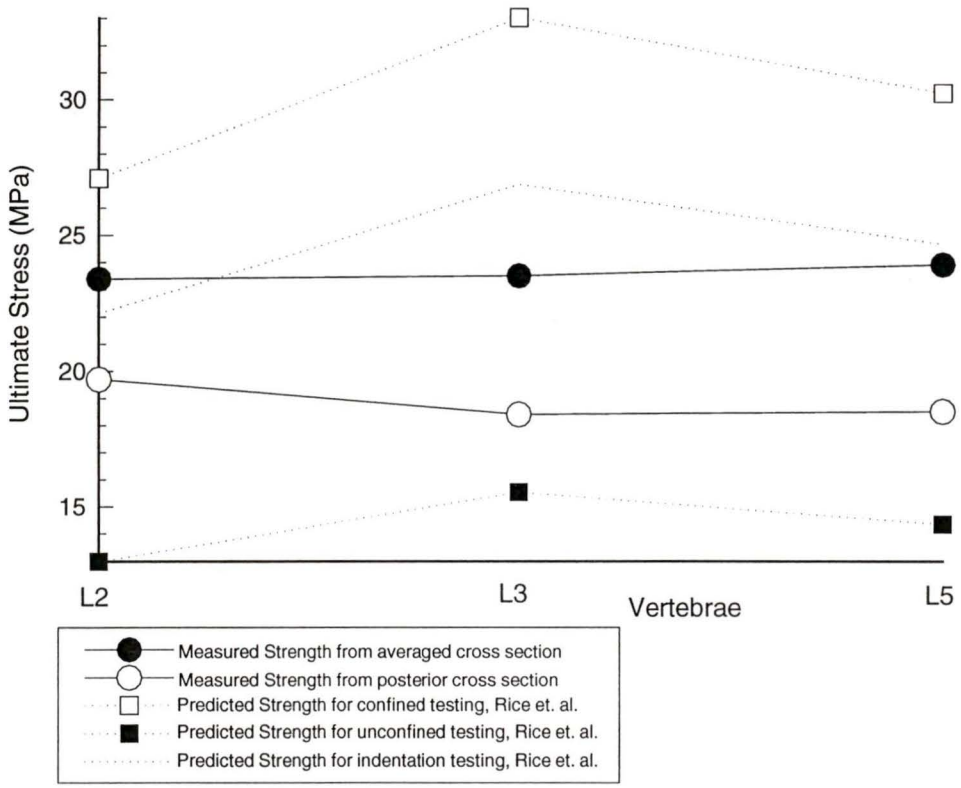

Figure 4-32: Comparison between Predicted Trabecular Bone Strength and Measured Vertebral Body Strength for the Bovine Specimens

To investigate this hypothesis, the predicted strength of trabecular bone is plotted with the measured strength of the bovine vertebral bodies. The three predicted strengths are based on compression tests using three methods: confined specimens, unconfined specimens, or indentation tests. As with the modulus predictions, the predictive formulas must be corrected for strain rate; the formulas for the strength (in MPa) of bovine

longitudinal specimens, normalized to 0.01 s^{-1}, are:

$$\begin{aligned} &\text{Confined:} && 2.45 + 63.05\rho^2 \\ &\text{Unconfined:} && 2.45 + 27.35\rho^2 \\ &\text{Indentation:} && 2.45 + 50.51\rho^2 \end{aligned} \tag{4-3}$$

Rice et al. [107] claimed that the quadratic strength model could explain 72.8% of the variance in strength and had a standard error of estimate of 3.80. (The complete model included both human and bovine data).

The measured vertebral body strengths lie between the different strength values predicted from the three trabecular bone testing methods. The stiffer outer shell of a vertebral body should act to partly confine the trabecular bone. Only the end surfaces are confined during trabecular bone testing. During vertebral testing, the lateral surface of a trabecular material element is constrained by the cortical and trabecular bone around it, thereby increasing local stress. This loading condition partly accounts for the lower strength of the vertebral bodies compared to the confined compression strength of bovine trabecular bone.

This same comparison has been made for human vertebral bodies and trabecular bone by Hansson et al. [100]. These authors plotted strengths of human lumbar trabecular bone and intact human lumbar vertebral bodies against bone mineral content (BMC) and found similar linear relationships for the two. The BMC of vertebrae measures the density of both the trabeculae and the cortical shell, thus better representing the vertebral structure than apparent density of trabecular bone as used in this study. Bell et al. [139] have also related vertebral strength to vertebral ash density, finding a power law relationship.

5 Model Stiffness Predictions

The shape and structure of the vertebral body made material testing difficult, and complicates modelling even more so. FEM bone model results are sensitive to modelling assumptions [48], [147]. Following a discussion of the simplifying assumptions for the bovine models, the results of three stiffness predictions are presented and compared to the material testing results. Finally the sensitivity of the model to various parameters is analyzed.

5.1 Initial Modelling Assumptions

5.1.1 Geometry

The highly curved surface of the vertebral body is approximated by the models. Assumptions must also be made about the inner structure of the body. The cortical shell thickness could not be measured accurately and hence only a single approximate thickness is used over the entire surface. The end-plate, made of an intermediate between trabecular and cortical bone, is not modelled at all as its dimensions could not be accurately measured and its material properties are not known.

5.1.2 Material Properties

Both cortical and trabecular bone are modelled as linear isotropic materials. Though this approximation is far from the truth, accurate values for more complex properties are not available for both bovine and human cortical bone [18]. Trabecular bone's density is the

key factor in the determination of strength and stiffness in osteoporosis, and the correlations of trabecular bone to density have only been made for Young's modulus. Hence, the isotropic model must suffice for trabecular bone.

The difficulty in choosing technical moduli for the models is illustrated in Table 5-1 which compares constants used for cortical bone in two human vertebral body models. Surprisingly, the same constants for the trabecular core and the end-plate were used in both models. Ueno and Liu [47] justified the low values for the cortical shell by claiming the shell is a mixture of both cortical and trabecular bone. Though their assumption is reasonable, it is not quantifiable so the models of the bovine vertebrae will use an average value for Young's modulus for bovine cortical bone as listed by Cowin [18].

Table 5-1: Comparison Between Two Human Vertebral Models' Choice of Cortical Technical Moduli

		Dietrich et al. [46]	Ueno and Liu [47]
Cortical Shell technical moduli	E_x, E_y (GPa)	11.3	0.7
	E_z (GPa)	22	1
	G_{xz},G_{yz} (GPa)	5.4	0.24
	G_{xy} (GPa)	3.8	0.24
	ν_{xz}, ν_{yz}	0.203	0.315
	ν_{xy}	0.45	0.484

Poisson's ratio for the cortical shell was equally difficult to determine accurately. The Poisson's ratios listed by Cowin [18] for cortical bone varied by as much as 0.2 between different experimental tests, but most were centered near 0.3.

Table 5-2: Poisson's Ratio for Trabecular Bone in the Human Lumbar Spine (adapted from [67])

Study	Sample size	Donor's age	Poisson's ratio
Yahia et al. [146]	30	25-35	0.301 (± 0.270)* 0.521 (± 0.443)
McElhaney [74]	28	45-79	0.14 (± 0.09)
Synder [148]	12	62-81	0.110 (± 0.087)* 0.952 (± 1.286) -0.372 - 4.602†

*The maximum and minimum mean values (standard deviation in parentheses) is listed when all six Poisson's ratios were found.
†Range is reported when available.

Few experiments have been conducted on the Poisson's ratio of trabecular bone, but the results suggest the ratio is highly variable (Table 5-2). Based on the rod and beam structure of trabecular bone, the ratio is likely dependent on density. Note that Poisson's ratio was measured negative and above four, while homogeneous materials have a range between zero and one half. Similar values for Poisson's ratio have been detected in other cellular solids [118]. The material constants used in the FEM models are listed in Table 5-3; the trabecular Poisson's ratio is assumed to be 0.3.

For osteoporosis prediction, the regional variation of density and modulus in the trabecular bone is an important consideration. As domestic animals do not reach old age, the bovine vertebral bodies in this study are not osteoporotic. The trabecular structure was dense in all regions compared to human specimens, so regional variation was not considered.

Table 5-3: Material Constants Used for Stiffness Predictions

Property		L5	L2	L3
Trabecular Bone	Young's modulus (GPa)	1.176	1.047	1.296
	Poisson's ratio	0.3	0.3	0.3
Cortical Bone	Young's modulus (GPa)	20.7	20.7	20.7
	Poisson's ratio	0.3	0.3	0.3
	Shell thickness (mm)	1.23	1.14	1.67
Dimensions	Height (mm)	69.5	72	72
	Average cross section-area (mm^2)	1881	1453	1574
Cement Fixing Agent	Top Young's modulus (GPa)	10.1	20.1	25
	Bottom Young's modulus (GPa)	7.1	7.2	10.6
	Poisson's ratio	0.18	0.18	0.18

Though trabecular bone is a two phase, porous structure composed of bone and marrow fluid in the pores, the fluid phase was not considered by using the empirical correlation of density to Young's modulus. Previous work has shown the fluid phase to affect only the higher strain rates [26], and the trabecular modulus value was corrected for strain rate through the 0.06 power law.

5.1.3 FEM Modelling

The FEM models use a linear equation solver. Hence geometric non-linearities, as can occur in a buckling failure, were not included. This study is preliminary and considers only the elastic range of the vertebral body, so at this stage nonlinear modelling is not necessary.

A simple boundary condition, or method of applying load, is considered in these models. The nodes on the end-plate surfaces of the body are constrained in all displacements and rotations, except for a specified inward displacement at one end causing the compression. This confined loading will induce a barreling effect, as the ends cannot expand during the compression. During the compression tests, the cement held the ends relatively fixed so this is a justified approximation. One model will include the cement fixation cylinders and will be used to confirm this assumption. The direction of loading was assumed to be along the longitudinal axis of the vertebral body.

All FEM models were built using the ANSYS® 5.0 software package from Swanson Analysis Inc., and run on Sparcstation ELC computer hardware from Sun Microsystems Inc. The solution procedure is based on the displacement formulation using iso-parametric elements. Three element types were used for all the FEM models: a shell element for the cortical bone, and two types of volume elements for trabecular bone.

The SHELL63 element [149] was used for the cortical bone because the outer cortical shell is thin compared to the vertebral body thickness. This is a classical shell element with well known behavior and is well tested. The element has both bending and membrane capabilities and permits both in-plane and normal loads. The element is usually defined by four nodes, but has the option to be triangular. Though the element should lie in a flat plane, small out-of-plane tolerance is permitted and is corrected by a warping factor.

For simple geometries, a SOLID45 3-D 8 node brick element was used for trabecular bone which uses linear shape functions. For more complex geometries, a SOLID92 3-D

10 node tetrahedral element was used. It has a quadratic displacement behavior with midside nodes.

These elements were chosen over other available elements for the following reasons. They can be used with the ANSYS® mesh generation algorithms. By allowing the software to mesh the FEM grid, a source for human error was eliminated and the model creation time was substantially decreased. These elements also proved to be efficient in keeping the size of the model small, an advantage because the ANSYS® package available for this work had a restriction on the size of the model it could run.

5.2 Modelling Progression

5.2.1 L5 FEM Model

After acquiring the digitized surface data using the techniques described in Appendix B, the surface points were input as keypoints. The keypoints were linked to lines generated between them; the lines were used to generate areas, and the areas generated a volume. The volume was described by 322 keypoints, 525 areas, and 834 lines (all generated manually). Due to the irregularity of the keypoint positions and their number, an efficient FEM model could not be built directly from this data. (Figure 5-1 depicts the volume.)

To simplify the surface while maintaining most of its shape, four cross-sections along the longitudinal axis were used to generate a "cross-section model". A new volume was generated with lines and areas between these cross-sections. Surfaces between these sections were linearly approximated.

Figure 5-2 depicts the surface approximation used for the cross-section models. The outer dotted line represents the maximum outer dimensions of the vertebral body viewed

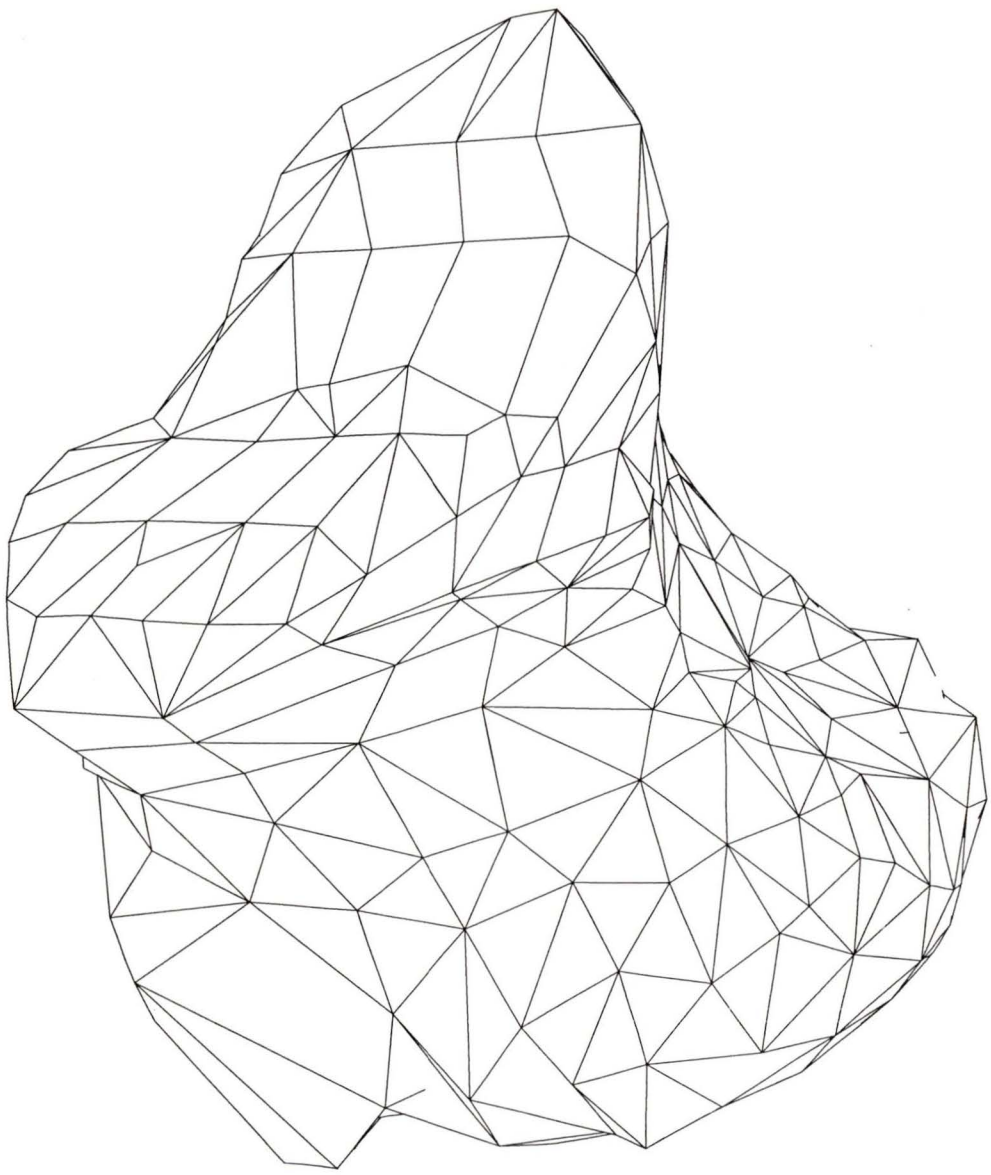

Figure 5-1: Surface Generated from Digitized L5 Point Data

laterally. To incorporate the entire height of the body into the model, the upper and lower cross-sections were moved along the longitudinal axis. The model's geometry was adjusted in this way to maintain the original volume of 131 cm^3 as measured from the data in Figure 5-1. The effect was to plane the top and bottom surfaces without drastically

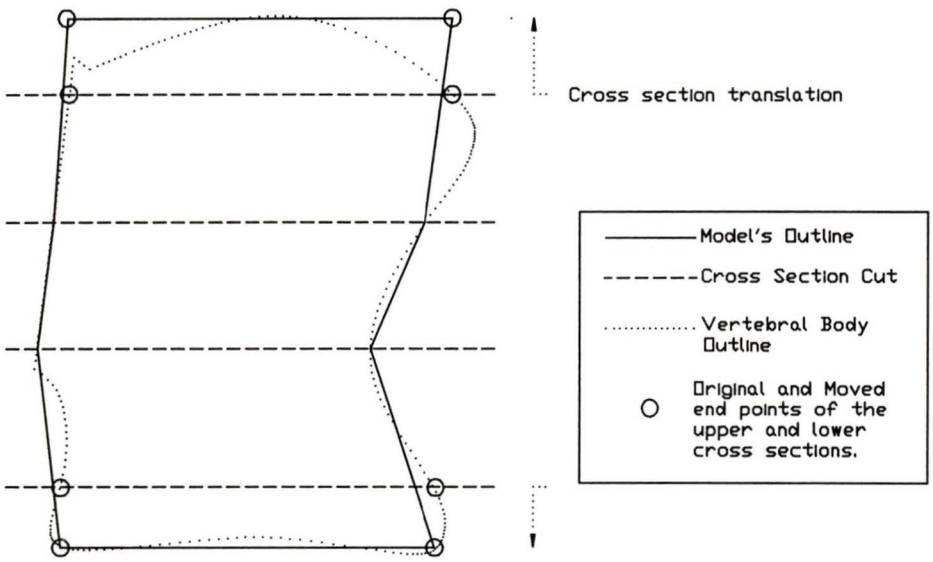

Figure 5-2: Manipulation of Cross-Sectional Longitudinal Position for Modelling

changing the height or width.

The cross-section model for L5 is shown in Figure 5-3. Information on the nodes and elements used in the model are listed in Table 5-4 on page 75 with the other models. The elements seen on the top and bottom surfaces are tetrahedral volume elements and the elements seen on the front and back surfaces are shell elements. The nodes and elements were generated automatically after an element size was specified. Two features are not present on the model: the curvature in the end-plates on the top and bottom surfaces, and the end of one cut, which was made to remove the pedicle.

5.2.2 FEM Cross-Section Models for L2 and L3

For L2 and L3, a similar technique to the one used for L5 was employed in order to form the cross-section models, except the traced cross-sections described in section 3.3 and section 4.1 were used. Because the vertebral bodies were cut during the measurement, the

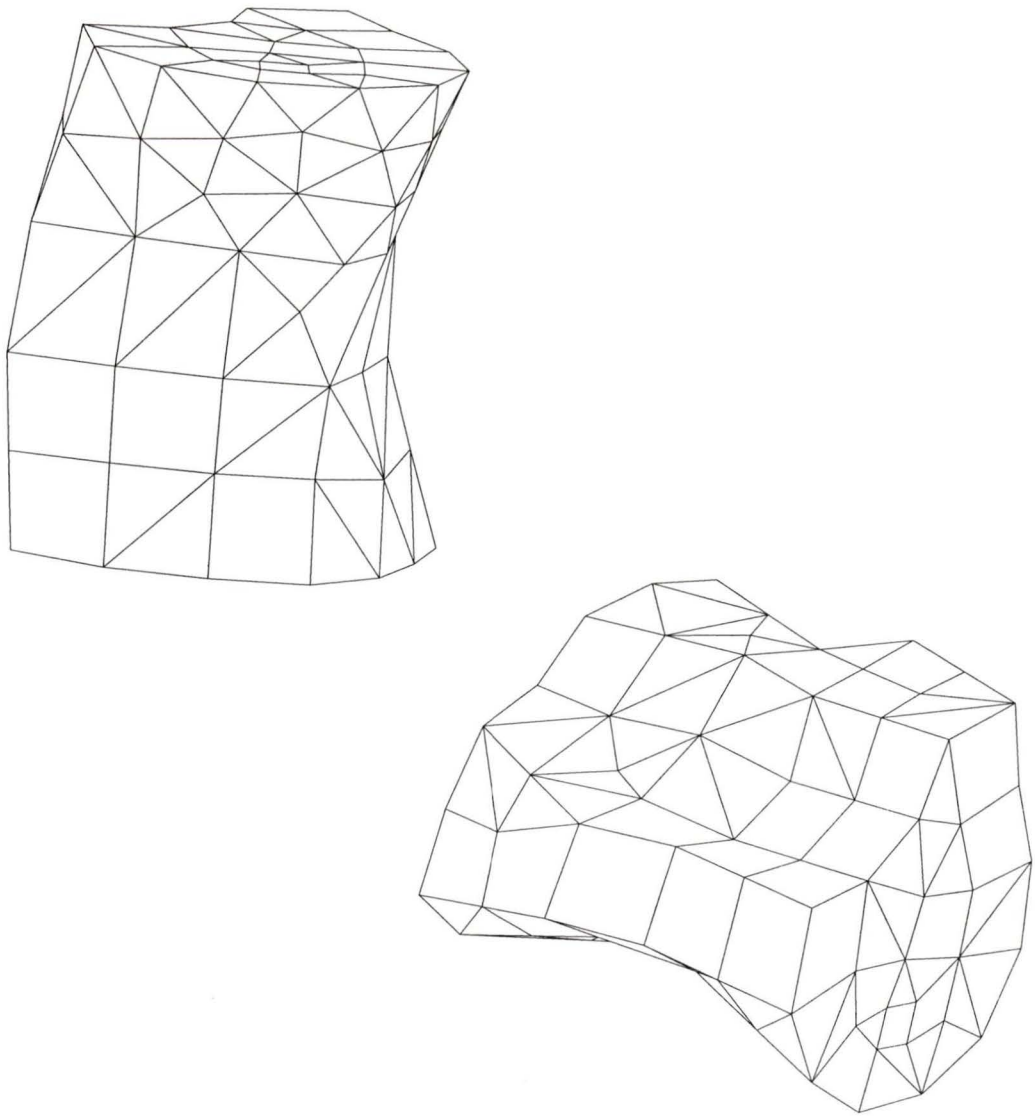

Figure 5-3: Cross-Section Model for L5

exact placement of the four cross-sections with respect to each other was not known. In order to assemble the cross-sections into a volume for the FEM model, assumptions were made about the placement based on the intact shape of the body.

It was assumed that the small projection in the middle of the back surface formed a straight line along the longitudinal axis, and the sharp bend in the middle of the front

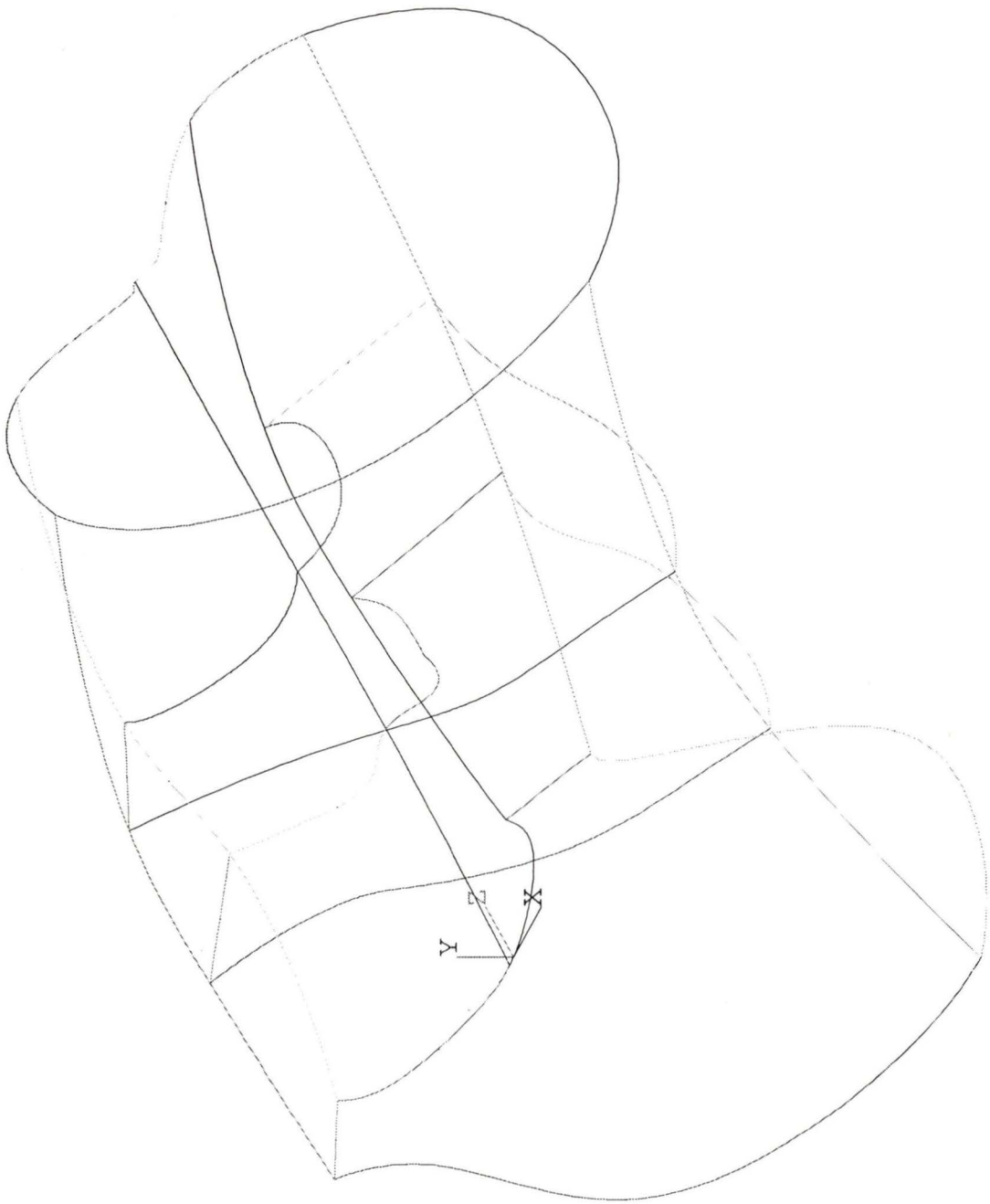

Figure 5-4: Volume Generated for the L3 Cross-Section Model

surface was situated directly forward to this line. To align the cross-sections with respect to these assumed lines, the cross-sections were rotated. Figure 5-4 shows the lines and cross-sections used to generate the L3 model. The line originating from the origin and

moving up the z -axis was assumed to contain the sharp change on the perimeter of the back surface for each cross-section. The light dotted line that connects the sharp change on the front side of the cross-section is situated on the negative side of the y axis. This line lies in the y-z plane. The model's geometry is simplistic, yet it includes the main features of the vertebral body. As with the L5 model, the curvature of the end-plate is not modelled. Also a definitive end to the cuts which removed the pedicles is not modelled.

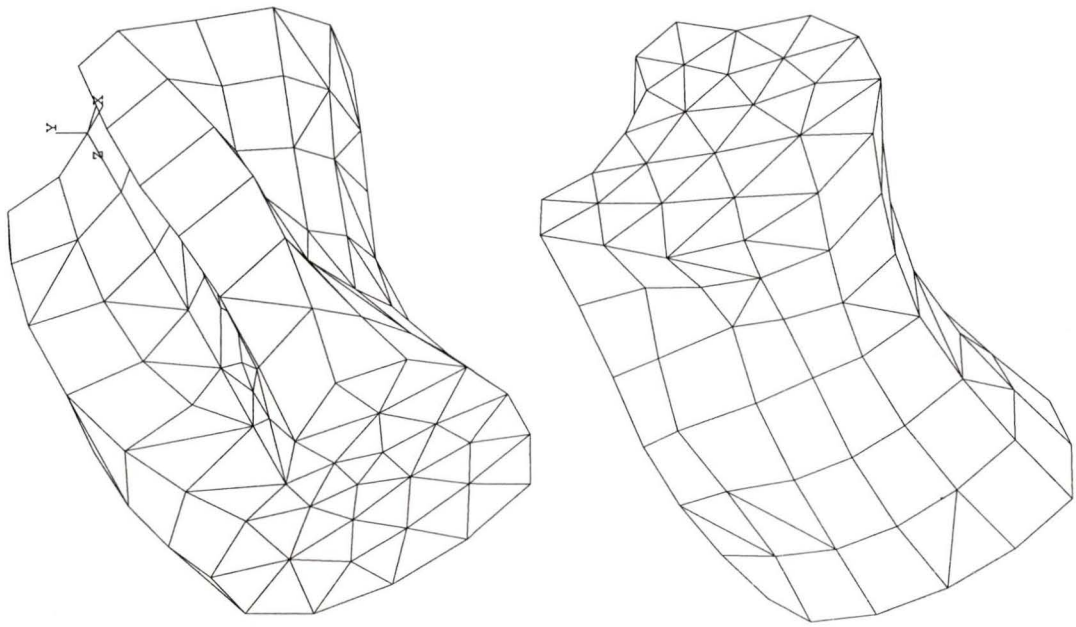

Figure 5-5: L2 Cross-Section Model

The longitudinal position of each cross-section was determined by the height where the cross-section was taken. The two end cross-sections were adjusted, as for L5, so the entire height of the vertebral body was modelled. The volumes of the L2 and L3 vertebral bodies were not known.

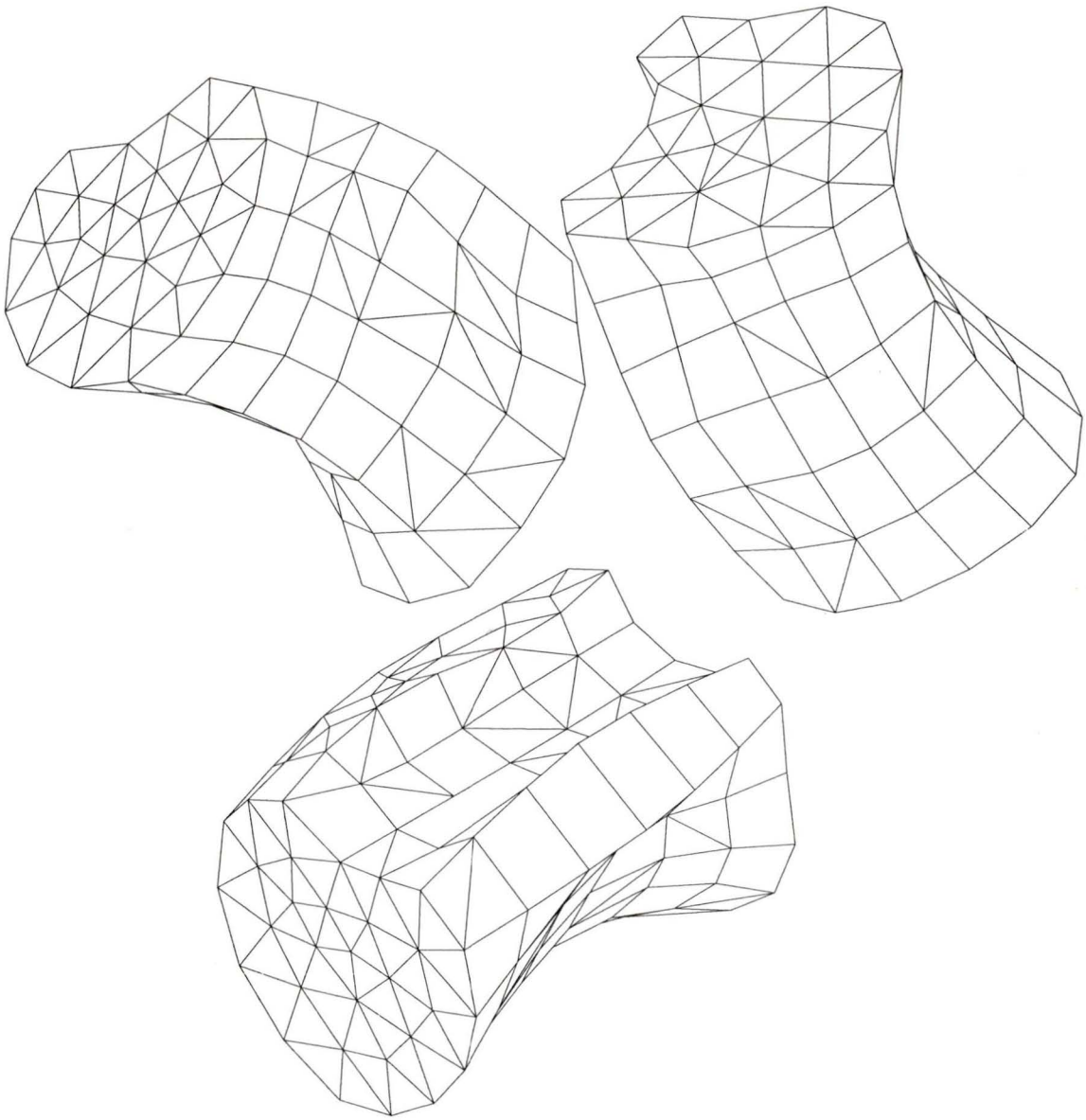

Figure 5-6: L3 Cross-Section Model

Plots of the L2 and L3 cross-section models are shown in Figure 5-5 and Figure 5-6. As the models for L2 and L3 were built using the same techniques, the number of generated elements and nodes are similar, as seen in Table 5-4.

5.2.3 FEM Cylinder Models

The cross-section models are relatively large and complex which makes checking their results difficult. A simpler model was built to compare and validate the cross-section models. Instead of using the complex geometry of the vertebral body, a cylinder surrounded with a stiff shell was used.

The cylinder used the height from the cross-section model and average cross-sectional area in Table 4-1 to determine a radius. A quarter of the cylinder was modelled by using symmetry as shown in Figure 5-7. Shell elements were used on the outer cylindrical wall

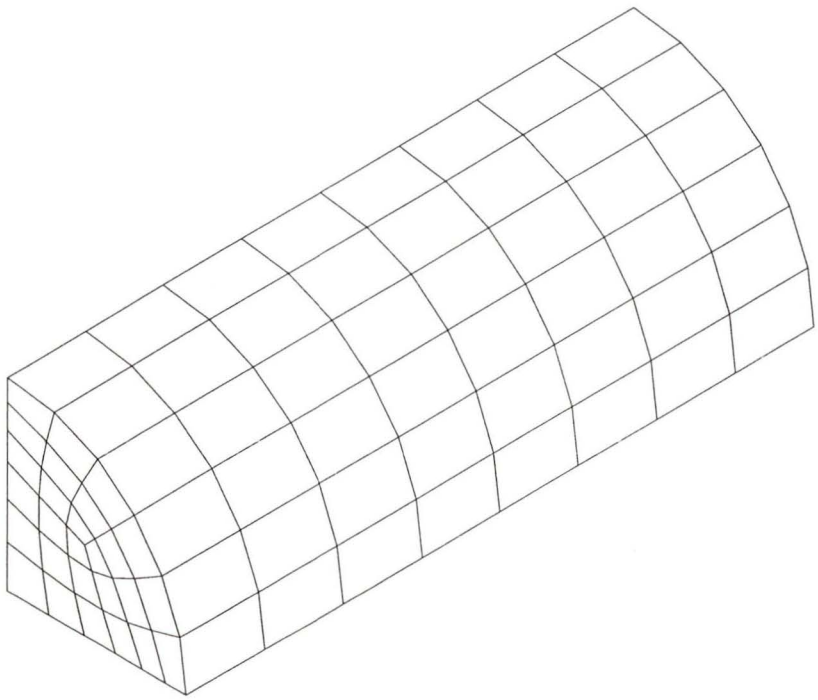

Figure 5-7: Cylinder Model for L3

to represent cortical bone, and 8-node brick elements are used to represent the interior trabecular bone. The model is parameterized; it can be used for all three vertebral bodies by changing the parameters for Young's modulus, shell thickness, height, and radius.

Before being used for the vertebral body models, the cylindrical FEM model was tested with more complex 8-node shell elements, and with a higher element resolution. The increased complexity of the model did not change its stiffness results significantly, providing confidence in the element resolution.

5.2.4 Modulus Summation Stiffness Prediction

The cylindrical model stimulated the formulation of an even simpler prediction of stiffness. It is included here as it can be compared to the cylindrical and cross-section models, and gives an indication of the accuracy of the more complex predictions.

The prediction assumes the stiffness of the vertebral body is the sum of the cortical and trabecular bone stiffness. A summation of cortical and trabecular moduli (E_c, E_{tb}) adjusted for the portion of the cross-sectional area covered by trabecular (A_{tb}) and outer cortical (A_c) bone was used as:

$$k = \left[E_{tb}A_{tb} + E_cA_c\right]/h \tag{5-1}$$

where k and h are the stiffness and height of the vertebral body respectively. The cross-sectional areas above can be related to the overall cross-sectional area (A) and cortical thickness (t_c) by assuming a cylindrical shell arrangement:

$$A_c = A - A_{tb}$$
$$A_{tb} = \left(\sqrt{A} - t_c\sqrt{\pi}\right)^2 \tag{5-2}$$

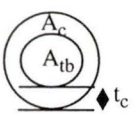

By substituting A_c and A_{tb} from Equation 5-2 into Equation 5-1, an algebraic prediction for stiffness is formed, dependent on three geometric variables (A, h, and t_c) and two material variables (E_{tb} and E_c).

5.2.5 Modelling of the Cement and Vertebral Body

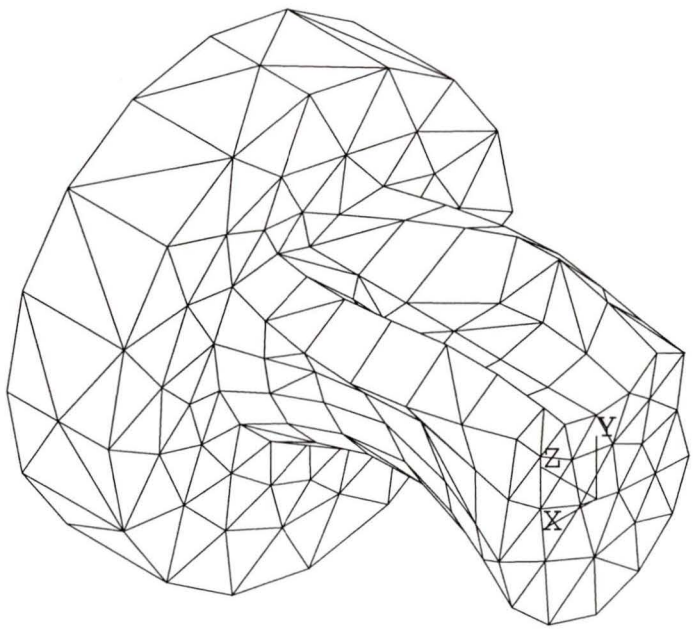

Figure 5-8: Cement Disk and L2 Vertebral Model

To better model the loading on the ends of the body, the stiffness of the cement fixation must be considered. There are a variety of ways which this can be done. The measured stiffness of the vertebral bodies could be corrected for the effect of the concrete using Equation 4-2, based on springs in series. Alternatively, the Airy stress function for cylindrical symmetry could be used for three contacted mediums (two concretes and the vertebral body), but this would require iteratively matching the boundary conditions of the stress functions in each medium until a solution is found. An easier way is to use FEM.

Two cement disks were added to the cross-section model for L2. Only one is shown in Figure 5-8 to provide an unobstructed view. The nodes on the surface of the cement disks,

Table 5-4: Size and Components of the FEM Models

Model		Shell Elements (type shell63)	Volume Elements		Nodes	DOF	Wave -front
			type	number			
Cross-section	L5	91	solid92	420	542	1611	308
	L2	100		598	788	2148	389
	L3	110		609	809	2184	374
Cylinder for L5, L2, and L3		48	solid45	216	333	798	147
L2 cross-section with cement ends		100	solid92 bone cement 1 cement 2	 598 615 642	2795	7371	659

which would contact with the aluminium cups, will be constrained. At one end, the nodes are assigned zero values for all degrees of freedom; at the other end, only the z displacement is given a non-negative value to apply a compression. As can be seen in Table 5-4, adding the cement disks greatly increases the size of the model.

5.3 Results with Comparisons to Experimentally Measured Stiffness

In general, all models predicted a higher stiffness than the material tests indicated (see Figure 5-14). The following section will analyze the model results, compare them to the material tests, and indicate reasons for this discrepancy.

5.3.1 Cylinder Model and the Loading of the Cortical Shell

As the results from the cylindrical model are easier to visualize, plots of the stress and displacement have been produced for them. Figure 5-9 depicts the deformed and

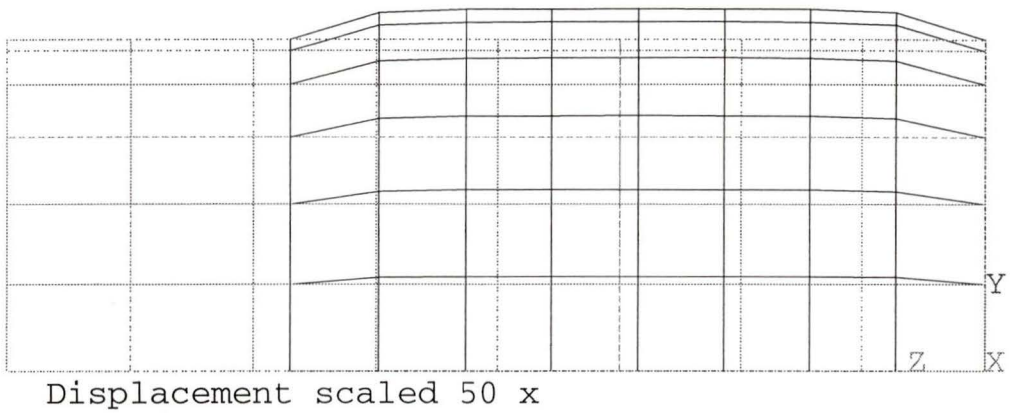

Figure 5-9: Deformed Shape of the L5 Cylinder Model

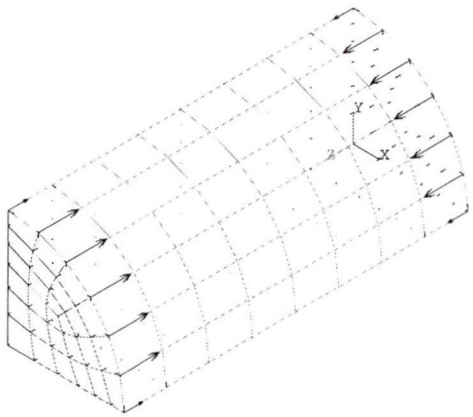

Figure 5-10: Reaction Forces on the L5 Cylinder Model

undeformed shape of the cylinder model. Here the effect of constraining the displacements at the ends can be seen as the shape becomes barreled after deformation. More interesting is Figure 5-10 which indicates the boundary forces at these constrained nodes as indicated by arrows. The forces on the shell elements are far greater than those on the brick elements. The smaller force seen on the corner shell nodes is due the symmetry condition. As the cortical shell has a much higher modulus and the displacement is constant on the ends, the shell element takes a great percentage of the

loading. Though the cement fixation constrain the ends somewhat, the large forces in the shell may indicate the need for a more realistic boundary condition.

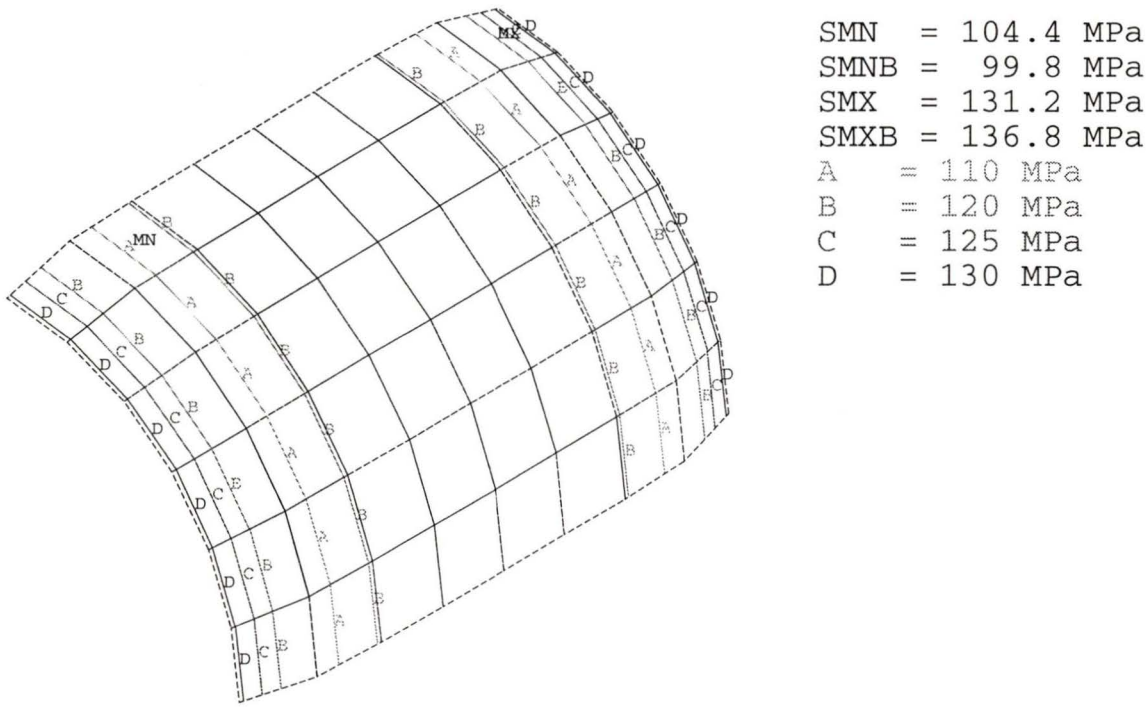

Figure 5-11: Von Mises Stress Contour Plot for the Shell Elements of the L5 Cylinder Model

A contour plot of the Von Mises stresses in the shell elements is shown in Figure 5-11. The SMN and SMX correspond to the maximum and minimum stress calculated in the elements and plotted on the contours as MN and MX. SMNB and SMXB are lower and upper bounds on SMN and SMX, considering the effect of discretization error. Close values between the bounds and the extrema indicate sufficient grid resolution. Due to the end constraints, the maximum stress values occur near the ends. The stress in the center is relatively constant.

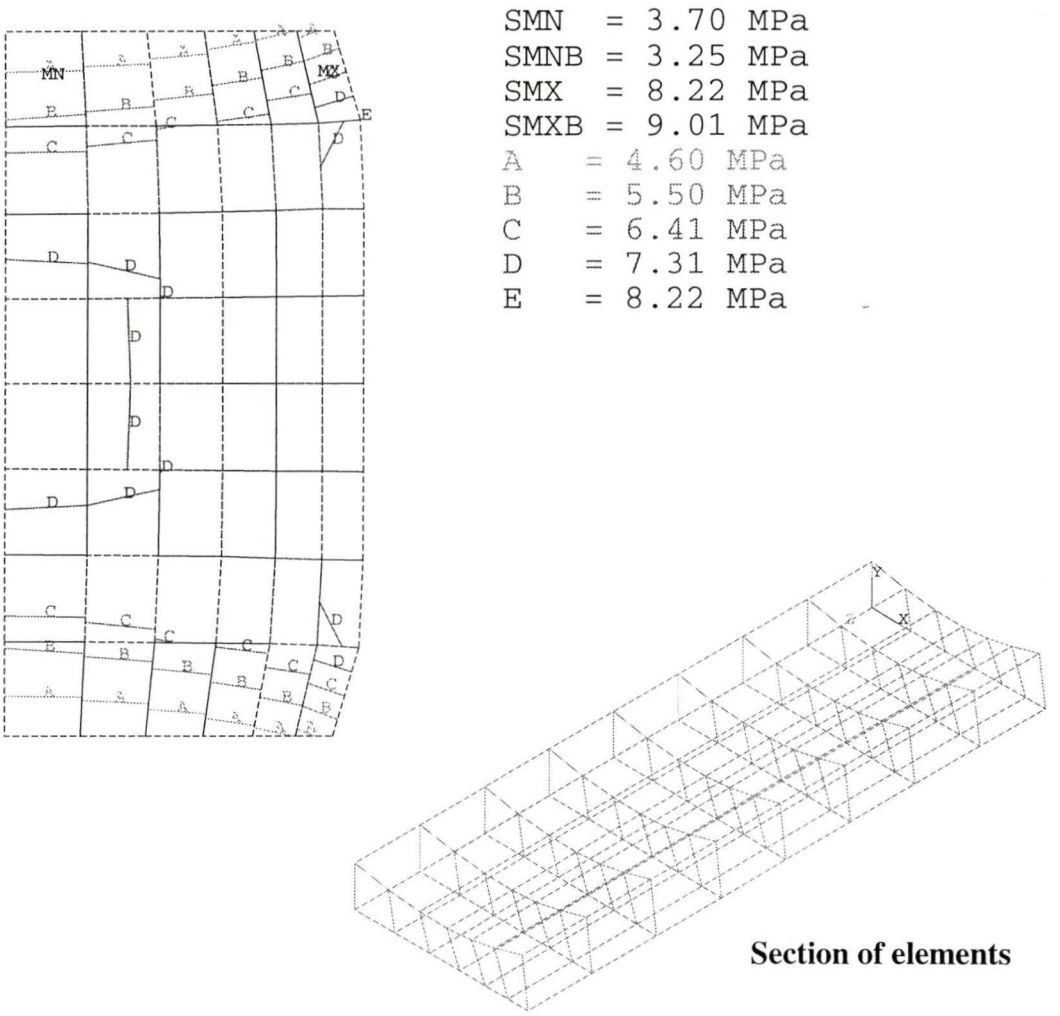

Figure 5-12: Von Mises Stress Contour Plot for a Section of Volume Elements in the L5 Cylinder Model

A similar plot for the trabecular elements indicates a drastic reduction in the stress magnitude. Figure 5-12 confirms that the cortical shell is taking a greater share of the applied load. The contours are taken through a section of the trabecular elements along the x-z plane. Again, the maximum value is near the ends and closer to where the surface begins to barrel out. In general, the center has higher stress than the ends and the surface, where the shell elements share more of the load.

5.3.2 The Loading of the L2 Cross-Section Model with Cement Disks

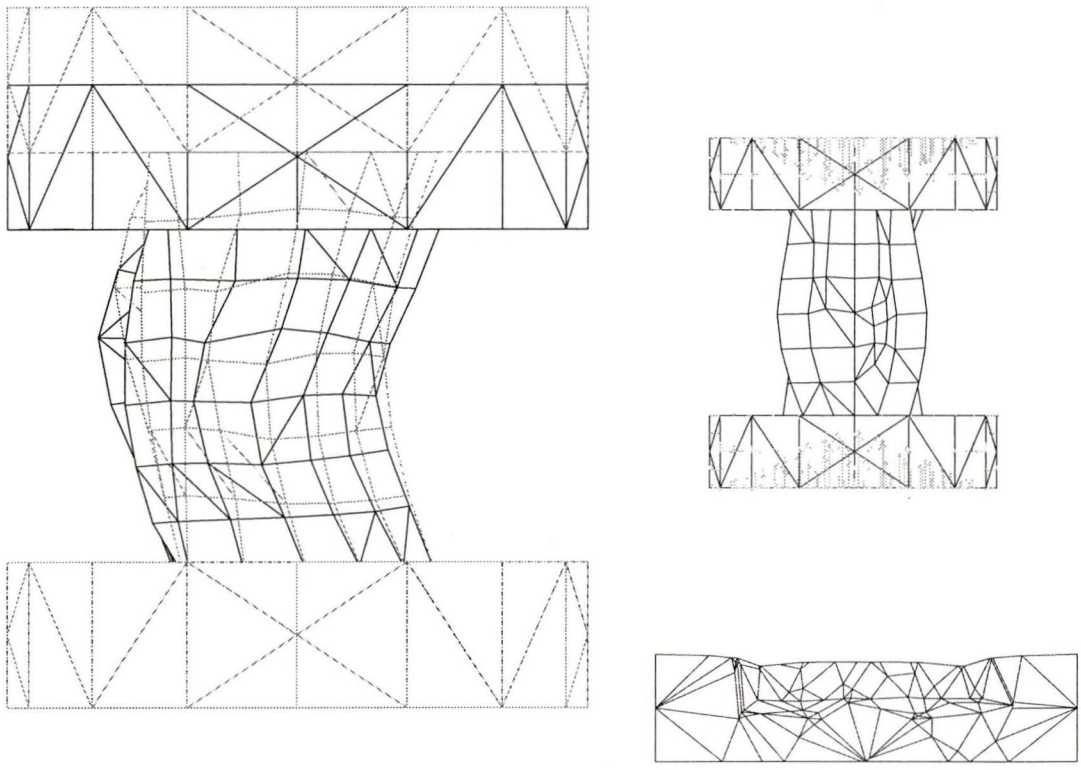

Figure 5-13: L2 Cross-Section Model with Cement Ends

In contrast to the simple cylindrical model, when the cement disks are included in the cross-section model, the boundary loading becomes more complex as shown in Figure 5-13. On the left hand side of the plot, the deformed and undeformed shape is shown with the deformed shape scaled up by about 30 times. The small lateral displacement in the center indicates that some 'buckling like' behavior has occurred. The top right figure displays the calculated boundary forces on the cement surface nodes. The force is centered in the middle of the vertebrae and trails off laterally. The lower right figure displays the deformed cement node shapes, scaled to 100 times. The figure is a cut

through the center of the disk and shows the various tetrahedral elements on one side as they would look if transparent. The shell of the vertebral body did not indent as much as the trabecular middle, causing less deformation in the middle of the top cement surface.

The difference in boundary loading proved to be of little consequence to the stiffness of the models. The L2/cement model predicted a stiffness of 49.5 kN/mm. For comparison, the L2 cross-section model's stiffness was adjusted by adding the cement stiffness through the relationships in Equation 4-2. A stiffness of 49.4 kN/mm was obtained. If these models were to be used for strength predictions, the boundary loading conditions would be of greater importance as different conditions can produce substantially different localized stress, but in accordance with Saint Venant's principle, the boundary conditions did not affect the overall stiffness properties.

5.3.3 Increased Grid Resolution for the Cross-Section Models

Table 5-5: Increased Grid Resolution for the Cross-Section Models*

Cross-Section Model	L5	L2	L3
Shell Element Number	123 (91)	151 (100)	148 (110)
Volume Element Number	616 (420)	1458 (598)	1015 (609)
Nodes	786 (542)	1947 (788)	1355 (809)
DOF	2394 (1161)	5481 (2148)	3696 (2184)
Wave-front	359 (308)	599 (389)	548 (374)
Stiffness Prediction (kN/mm)	65.2 (61.5)	61.0 (57.0)	94.3 (91.9)

* Original value for the model given in brackets

Increasing the resolution of the FEM grid is a standard technique to determine the accuracy of the predicted displacements and stress. The cross-section model for each

vertebral body was regenerated with a smaller specified element size. These larger models are compared to the original cross-section models in Table 5-5. By increasing the resolution of the model, an increase in stiffness was predicted. The percent difference between the original and new stiffness prediction was between 2.6% and 6.4%.

5.3.4 Lower Constants for the Cross-Section Models

All stiffness predictions were higher than the measured values. This may have been a result of overlooking the stiffness of the components in the load train, such as the aluminium cups. Other consistent experimental error such as a slippage in the extensometer attachments could also have caused error. But the discrepancy likely occurred in the measurement of the material constants and geometry of the trabecular and cortical bone.

To investigate this possibility, lower constants were used in the cross-section models. These constants (in Table 5-6) correspond to a standard deviation less than the mean of the Young's modulus for trabecular bone and cortical shell thickness measured. The cortical Young's modulus is set to the lowest value measured for bovine cortical bone, according to the review by Cowin [18]. These models produced much lower stiffness predictions.

Table 5-6: Lower Constants Used for Stiffness Predictions

Property		L5	L2	L3
Trabecular Bone	Young's modulus (GPa)	0.954	0.860	0.937
Cortical Bone	Young's modulus (GPa)	18.1	18.1	18.1
	Shell thickness (mm)	0.53	0.64	1.07

5.3.5 Stiffness Predictions Compared to Material Test Measurements

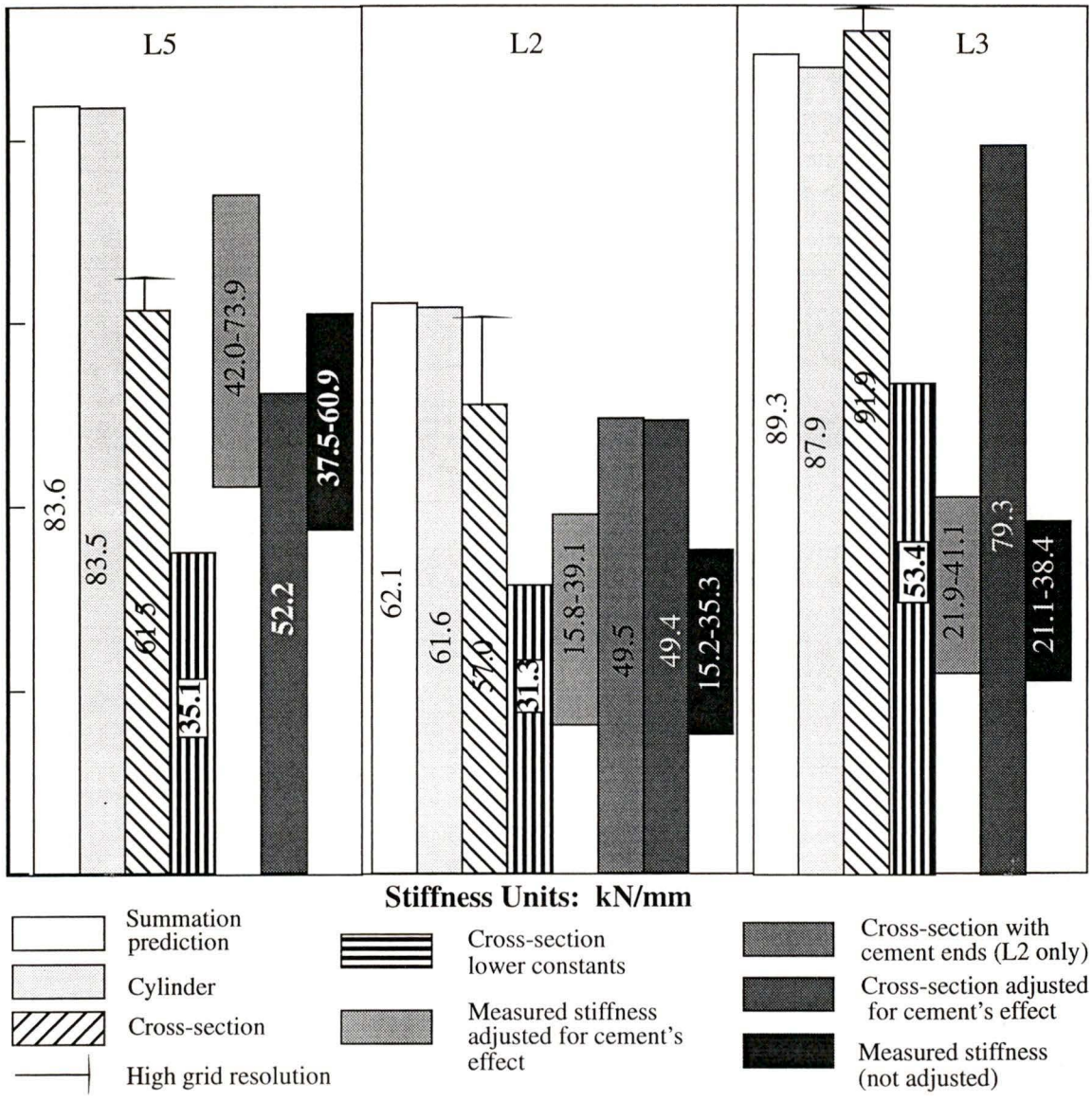

Figure 5-14: Stiffness Predictions from the Various Models Compared to Experimental Measurement

The stiffness predictions from the various models are shown in the bar graphs in Figure 5-14. The number inside each bar is the stiffness in kN/mm. The two smaller off-axis bars represent the ranges of stiffness determined from the material tests. The lighter off-axis bar has been adjusted by Equation 4-2 to remove the stiffness of the cement

fixation from the experimental results. For comparison, the cross-section models were also adjusted to include the cement stiffness using the same relationship, and the results are shown in the second darkest bars. The line segments above the cross-section bar show the stiffness predictions when the grid resolution was increased for these models. The models, which predicted the stiffness shown by the bars in the graph, are listed underneath.

The summation stiffness prediction and the cylindrical model's prediction were similar for all the vertebral bodies. The L5 cross-section model predicted a stiffness within the range experimentally measured by using the mean values of the measured material parameters. Using the lower valued parameters, the L2 cross-section model also compared favorably to the material testing results.

6 Discussion

6.1 Material Tests

The material results indicated that bovine vertebral bodies have denser trabecular bone and a higher stiffness than human bodies, as would be expected in a larger heavier, animal (see Appendix C for a detailed comparison to human vertebral bodies). But the measurements were not precise enough for the FEM models to consistently predict stiffness.

6.1.1 Shell Thickness

The end-plates were not only the thickest region, they were also the most variable. As force is transferred through the semi-fluid disk below the end-plate, this thickness has structural significance. Previous work has been done in humans to investigate the deformation [140] and the regional stiffness [56] of the end-plate. But the greater "cortical" thickness of the end-plate is misleading as will presently be discussed.

The dense outer shell covering vertebral bodies is not pure cortical bone. Some of the soft outer cartilaginous layers are inseparably mixed with the dense bone material. These layers provide attachment sites for external cartilage and ligaments. To further complicate the boundary between the outer shell and the inner trabeculae, the dense bone near the boundary can have the appearance of trabecular bone. During normal 'bone turnover', less bone is replaced than is removed on the inner surface, resulting in a net loss manifested as cortical-endosteal resorption. In doing so, this bone has the appearance of

trabecular bone, but was in fact originally cortical bone. Hence, the dense outer layer of the vertebrae is a composite of cortical bone, cartilage, and partly eroded cortical bone. Nowhere is this more evident than at the end-plate where cartilage, which attaches to the disk, contributes to a good percentage of the thickness. It has been suggested that a modulus between 1150 to 9650 MPa is more correct than the 18000 MPa of human cortical bone for areas such as the vertebral end-plates [67].

Hence, though this thickness has been denoted as cortical bone, it must be emphasized that the thickness actually relates to a more complex material that varies its properties depending on the region. Because a definitive boundary does not exist between the shell and the inner trabecular bone, there are high standard deviations in the results.

Another source of error may have influenced the measurement. If the band saw is angled with respect to the shell surface normal, the shell thickness will appear thicker. Though not shown in the table, the cortical bone near the pedicles was very thick, ranging from 2 to 6 mm. This has also been observed in human subjects [10].

6.1.2 Trabecular Bone Density and Modulus

The large variation in density measured within each vertebral body was due to regional differences in that body. Bone in the central portion of the body will be subject to more vertical forces whereas the outer trabecular bone will undergo forces dependent on the boundary forces on the body. These differences in loading are reflected in bone growth; with denser bone in regions of greater stress.

Error in the volume and weight measurements, used to determine density and modulus, were large as indicated by the error bars in Figure 4-6 through Figure 4-8. Three

factors contributed to these measurement errors. Due to the wet porous surface of the cube/prisms, cutting and sanding flat smooth faces was not always possible. Secondly, though the removal of the soft tissue through jet spraying and ultrasonic cleaning was effective, it is impossible to know if all the material was removed. Third, as the cube/ prisms were weighed in a wet state in air, evaporation took place. Upon observing this, repeated measurements were done on all the cubes in an attempt to find a consistent weight.

Other reasons exist for the variability. As discussed in the previous section, the boundary between cortical and trabecular bone is indistinct. Some of the cube/prisms taken close to the surface may have a higher density due the presence of bone taken to be very dense trabecular bone, but in fact is more cortical in nature. Also, the central bone contains large pores or canals for the passage of blood vessels. Irregularly large pores running through the middle of a cube/prism specimen cause that specimen to have a low density.

The measured apparent density and calculated modulus were in the ranges previously measured for bovine specimens. In general, trabecular bone has a modulus near zero to 2 GPa, with density ranges from near zero to slightly over 1 g cm^{-3} [63],[67]. No reference could be found for bovine vertebral trabecular bone. Instead, Table 6-1 shows values obtained from other locations in the bovine.

Table 6-1: Bovine Trabecular Modulus from Previous Works

Location	Apparent Density ($g\ cm^{-3}$)		Compressive Young's Modulus (GPa)			Sample Size	References
	Mean and Standard Deviation	Range	Mean and Standard Deviation	Range	Strain rate s^{-1}		
Distal femoral condyles	0.46 ± 0.13	0.17-0.71	1.0 ± 0.6	0.22-1.9	0.014 ± 0.005	61	[113]
		0.27-0.79*		0.15-2.3*	~0.002†	62	[106]
Humerus	0.54 ± 0.18 0.56 ± 0.11	0.29-0.94 0.34-0.74	1.0 ± 0.8 1.5 ± 0.8	0.13-2.3 0.32-2.1	0.005	30 29	[117]
Many locations		0.35-0.93*		0.2-2.0*		22	[17]

* Values measured from a graph in the reference.
† 1 mm/min displacement rate for 9.9-10.6 mm long specimens.

6.2 Compression Testing

The compression tests were also subject to experimental error. The alignment of the vertebral body to the direction of loading would be more reproducible using an alignment jig. Such a jig could use x-rays of the vertebral bodies to align the internal orientation of the trabecular bone with the loading direction. The displacement cycle used to measure stiffness was incorrectly set for bovine tests due to the pretest of the L6 vertebral body.

6.2.1 The L6 Body Pretest and Strength Measurement

The vertebral bodies fixed with cement had a much higher ultimate load and contraction than did the L6 body fixed with epoxy (see Table 2-2 and Table 4-5). It can be concluded that the failure which occurred during the L6 epoxy tests was due to the epoxy and not the vertebral body. The choice of a fixing agent with known properties, as discussed in

Chapter 2, is crucial to the accuracy of compression tests made on bones with curved ends.

Had the tests made on human lumbar vertebral bodies been reviewed in detail at this time, the error in choosing the fixing agent may have been detected. The percent contraction measured for L6 is smaller than that measured from human specimens as seen in Figure 6-1.

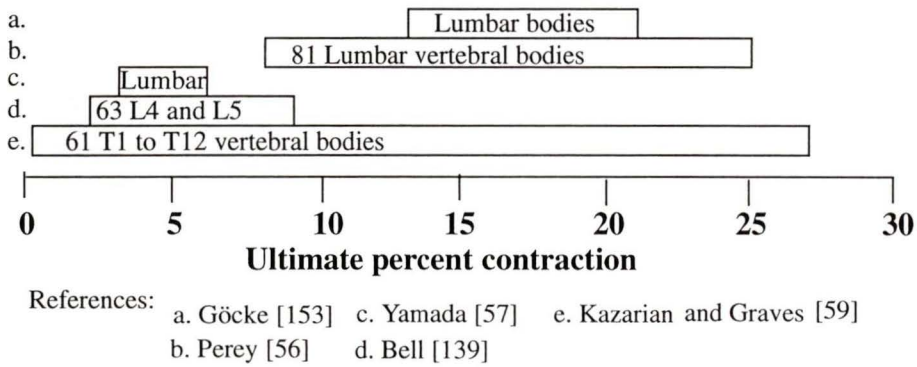

Figure 6-1: Range of Ultimate Contraction for Human Lumbar Vertebral Bodies

The bars represent the range measured by the researchers (referenced by the letter to the left of the bar). As shown in Appendix C, the ultimate load and stiffness of human specimens is much less than that of bovine.

During the compression cycles for the cement mounted vertebral bodies, difficulties were encountered at the higher displacement and load values due to setting the displacements based on the L6 test. If the maximum displacement did not fail the vertebral body, a relaxation would occur at the fixed displacement, which compromised the strength measurement meant to be taken at the given strain rate. Fortunately, the measurement of stiffness was the primary goal of the material tests, as the FEM models

were used to predict stiffness. The ultimate load was a secondary consideration. Hence, the different loading cycles, with different unloading, were not a major setback.

Surprisingly, the strength measurements made for the cement-fixed vertebral bodies did provide some interesting results. The measurements confirmed that the vertebral bodies had increased ultimate load with lower position along the spine, as seen in human specimens (see Appendix C). A more accurate means of measuring vertebral body cross-sectional area was used in the strength measurements which can be used for human tests. Finally, a relationship between vertebral body strength and trabecular bone strength was shown to exist which provides evidence that the vertebral body fails in the trabecular bone and not the outer shell.

6.2.2 Stiffness

The stiffness of the vertebral body was seen to increase with each displacement cycle until a substantially large displacement was reached. Then the stiffness would decrease indicating a weakening of the vertebral body, possibly due to the accumulation of damage to individual trabeculae. It can be concluded that the stiffness of a vertebral body depends on the level of load at that time, and the previous loading it has encountered.

L5 exhibited the greatest stiffness decrease, with the last recorded value (37 kN/mm) being 61% of the maximum (61 kN/mm). In contrast, L3 did not exhibit a large stiffness decrease before the relaxation at the maximum displacement damaged the vertebral body. The large range of stiffness values recorded for each vertebra reflect the need for a detailed report of loading history during material tests.

An error estimate for stiffness cannot be easily formulated, as there was no check or approximation for the results. Errors could have been introduced in the displacement measurement either by uncorrected compliance in the load train, or by a gradual slippage in the extensometer attachment. The concrete's compliance was corrected by using the spring approximation, though the interface between the concrete and the aluminum cup was not considered. The correction adds the assumption that the concrete test samples had the same modulus as the concrete used in the aluminum cups. Based on the large range of values measured for the concrete moduli, this assumption is weak. Fortunately, the correction only affected the higher stiffness values as seen in Figure 4-31. The greatest change occurred for L5, where the maximum stiffness went from 61 to 74 kN/mm. The lower values were unaffected (L3's lowest value changed from 15.2 to 15.8 kN/mm).

The stiffness of the L5 vertebral body was substantially higher than the stiffness measured for L2 and for L3. The exact reason for this is not known. Though L5 had a higher measured trabecular modulus than L2, it had a lower one than L3. The cortical shell thickness measurements were inexact so the differences in shell thickness are unknown. A thick cortical shell may have been a factor, as could the thicker cross-sectional area and different geometry.

6.3 FEM Models Stiffness Predictions

In general, the cross-section models predicted a lower stiffness than the other predictions. The difference between the cylindrical model and the algebraic summation prediction model is small, indicating that the accuracies for both models were similar. The differences in stiffness prediction between the cross-section models and the other

predictions for the same vertebral body are due to a more accurate representation of the body's geometry. The L5 cross-section model predicted a far lower stiffness compared to the other L5 models. This is due to the curvature of the body along the long axis, seen in Figure 5-3. The L2 and L3 models did not include this curvature as their surface was not digitized. Consequently, the L2 cross-section model had a low stiffness, and the L3 cross-section had a higher stiffness compared to other models for the vertebral body.

The three vertebral bodies have different predicted stiffness due to differences in the material properties and geometry. The large stiffness predicted by all the L3 models is due to the higher values for trabecular modulus and cortical shell thickness. The accuracy of the prediction depends on how well those quantities were measured and modelled. The experimentally measured stiffness, though close to the actual value, will also have some error.

Increasing the grid resolution of the cross-section models increased stiffness. Though the FEM's displacement formulation with iso-parametric elements always underestimates displacement when forces are specified on the boundary, this statement does not necessarily hold when displacements are specified on the boundary, and the reaction forces are calculated from this displacement field. Therefore, it is not inconsistent with theory that the better resolution grids predicted higher reaction forces and higher stiffness.

The increase in stiffness due to better grid resolution is small when compared to the differences between experimentally measured stiffness and the model predictions (Figure 5-14). The discrepancy between model and experimental stiffness cannot be explained by inaccuracies in the numerical computation, and must lie in the modelling assumptions made. Hence, the computational accuracy of the FEM models is better than their validity.

The lower constants used in the cross-section models predicted a stiffness that was 55% to 60% of that determined with the mean constants. Not only does this indicate a need for more accurate measurement (as the lower constants are only a standard deviation less than the mean), it also indicates the sensitivity of the model to these parameters. Only the L3 model consistently had a higher predicted stiffness than the experimentally measured values with the lower constants.

Including the cement ends in the L2 cross-section model did not improve the prediction, as the L2 cross-section model when corrected through Equation 4-2 produced similar results. But applying the correction is not straight forward. The correction affects larger stiffness values more than smaller ones. Therefore, when the correction is applied to the high stiffness predictions from the FEM models, a large change is made, but when applied to the lower valued experimental results, a small change is made. The correction of the cement's stiffness must be considered as an approximation dependent on the vertebral body's stiffness value.

6.3.1 Cortical and Trabecular Contribution to Stiffness

Of theoretical importance is the relative contribution of the cortical shell and the trabecular bone to the stiffness and strength of the body. High stress values were seen in the shell of the cylindrical model, reflecting that most of the support comes from the shell. However, the fixed displacement constraint on the end nodes required the stiffer shell to take more of the load, as explained in the results.

Although the end effects of the chosen loading induced high stress in the shell elements, this does not greatly influence the stiffness prediction of the cross-section model

when compared to the same model with cement disks. Also, some experimental evidence suggests that the cortical shell provides most of the support in human vertebral bodies. Rockoff et al. measured the relative contribution of trabecular and cortical bone to compressive strength of vertebral bodies. In their study, whole bodies, and bodies with the cortical shell removed, were compressed; 45-75% of the strength was attributed to the cortical shell [150]. Yoganandan et al. [151] undertook similar experiments with similar results, though both studies noted that the higher cortical shell contributions occurred in osteoporotic vertebral bodies.

Using the summation stiffness prediction with the L5 data, the cortical shell contributes 65.6% (54.9 kN/mm) and the trabecular bone 34.3% (28.7 kN/mm) to the total stiffness. By removing the shell elements from the cylindrical model, the trabecular bone alone had a stiffness of 29.6 kN/mm or 35.4% of the complete model's stiffness. Hence, the models have predicted that the shell contributes 60-70% to the stiffness of the vertebral body, just as would be expected in humans specimens.

6.3.2 Sensitivity of the Summation Stiffness Prediction

The use of lower values for trabecular modulus, cortical modulus, and cortical shell thickness in the cross-section models has demonstrated that stiffness predictions are sensitive to these parameters within the range measured. To improve the FEM models, these parameters must be more accurately measured. It would also be useful to know which of these parameters most affected the stiffness values so that future work may concentrate on a better measurements of these.

The algebraic summation prediction was solved with these parameters to investigate

their effect on stiffness. To visualize these results, the three parameters were assigned coordinates on a three-dimensional space. Appropriate intervals over which the equation was solved were determined from the material measurements and published results [18]. The other parameters in the summation prediction (height and cross-sectional area) were assigned constant values for L3. A constant value of stiffness will define a surface in the 3-D space.

Plots of these surfaces for 130, 75 and 20 kN/mm are shown in Figure 6-2. The box surrounding the surface defines the space in which that stiffness can exist. The same limits are used for the cortical modulus (x-axis) in the three plots and the above two plots have the same limits for the trabecular modulus (y-axis), but the cortical shell limits (z-axis) become progressively larger for the higher valued stiffness. The 20 kN/mm stiffness requires both a low cortical shell thickness and a low trabecular bone modulus.

Trabecular modulus is shown to have a strong affect on stiffness over the range in which it was measured during the material tests. This parameter was measured more accurately than the other two. Though improvements in its measurements can be made, the other parameters are a greater concern.

Cortical modulus could be much lower than the 20.7 GPa used in this study, considering that the shell is not pure cortical bone but a combination of cortical and trabecular bone. Decreasing the modulus will reduce the predicted stiffness. But the effect is small, unless the modulus is much lower than cortical bone. It is possible that the modulus is lower than the lower limit of 15 GPa used in the Figure (see Table 5-1 where a modulus of 1 GPa was used by Ueno and Liu [47]). Some form of measurement for the cortical shell modulus on the vertebral body would improve the accuracy of the model.

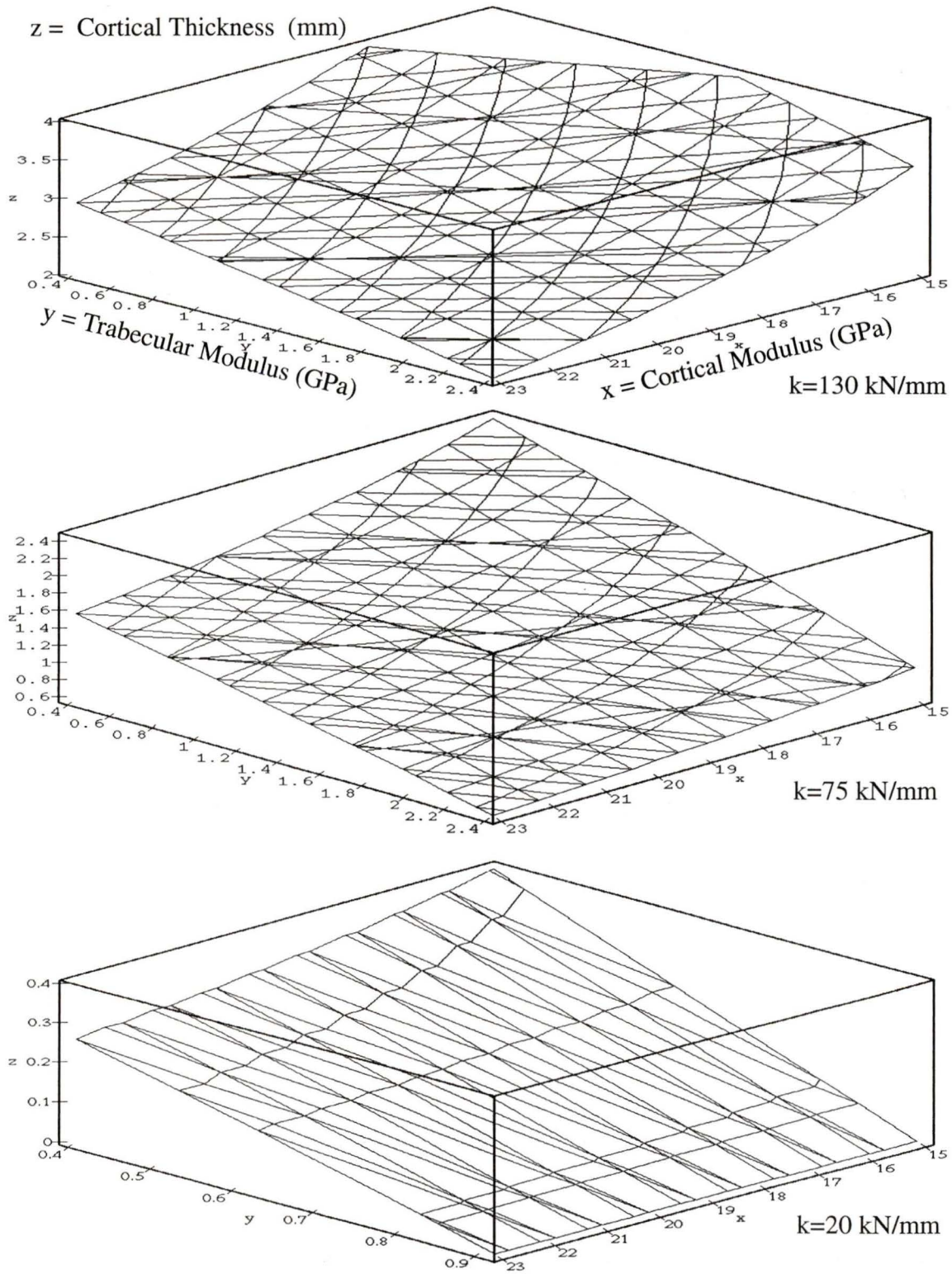

Figure 6-2: Surface Plot of the Summation Model's Stiffness Prediction in a Three Dimensional Space with Cortical Modulus, Trabecular Modulus, and Cortical Thickness as Coordinates

Considered over the range in Figure 6-2, the cortical shell thickness affects stiffness the most: a stiffness of 20 kN/mm is impossible with a shell thicker than 0.4 mm, and a stiffness of 130 kN/mm is equally impossible with a shell less than 2 mm thick. The methods used in this study to measure shell thickness did not provide acceptable accuracy. Accurate measurement of cortical shell thickness is of prime importance for better stiffness predictions.

7 Conclusions and Future Improvements

7.1 Conclusions

The FEM models did not accurately predict the stiffness of the vertebral bodies determined from the material tests. One out of the three cross-section models predicted a stiffness within the range measured experimentally. Despite the disagreement between the predictions and the experimental results, this study has produced a much better understanding of the nature of the material properties of bovine vertebral bodies.

In particular, three points can be made from these findings:

1. The thickness and modulus of the cortical bone shell are important parameters when predicting the stiffness of vertebral bodies. The shell may contribute as much as 70% to the total stiffness of the body.
2. The thickness of the shell was troublesome to measure which led to inaccurate prediction of stiffness.
3. Stiffness prediction improved when accurate geometric data was incorporated into the models.

7.2 Future Improvements

The accuracy of the material tests can be improved. The digitized surface of L5 provided the best geometrical measurement and improved stiffness predictions, yet the measurements were time-consuming. A more efficient digitization of the surface could be achieved using only the most relevant surface points. This would allow the modelling of the curved end-plates.

The measurement of apparent density was affected by evaporation of water from the trabecular bone; timed cycles of centrifuging and weighing could improve the weight measurement.

Compression cycles for testing the vertebral bodies should be of a more adaptable nature in future work. Due to the viscoelastic behavior of vertebral bodies, stiffness changes with the level of load and the previous loading history. A more sophisticated theory of the failure such as fatigue life, low cycle fatigue, or cumulative fatigue damage would better represent the compression of vertebral bodies.

Improvements can be made on the FEM models by adding curved end-plates and accounting for the longitudinal curvature of the body (not done for L2 and L3). Anisotropic material properties would more correctly model bone, but consistent measurement of technical constants are required before they can be used in the FEM models. The FEM models were limited by the inaccurate values given for cortical modulus, and more importantly cortical shell thickness. Until these inaccuracies are addressed, further model complications such as nonlinear material and geometrical analysis should not be considered.

The FEM predictions would be improved if the cortical shell thickness could be accurately measured. Observations of the cortical/trabecular interface through a travelling microscope could provide far more significant data, but making such measurements over the entire vertebral body would be laborious.

The measurement of average shell thickness, apparent density, and outer dimensions can all be done with QCT where bone density (expressed as bone mineral content) is determined from x-ray absorption. In addition, the bone mineral content would indicate

the density of the cortical shell, enabling a better approximation for the shell's modulus. Measuring the above parameters using QCT will be more efficient and likely more accurate.

Bibliography

[1] R. Huiskes and S. J. Hollister. From structure to process, from organ to cell: recent developments of fe-analysis in orthopaedic biomechanics. *ASME Journal of Biomechanical Engineering*, 115: 520-527, 1993.

[2] R. L. Spilker and B. R. Simon, eds. *Computational Methods in Bioengineering.* Full length papers based on presentations at the ASME Winter Annual Meeting, Chicago, Illinois, November 27-December 2, 1988.

[3] E. A. Chrischilles, D. Butler, C. S. Davis, and R. B. Wallace. A model of lifetime osteoporosis impact. *Archives of Internal Medicine*, 151: 2026-2032, 1991.

[4] M. Parniapour, M. Nordin, M. L. Skovron, and V. H. Frankel. Environmentally induced disorders of the musculoskeletal systems. *Environmental Medicine: Medical Clinics of North America*, 74(2): 347-357, 1990.

[5] B. E. C. Nordin, A. G. Need, A. Bridges, and M. Horowitz. Relative contributions of years since menopause, age, and weight to vertebral density in postmenopausal women. *Journal of Clinical Endocrinology and Metabolism,* 74(1): 20-23, 1992.

[6] K. G. Faulkner, C. E. Cann, and B. H. Hasegawa. Effect of bone distribution on vertebral strength: assessment with patient-specific nonlinear finite element analysis. *Radiology*, 179: 669-674, June 1991.

[7] J. Currey. *The Mechanical Adaptions of Bones*. Princeton University Press, 1984.

[8] H. M. Frost. *Intermediary Organization of the Skeleton.* Boca Raton, Florida: CRC Press, 1986.

[9] P. C. Cotterill, J. P. Kostuik, G. D'Angelo, G. R. Fernie, and B. E. Maki. An anatomical comparison of the human and bovine thoracolumbar spine. *Journal of Orthopaedic Research*, 4: 298-303, 1986.

[10] H. Gray. *Anatomy: Descriptive and Surgical.* 1st edition. Toronto, Canada: B. Mitchell, 1991.

[11] H. J. Swatland. *Structure and Development of Meat Animals.* Englewood Cliffs, New Jersey: Prentice-Hall, Inc., 1984.

[12] A. P. Spence. *Basic Human Anatomy.* 2nd. edition. Menlo Park, California: The Benjamin/Cummings Publishing Company, Inc., 1986.

[13] C. L. Brown and C. E. Gustafson. A key to postcranial skeletal remains of cattle/bison, elk, and horse. *Reports of Investigations*, No. 57. Laboratory of Anthropology, Washington State University, 1979.

[14] A. A. White and M. M. Panjabi. *Clinical Biomechanics of the Spine.* 2nd ed. J. B. Lippincott Company: Philadelphia, Pennsylvania, 1990.

[15] L. Mosekilde. Age-related loss of vertebral trabecular bone mass and structure - biomechanical conse-

quences. In: *Biomechanics of Diarthrodial Joints Volume II.* V. C. Mow, A. Ratcliffe, S. L-Y. Woo, eds. New York: Springer-Verlag, 1990.

[16] K. Short. Mechanical properties of vertebral cancellous bone. In: *Material properties and stress analysis in biomechanics*. A. L. Yettram ed. Manchestor: University Press, 1989.

[17] S. C. Cowin. The mechanical properties of cancellous bone. In: *Bone Mechanics*. S. C. Cowin ed. Boca Raton, Florida: CRC Press, 1991.

[18] S. C. Cowin. The mechanical properties of cortical bone. In: *Bone Mechanics*. S. C. Cowin ed. Boca Raton, Flworida: CRC Press, 1991.

[19] M. Dietrich, K. Kedzior, and T. Zagrajek. A biomechanical model of the human spinal system. *Proceedings of the Institution of Mechanical Engineers 205(H1), Journal of Engineering in Medicine*, 19-26, 1991.

[20] M. Dietrich, K. Kedzior, and T. Zagrajek. Modeling of muscle action and stability of the human spine. In: *Multiple Muscle Systems: Biomechanics and Movement Organization*. J. M. Winters and S. L.-Y. Woo, eds. New York: Springer-Verlag, 1990.

[21] C. Breau, A. Shirazi-Adl, and J. de Guise. Reconstruction of a human ligamentous lumbar spine using CT images -- A three dimensional finite element mesh generation. *Annals of biomedical Engineering*, 19: 291-302, 1991.

[22] A. Shirazi-Adl, C. Breau, and J. DeGuise. From computer-assisted tomography to finite element modelling -- A 3-D finite element grid of the human lumbar spine. In: *1991 Biomechanics Symposium : presented at the ASME Applied Mechanics Conference*, Columbus, Ohio, pages 369-372, June 1991.

[23] A. Shirazi-Adl and M. Parnianpour. Nonlinear response analysis of the human ligamentous lumbar spine in compression. On mechanisms affecting the postural stability. *Spine*, 18(1): 147-158, 1993.

[24] A. Shirazi-Adl. Nonlinear stress analysis of the whole lumbar spine in torsion -- Mechanics of facet articulation. *Journal of Biomechanics*, 27(3): 289-299, 1994.

[25] F. Linde and I. Hvid. Stiffness behavior of trabecular bone specimens. *Journal of Biomechanics,* 20: 83-89, 1987.

[26] D. R. Carter and W. C. Hayes. The Compressive behavior of bone as a two-phase porous structure. *Journal of Bone and Joint Surgery*, 59A(7): 954-962, 1977.

[27] A. F. Tencer and T. G. Mayer. Soft tissue strain and facet face interaction in the lumbar intervertebral joint -- Part I: Input data and computational technique. *Journal of Biomechanical Engineering*, 105: 201-209, 1983.

[28] R. Kurowski and A. Kubo. The relationship of degeneration of the intervertebral disc to mechanical loading conditions on lumbar vertebrae. *Spine*, 11(7): 726-731, 1986.

[29] H. S. Ranu. The role of finite element modelling in biomechancis. In: *Material properties and stress analysis in biomechanics*. A. L. Yettram ed. Manchester: Manchester University Press, 1989.

[30] M. Kasra, A. Shirazi-Adl, and G. Drouin. Dynamics of the human lumbar intervertebral joints: experimental and finite-element investigations. *Spine,* 17(1): 93-102, 1992.

[31] J. P. Laible, D. S. Pflaster, M. H. Krag, B. R. Simon, and L. D. Haugh. A poroelastic-swelling finite element model with application to the intervertebral disc. *Spine*, 18(5): 659-670, 1993.

[32] T. P. Belytschko, T. F. Andriacchi, A. B. Schultz, and J. O. Galante, Analog studies of forces in the human spine: Computational techniques. *Journal of Biomechanics,* 6, 361-371, 1973.

[33] T. P. Belytschko, R. F. Kulak, and A. B. Schultz. Finite element stress analysis of an intervertebral disc. *Journal of Biomechanics,* 7, 277-285, 1974.

[34] V. K. Goel, J. M. Winterbottom, and Y. E. Kim. Load sharing among spinal elements of a motion segment in extension and lateral bending. *ASME Journal of Biomechanical Engineering*, 109: 291-297, 1987.

[35] V. K. Goel and Y. E. Kim. Effects of injury on the spinal motion segment mechanics in the axial compression mode. *Clinical Biomechanics*, 4: 161-167, 1989.

[36] Y. E. Kim and V. K. Goel. Effect of testing mode on the biomechanical response of a spinal motion segment. *Journal of Biomechanics*, 23(3): 289-291, 1990.

[37] L. Gilbertson, V. K. Goel, and A. G. Patwardhan. Role of facet orientation in producing thoracolumbar spinal fractures. In: *1991 Biomechanics Symposium : presented at the ASME Applied Mechanics Conference*, Columbus, Ohio, pages 357-360, June 1991.

[38] Y. E. Kim, V. K. Goel, J. N. Weinstein, and T.-H. Lim. Effect of disc degeneration at one level on the adjacent level in axial mode. *Spine*, 16(3): 331-335, 1991.

[39] V. K. Goel, W. Kong, J. S. Han, J. N. Weinstein, and L. G. Gilbertson. A combined finite element and optimization investigation of lumbar spine mechanics with and without muscles. Spine, 18(11): 1531-1541, 1993.

[40] K. H. Yang, R. Sofranko, and D. B. Burr. Stress redistribution of osteoporotic spine. In: *Computational Methods in Bioengineering.* Full length papers based on presentations at the ASME Winter Annual Meeting, Chicago, Illinois, pages 427-436, November 27-December 2, 1988.

[41] A. Shirazi-Adl, S. C. Shrivastava, and A. M. Ahmed. Stress analysis of the lumbar disc-body unit in compression: A three-dimensional nonlinear finite element study. *Spine*, 9(2): 120-134, 1984.

[42] A. Shirazi-Adl, A. M. Ahmed, and S. C. Shrivastava. A finite element study of a lumbar motion segment subjected to pure sagittal plane moments. *Journal of Biomechanics,* 19(4): 331-350, 1986.

[43] A. Shirazi-Adl and G. Drouin. Load-bearing role of facets in a lumbar segment under sagittal plane loadings. *Journal of Biomechanics,* 20(6): 601-613, 1987.

[44] A. Shirazi-Adl and G. Drouin. Nonlinear gross response analysis of a lumbar motion segment in combined sagittal loadings. *ASME Journal of Biomechanical Engineering*, 110: 216-222, 1988.

[45] A. Shirazi-Adl. Finite-element simulation of changes in the fluid content of human lumbar discs: Mechanical and clinical implications. *Spine,* 17(2): 206-211, 1992.

[46] M. Dietrich, K. Kedzior, A. Wittek, and T. Zagrajek. Non-linear finite element analysis of formation and treatment of intervertebral disc herniae. *Proceedings of the Institution of Mechanical Engineers 206(H1), Journal of Engineering in Medicine*, 225-231, 1992.

[47] K. Ueno and Y. K. Liu. A three-dimensional nonlinear finite element model of lumbar intervertebral joint in torsion. *ASME Journal Biomechanical Engineering*, 109: 200-209, 1987 .

[48] W. Suwito, T. S. Keller, P. K. Basu, A. M. Weisberger, A. M. Strauss, and D. M. Spengler. Geometric and material property study of the human lumbar spine using the finite element method. *Journal of Spinal Disorders*, 5(1): 50-59, 1992.

[49] J. Mizrahi, J. Silva, T. M. Keaveny, W. T. Edwards, and W. C. Hayeś. Finite-element stress analysis of the normal and osteoporotic lumbar vertebral body. *Spine,* 18(14): 2088-2096, 1993.

[50] N. S. Hakim and A. I. King. A three dimensional finite element dynamic response analysis of a vertebra with experimental verification. *Journal of Biomechanics,* 12: 277-292, 1979.

[51] E. Alici, O. Z. Alku, and S. Dost. Prostheses designed for vertebral body replacement. *Journal of Biomechanics*, 23(8): 799-809, 1990.

[52] F. Lavaste, W. Skalli, S. Robin, R. Roy-Camelle, and C. Mazel. Three-dimensional geometrical and mechanical modelling of the lumbar spine. *Journal of Biomechanics*, 25(10): 1153-1164, 1992.

[53] W. Skalli, S. Robin, F. Lavaste, and J. Dubousset. A biomechanical analysis of short segment fixation using a three-dimensional geometric and mechanical model. *Spine*, 18(5): 536-545, 1993.

[54] J. H. Keyak, J. M. Meagher, H. B. Skinner, and C. D. Mote. Automated three-dimensional finite element modeling of bone: a new method. *Journal of Biomedical Engineering*, 12: 386-397, 1990.

[55] K. J. Bozic, J. H. Keyak, H. B. Skinner, H. U. Bueff, and D. S. Bradford. Three-dimensional finite element modeling of a cervical vertebra: a new approach to investigating injury mechanism in the cervical spine. In *Proceedings of the Twelfth Southern Biomedical Engineering Conference*, New Orleans, Louisiana, pages 51-53, April 1993.

[56] O. Perey. Fracture of the verebral end-plate in the lumbar spine. An experimental biomechanical investigation. *Acta Orthopaedica Scandinavica (Suppl),* 25: 1-102, 1957.

[57] H. Yamada. *Strength of Biological Materials*. F. G. Evans ed. Baltimore, Maryland: The Williams and Wilkins Company, 1970.

[58] N. Yoganandan, F. Pintar, C. R. Wilson, and A. Sances, Jr. In vitro biomechanical study of female geriatric cervical vertebral bodies. *Journal of Biomedical Engineering,* 12: 97-101, 1990.

[59] L. Kazarian and G. A. Graves. Compressive strength characteristics of the human vertebral centrum. *Spine*, 2(1): 1-14, 1977.

[60] S. A. Gozulov, Y. Korzhen, V. G. Skrupknik, and Y. N. Sushkov. Issledovaniye prochnosti pozvonkov cheloveka na szhatiye. *Arkhiv Anatomii, Gistologii, i Embriologii*, 43-51, 1966.

[61] O. Messerer. *Uber Elasticitat und Festigkeit der menschlichen Knochen*. Stuttgart, Germany, 1880.

[62] J. Cholewicke, S. M. McGill, and R. W. Norman. Lumbar spine loads during the lifting of extremely heavy weights. *Medicine and Science in Sports and Exercise,* 23(10): 1179-1186, 1991.

Trabecular Bone review papers:

[63] S. A. Goldstein. The mechanical properties of trabecular bone: Depenence on anatomic location and function. *Journal of Biomechanics*, 20(11/12): 1055-1061, 1987.

[64] R. B. Ashman. Experimental techniques. In: *Bone Mechanics*. S. C. Cowin ed. Boca Raton, Florida: CRC Press, 1991.

[65] R. B. Martin. Determinants of the mechanical properties of bones. *Journal of Biomechanics*, 24(Suppl. 1): 79-88, 1991.

[66] T. M. Keaveny and W. C. Hayes. A 20-year perspective on the mechanical properties of trabecular bone. *ASME Journal of Biomechanical Engineering,* 115: 534-542, 1993.

[67] T. M. Keaveny and W. C. Hayes. Mechanical properties of cortical and trabecular bone. In: *Bone Volume 7: Bone Growth --B.* B. K. Hall ed. CRC Press, 1993.

[68] W. C. Hayes. Biomechanical measurements of bone. In: *CRC Handbook of Engineering in Medicine and Biology.* D. G. Fleming and B. N. Feinberg eds. Boca Raton, Florida: CRC Press, 1978.

Apparent density and Modulus correlations papers

[69] M. H. Bartely Jr., J. S. Arnold, R. K. Haslam, and W. S. S. Gee. The relationship of bone strength and bone quantity in health, disease, and aging. *Journal of Gerontonolgy*, 21: 517-521, 1966.

[70] J. H. McElhaney. Dynamic response of bone and muscle tissue. *Journal of Applied Physiology*, 21: 1231, 1966.

[71] J. K. Weaver and J. Chalmers. Cancellous bone: its strength and changes with aging and an evaluations of some methods for measuring its mineral content. *Journal of Bone and Joint Surgery*, 48A: 289-298, 1966.

[72] J. D. Currey. The mechanical consequences of variation in the mineral content of bone. *Journal of Biomechanics*, 2: 1, 1969.

[73] J. Galante, W. Rostoder, and R. D. Ray. Physical properties of trabecular bone. *Calcified Tissue Research*, 5: 236-246, 1970.

[74] J. H. McElhaney, N. Alem, and V. Roberts. A porous block model for cancellous bones. American Society of Mechanical Engineers, publication 70-WA/BHF-2, 1970.

[75] J. H. McElhaney, J. L. Fogle, J. W. Melvin, R. R. Haynes, V. L. Roberts, and N. M. Alem. Mechanical properties of cranial bone. *Journal of Biomechanics*, 3: 495-511, 1970.

[76] J. W. Pugh, R. M. Rose, and E. L. Radin. Elastic and viscoelastic properties of trabecular bone: dependence on structure. *Journal of Biomechanics*, 6: 475, 1973.

[77] J. C. Behrens, P. S. Walker, and H. Shoji. Variation in strength and structure of cancelous bone at the knee. *Journal of Biomechanics*, 7: 201-207, 1974.

[78] R. D. Crowninshield and M. H. Pope. The response of compact bone in tension at various strain rates. *Annals of Biomedical Engineering*, 2: 217, 1974.

[79] C. M. Schoenfeld, E. P. Lautenschlager, and P. R. Meyer Jr. Mechanical properties of human cancelleous bone in the femoral head. *Medical and Biological Engineering*, 12: 313-317, 1974.

[80] J. C. Runkle and J. W. Pugh. The micromechanics of cancelleous bone. II. Determination of the elastic modulus of individual trabeculae by a buckling analysis. *Bulletin of the Hospital for Joint Diseases*, 36: 2, 1975.

[81] P. R. Townsend, R. M. Rose, and E. L. Radin. Buckling studies of single human trabeculae. *Journal of Biomechanics*, 8: 199, 1975.

[82] W. C. Hayes and D. R. Carter. Postyield behavior of subchondral trabecular bone. *Journal of Biomedical Material Research*, 10(7): 537-544, 1976.

[83] D. R. Carter and W. C. Hayes. Bone compressive strength: the influence of density and strain rate. *Science*, 194: 1174-1176, 1976.

[84] T. M. Wright and W. C. Hayes. Tensile testing of bone over a wide range of strain rates: effects of strain rate, microstructure and density. *Medical and Biological Engineering*, 14: 671, 1976.

[85] O. Lindahl. Mechanical properties of dried defatted spongy bone. *Acta Orthopaedica Scandinavica*, 47: 11-19, 1976.

[86] O. Lindahl and A. G. H. Lindgren. Grading of osteoporosis in autopsy specimens. *Acta Orthopaedica Scandinavica*, 32: 85-100, 1962.

[87] P. Ducheyne, L. Heymans, M. Martens, E. Aernoudt, P. D. Meester, and J. C. Mulier. The mechanical behavior of intracondylar cancellous bone of the femur at different loading rates. *Journal of Biomechanics*, 10: 747-762, 1977.

[88] T. D. Brown and A. B. Ferguson. Mechanical property distributions in the cancellous bone of the human proximal femur. *Acta Orthopaedica Scandinavica*,51: 429, 1980.

[89] D. R. Carter, G. H. Schwab, and D. M. Spengler. Tensile fracture of cancellous bone. *Acta Orthopaedica Scandinavica*, 51: 733-741, 1980.

[90] L. S. Gibson and M. F. Ashby. The mechanics of three-dimensional cellular materials. *Proceedings of the Royal Society of London*, A382: 43-59, 1982.

[91] J. L. Williams and J. L. Lewis. Properties and an anisotropic model of cancellous bone from the proximal tibial epiphysis, *Journal of Biomechical Engineering,* 104: 50-56, 1982.

[92] J. S. Bensusan, D. T. Davy, K. G. Heiple, and P. J. Verdin. Tensile, compressive and torsional testing of cancellous bone. *Transactions of the 29th Orthopedic Research Society*, 8: 132, 1983.

[93] M. Martens, R. VanAudekercke, P. Delport, P. DeMeester, and J. C. Muelier. The mechanical characteristics of cancellous bone at the uper femoral region. *Journal of Biomechanics*, 16: 971-983, 1983.

[94] J. L. Stone and G. S. Beaupre, W. C. Hayes. Multiaxial strength characteristics of trabecular bone. *Journal of Biomechanics*, 16: 743-752, 1983.

[95] S. A. Goldstein, D. L. Wilson, D. A. Sonstegard, and L. S. Matthews. The mechanical properties of human tibial trabecular bone as a function of metaphyseal location. *Journal of Biomechanics*, 16: 965-969, 1983.

[96] L. J. Gibson. The mechanical behavior of cancellous bone. *Journal of Biomechanics*, 18(5): 317-328, 1985.

[97] S. J. Kaplan, W. C. Hayes, J. L. Stone, and G. S. Beaupre. Tensile strength of bovine trabecular bone. *Journal of Biomechanics*, 18: 723-727, 1985.

[98] F. Linde, I. Hvid, and N. Jensen. Material properties of cancellous bone in repetitive axial loading. *Engineering in Medicine*, 14(4): 173-177, 1985.

[99] M. J. Ciarelli, S. A. Goldstein, D. Dickie, J. L. Ku, M. Kapper, J. Stanley, M. J. Flynn, and L. S. Matthews. Experimental determination of the orthogonal mechanical properties, density, and distribution of human trabecular bone from the major metaphyseal regions utilizing materials testing and computed tomography. *Transactions of the 32nd Orthopedic Research Society*, 11: 42, 1986.

[100] T. H. Hansson, T. S. Keller, and M. M. Panjabi. A study of the compressive properties of lumbar vertebral trabeculae: effects of tissue characteristics. *Spine*, 11(10):56-62, 1986.

[101] S. D. Ryan and J. L. Williams. Tensile testing of individual bovine trabeculae. In: *Proceedings of the 12th Annual North-East Bio-Eengineering Conference*, S. C. Orphanoudakis ed., p. 35-36, 1986.

[102] R. B. Ashman, J. D. Corin, and C. H. Turner. Elastic properties of cancellous bone: measurement by an ultrasonic technique. *Journal of Biomechanics*, 20: 979-987, 1987.

[103] J. L. Kuhn, (J. L. née Ku), S. A. Goldstein, K. W. Choi, M. Landon, M. A. Hezig, and L. S. Matthews. The mechanical properties of single trabeculae. *Transactions of the 33rd Orthopedic Research Society*, 12: 48, 1987.

[104] P. L. Mente and J. L. Lewis. Young's modulus of trabecular bone tissue. *Transactions of the 33rd Orthopedic Research Society*, 12: 49, 1987.

[105] R. B. Ashman and J. Y. Rho. Elastic modulus of trabecular bone material. *Journal of Biomechanics*, 21: 177-181, 1988.

[106] K. Brear, J. D. Currey, S. Raines, and K. J. Smith. Density and temperature effects on some mechanical properties of cancellous bone. *Engineering in Medicine*, 17(4): 163-167, 1988.

[107] J. C. Rice, S. C. Cowin, and J. A. Bowman. On the dependence of the elasticity and strength of cancellous bone on apparent density. *Journal of Biomechanics*, 21(2): 155-168, 1988.

[108] S. C. Cowin and M. M. Mehrabadi. Identification of the elastic symmetry of bone and other materials. *Journal of Biomechanics*, 22: 503-515, 1989.

[109] S. I. Esses, J. C. Lotz, and W. C. Hayes. Biomechanical properties of the proximal femur determined in-vitro by single-energy quantitative computed tomography. *Journal of Bone Mineral Research*, 4: 715-722, 1989.

[110] I. Hvid, S. M. Bentzen, F. Linde, L. Mosekilde, and B. Pongsoipetch. X-ray quantitative computed tomography: the relations to physical properties of proximal tibial trabecular bone specimens. *Journal*

of Biomechanics, 22: 837-844, 1989.

[111] T. S. Keller, T. H. Hansson, A. C. Abram, D. M. Spengler, and M. M. Panjabi. Regional variations in the compressive properties of lumbar vertebral trabeculae. *Spine*, 14(9): 1012-1019, 1989.

[112] F. Linde, I. Hvid, and B. Pongsoipetch. Energy absorptive properties of human travecular bone specimens during axial compression. *Journal of Orthopedic Research*, 7: 432-439, 1989.

[113] C. H. Turner. Yield behavior of bovine cancellous bone. *ASME Journal of Biomechanical Engineering*, 111: 256-260, August 1989.

[114] J. C. Lotz, T. N. Gerhart, and W. C. Hayes. Mechanical properties of trabecular bone from the proximal femur: a quantitative CT study. *Journal of Computer Assisted Tomography*, 14: 107-114, 1990.

[115] F. Linde, P. Nørgaard, I. Hvid, A. Odgaard, and K. Søballe. Mechanical properties of trabecular bone. Dependency on strain rate. *Journal of Biomechanics*, 24(9): 803-809, 1991.

[116] J. Y. Rho, R. B. Ashman, and C. H. Turner. Young's modulus of trabecular and cortical bone material: ultrasonic and microtensile measurements. *Journal of Biomechanics*, 26(2): 111-119, 1993.

[117] T. M. Keavenly, R. E. Borchers, L. J. Gibson, and W. C. Hayes. Trabecular bone modulus and strength can depend on specimen geometry. *Journal of Biomechanics*, 26(8): 991-1000, 1993.

End of Apparent density versus Young's Modulus papers

[118] L. J. Gibson and M. F. Ashby. *Cellular solids, structure and properties*. Oxford: Pergamon Press, 1988.

[119] J. Wolff. Das Gesetz der Transformation der Knochen. Berlin: Hirschwald, 1892.

[120] S. A. Goldstein, S. J. Hollister, J. L. Kuhn, and N. Kikuchi. The mechanical and remodeling properties of trabecular bone. In: *Biomechanics of Joints Volume II.* V. C. Mow, A. Ratcliffe, S. L-Y. Woo, eds. New York: Springer-Verlag, 1990.

[121] B. D. Snyder and W. C. Hayes. Multiaxial structure-property relations in trabecular bone. In: *Biomechanics of Diarthrodial Joints Volume II.* V. C. Mow, A. Ratcliffe, S. L-Y. Woo, eds. New York: Springer-Verlag, 1990.

[122] B. D. Snyder, W. T. Edwards, and J. M. van der Linde, A. A. White, W. C. Hayes. Steriologic assessment of trabecular structure in the lumbar vertebral body: Biomechanical implications. *Transactions of the 35th Orthopedic Research Society*, 14: 262, 1989.

[123] R. W. Goulet, L. A. Feldkamp, D. J. Kubinski, and S. A. Goldstein. Predicting the architectural orientation of trabecular bone. *Transactions of the 35th Orthopedic Research Society*, 14: 263, 1989.

[124] R. W. Goulet, M. J. Ciarelli, S. A. Goldstein, J. L. Kuhn, L. A. Feldkamp, D. Kruger, D Viviano, and F. Chapmplain. The effects of architecture and morphology on the mechanical properties of trabecular bone. *Transactions of the 34th Orthopedic Research Society*, 13: 73, 1988.

[125] T. Harrigan and R. W. Mann. Charaterization of microstructural anisotropy in orthotropic materials using a second rank tensor. *Journal of Material Science*, 19: 761, 1984.

[126] F. Linde, K. Hvid, and F. Madsen. The effect of specimen geometry on the mechanical behavior of trabecular bone specimens. *Journal of Biomechanics*, 25: 359-368, 1992.

[127] M. Zhu, T. S. Keller, and D. M. Spengler. The effect of specimen load-bearing and free surface layers on the compressive mechanical properties of cellular materials. *Journal of Biomechanics*, 27(1): 57-66, 1994.

[128] J. K. Gong, J. S. Arnold, and S. H. Cohn. Composition of trabecular and cortical bone. *Anatomical Record*, 149: 325-332, 1964.

[129] S. M. Bowman, T. M. Keavenly, L. J. Gibson, W. C. Hayes, and T. A. McMahon. Compressive creep behavior of bovine trabecular bone. *Journal of Biomechanics*, 27(3): 301-310, 1994.

[130] M. C. Michel, X. E. Guo, J. L. Gibson, T. A. McMahon, and W. C. Hayes. Compressive fatigue behavior of bovine trabecular bone. *Journal of Biomechanics,* 26(4/5): 453-463, 1993.

[131] J. E. Smeathers and D. N. Joanes. Dynamic compressive properties of human lumbar intervertebral joints: a comparison between fresh and thawed specimens. *Journal of Biomechanics,* 21(5): 425-433, 1988.

[132] R. W. Porter, M. A. Adams, and W. C. Hutton. Physical activity and the strength of the lumbar spine. *Spine,* 14(2): 201-203, 1989.

[133] M. J. Pearcy, and R. J. Hindle. Axial rotation of lumbar intervertebral joint in forward flexion. *Proceedings of the Institution of Mechanical Engineers 205(H4), Journal of Engineering in Medicine*, 1991.

[134] M. Shea, T. W. Edwards, A. A. White, and W. C. Hayes. Variations of stiffness and strength along the human cervical spine. *Journal of Biomechanics,* 24(2): 95-107, 1991.

[135] P. Brinckmann, M. Biggemann, and D. Hilweg. Prediction of the compressive strength of human lumbar vertebrae. *Spine,* 14(6): 606-610, 1989.

[136] D. Kunz, R. Vanderby Jr., T. Zdeblick, R. McCabe, and M. Markel. A multi-axis system for biomechanical testing: Application of pure loads in axial, torsional or flexural directions. *Closed Loop,* 17(4): 4-10, 1993.

[137] A. L. Osvalder, P. Neumann, P. LÖvsund, and A. Nordwall. Ultimate strength of the lumbar spine in flexion -- an in vitro study. *Journal of Biomechanics,* 23(5): 453-460, 1990.

[138] T. H. Hansson, R. Bengt, and A. Nachemson. The bone mineral content and ultimate compressive strength of lumbar vertebrae. *Spine,* 5(1): 46-55, 1980.

[139] G. H. Bell, O. Dunbar, J. S. Beck, and A. Gibb. Variations in strength of vertebrae with age and their relation to osteoporosis. *Calcified Tissue Research*, 1:75-86, 1967.

[140] S. D. Rolander, and W. E. Blair. Deformation and fracture of the lumbar vertebral end plate. *Orthopedic Clinics of North America,* 6(1), 1975.

[141] P. Brinckmann, N. Johannleweling, D. Hilweg, and M. Biggemann. Fatigue fracture of human lumbar vertebrae. *Clinical Biomechanics,* 2: 94, 1987.

[142] R. M. Pilliar, R. Blackwell, I. Macnab, and H. U. Cameron. Carbon fiber-reinforced bone cement in orthopedic surgery. *Journal of Biomedical Material Research*, 10: 893-906, 1976.

[143] C. T. Lynch, ed. *CRC Handboook of Material Science. Volume 1: General Properties*. Boca Raton, Florida: CRC Press, 1988.

[144] E. D. Sedlin and C. Hirsch. Factors affecting the determination of the physical properties of fermoral cortical bone. *Acta Orthopaedica Scandinavica,* 38: 148-62, 1966.

[145] S. Struhl, S. A. Goldstein, D. L. Dickie, M. J. Flynn, and L. S. Mattews, L. S. The distribution of mechanical properities of trabecular bone within vertebral bodies and iliac crest: correlations with computed tomography density. *Transactions of the 33th Orthopedic Research Society*, 12: 262, 1987.

[146] L. H. Yahia, G. Drouin, and P. Duval. A methodology for mechanical measurements of technical constants of trabecular bone. *Engineering in Medicine*, 17(4):169-173, 1988.

[147] Z. M. Oden, R. T. Hart, and D. B. Burr. The influence of assumed relationships between bone's mechanical properties and CT density on results of finite element analyses. In *Proceedings of the Twelfth Southern Biomedical Engineering Conference*, New Orleans, Louisiana, pages 57-58, April 1993.

[148] B. D. Snyder. Anisotropic Structure-Property Relations for Trabecular Bone. Ph. D. dissertation, University of Pennsylvania, Philadelphia, 1991.

[149] *ANSYS User's Manual Vol. III Elements*. Version 5.0. Houston, PA: Swanson Analysis Systems, Inc., 1993.

[150] S. D. Rockoff, E. Sweet, and J. Bleustein. The relative contribution of trabecular and cortical bone to the strength of human lumbar vertebrae. *Calcified Tissue Research*, 3: 163-175, 1969.

[151] N. Yoganandan, J. B. Myklebust, C. R. Wilson, J. R. Cusick, and A. Sances. Functional biomechanics of the thoracolumbar vertebral cortex. Clinical Biomechanics, 3: 11-18, 1988.

[152] L. E. Malvern. *Introduction to the Mechanics of a Continuous Medium*. Englewood Cliffs, New Jersey: Prentice-Hall, Inc., 1969.

[153] C. Göcke. Das Verhalten der Bandscheiben Wirbelverletzungen. *Archiv fuer Orthopaedische und Unfall-Chirurgie*, 31: 42-80, 1932.

[154] A. Rauber. *Elasticitat und Festigkeit der Knochen*. Leipzig, Germany, 1876.

[155] S. Ruff. Brief acceleration less than one second. German Aviation Medicine World War II, The Surgeon General U.S. Air Force, 584, 1950.

Appendix A: Anatomy of the Bovine and Human Spine

Complex structure occurs at all levels and dimensions in living systems [7],[8]. Models of such systems are limited by definition: they can only reflect a small subset of its complexity and hence can only predict a small subset of its function. It would be impossible to include all the details of a vertebral body in a model but a detailed awareness of physiology and anatomy is necessary if one is to evaluate the success of the model. Thus, the structure of human and bovine spines will be reviewed from the gross level to the microscopic.

A.1 Orientation Definitions

Anatomical directions are described by paired terms. 'Anterior' (top) refers to the direction the head is facing, whereas 'posterior' (bottom) refers to a position towards the rear. 'Ventral' (front) is toward the belly or abdominal area and 'dorsal' (back) is toward the back. Since humans stand upright, these terms are used differently for humans and bovines: the head faces the same direction as the abdomen so 'anterior' and 'ventral' are synonymous. Hence, extra terms are needed for humans: 'superior' (cranial) means toward the head and 'inferior' means away from the head. In both animals and humans, 'lateral' is the direction through the plane of symmetry in the body.

A.2 The Spinal Column

The spine or vertebral column consists of a series of bones called vertebrae. In humans there are 33 vertebrae: 7 cervical in the head and neck, 12 thoracic or dorsal attaching to the ribs, 5 lumbar in the lower back, and 9 which are fused to form the sacrum and coccyx

(see Figure A-1). The average length of the vertebral column for an adult man is 71 cm. The adult bovine vertebral column is approximately 280 cm long consisting of 49-51 vertebrae, 35 vertebrae if the tail is excluded. The bovine has 7 cervical, 13 thoracic, and 6 lumbar [9]. Each vertebrae is designated a letter referring to its region and a number referring to its placement within the region. (e.g., L1 refers to the 1st lumbar vertebra).

Although osteoporosis usually affects the cervical and thoracic spine, the lumbar spine is easier to study because of its larger diameter and accessibility for dissection. Conclusions based on lumbar models can be applied to other areas of the spine. For this reason, the following will concentrate on the lumbar spine. A dorsal view of a bovine lumbar spine is shown in Figure A-2

Running through the vertebrae is the spinal canal which houses and protects the spinal cord. Surrounding the vertebrae in the spine is a variety of connective tissues.

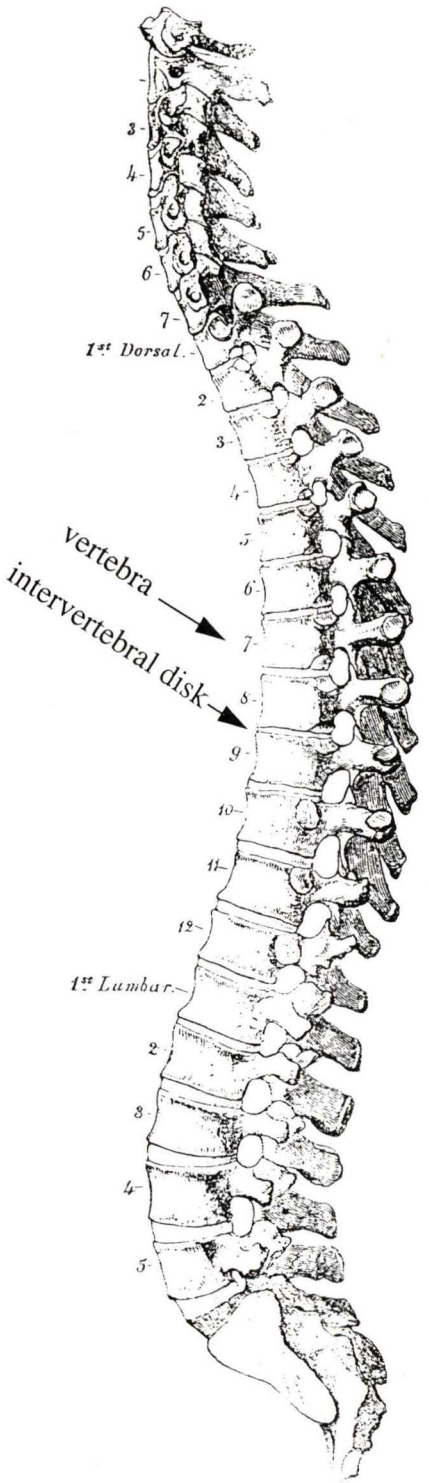

Figure A-1: Lateral View of the Human Spine (adapted from [10])

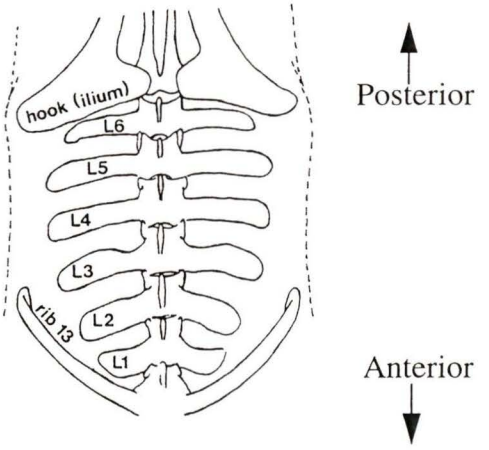

Figure A-2: Dorsal View of the Bovine Lumbar Spine (adapted from [11])

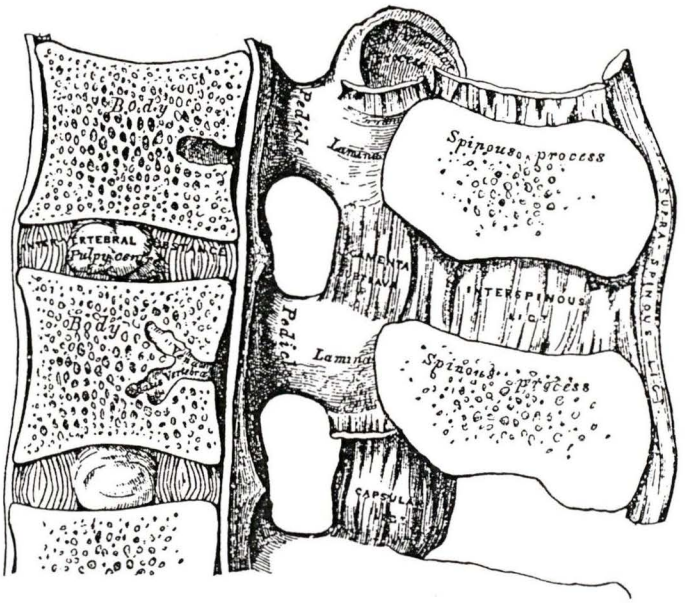

Figure A-3: Lateral View through the Center of the Lumbar Spine Showing Ligaments in Humans (from [10])

Ligaments are cable-like supports which attach to bones (see Figure A-3). Muscles provide active support and attach to the vertebrae through tendons. The vertebrae also attach directly to each other through articular joints. These joints are flexible as smooth lubricated synovial cartilage is used in between the bones.

A.3 The Vertebrae

Each vertebra shown in Figure A-4 consists of two parts, the body (a ventral solid segment forming the chief pillar of support) and the arch (a dorsal segment forming part of the spinal canal). The arch is formed of two pedicles and two laminae. Attached to the arch are seven processes. The spinous process and two transverse processes are used to attach ligaments and muscles. The other four articular processes form the articular joints above and below, joining with neighboring vertebrae in the spinal column.

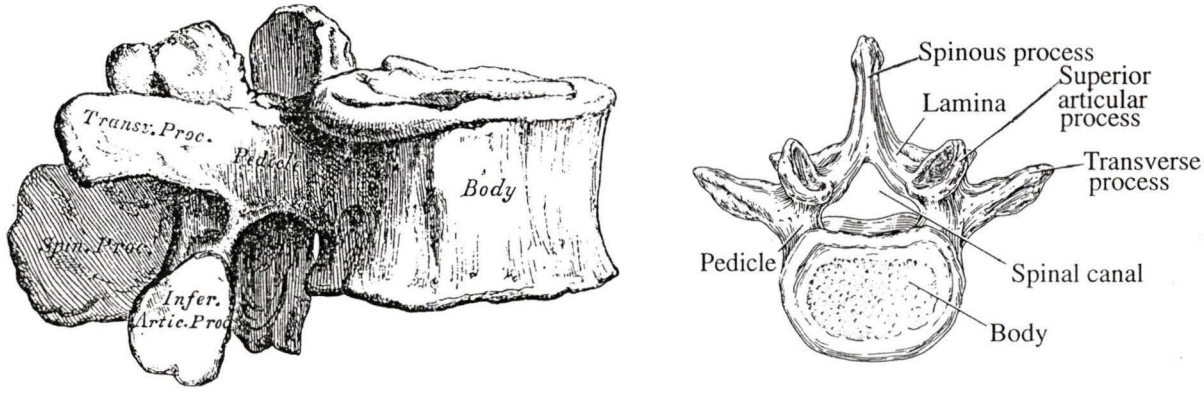

Figure A-4: Human Lumbar Vertebrae (adapted from [10] **and** [12])

The bovine lumbar vertebrae are larger than human, though both have a lateral width through the body of 3 to 5 cm. The transverse processes are substantially longer and wider in the bovine (approximate length is 16-17 cm), while the spinous and articular processes is not much larger as shown in Figure A-5.

A.4 The Disk

The bodies of the vertebrae are held together by a fibrous intervertebral disk. Each disk is composed of a firm outer portion, called the annulus fibrosus, and a softer central portion,

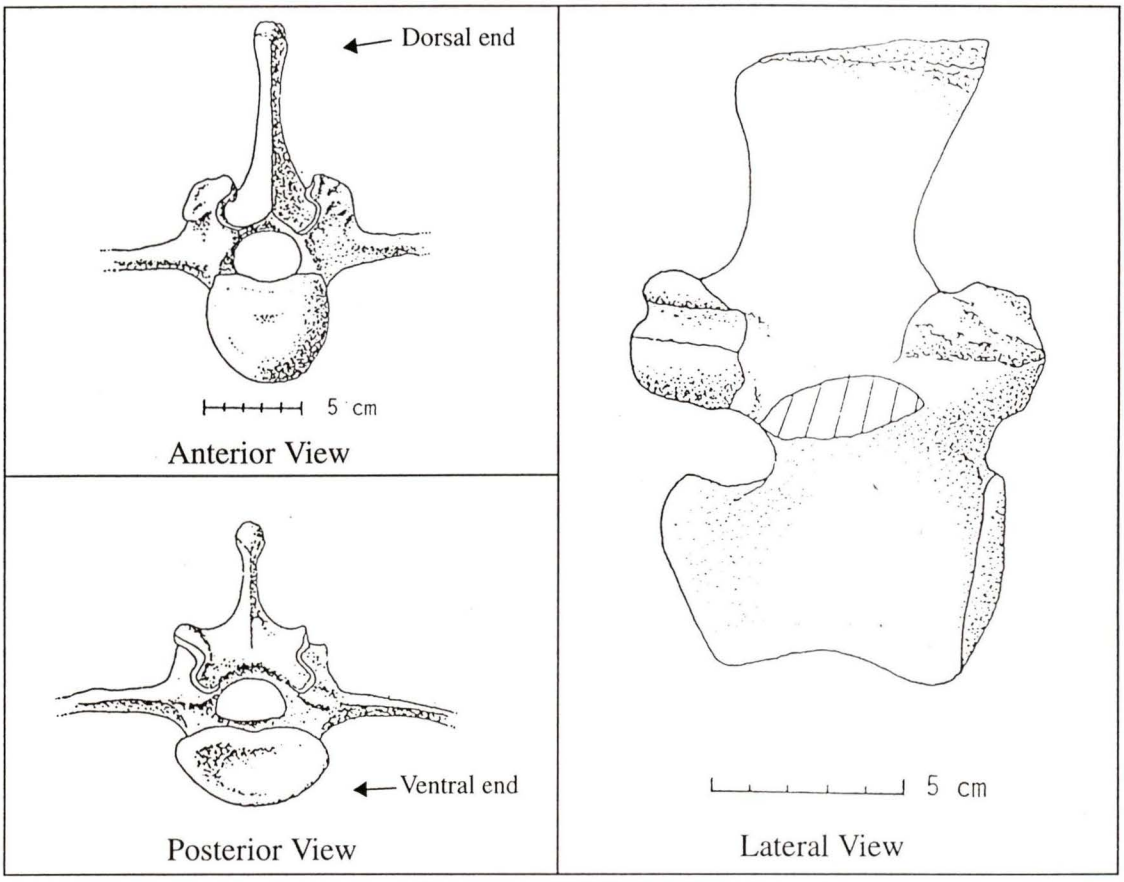

Figure A-5: Bovine Lumbar Vertebrae (adapted from [13])

the nucleus pulposus. The disk adds flexibility as well as shock absorption to the spine. The disk contains fluid. During the day, some of this fluid is lost which accounts for the loss of height a person undergoes from morning to night. The fluid content of the disk also decreases with age. Some weak or overused disks rupture and spill their gelatinous contents which may contact spinal nerves. This is one of the major cases of low back pain and much research has been done on the intervertebral disk for this reason [14].

The disk, however, is not the weak component in the compression of the spine. Disk herniation or rupture does not typically occur when two vertebrae and the intervening disk are compressed. The vertebrae typically fracture at the end-plate. Osteoporotic vertebrae

show extensive collapse of the end-plate and the underlying bone at relatively low loads [14]. Hence, the vertebral body is important to the compressional strength of the spine.

A.5 The Lumbar Vertebral Body

Supporting the upper torso, the lumbar vertebral body is roughly cylindrical. In humans, the lumbar vertebral body is broad with flat or slightly concave inferior and superior surfaces. The sides of the body are slightly bowed causing a smaller cross-section in the middle of the body than at the ends. In comparison, bovine lumbar vertebral bodies have a greater height, with end-plates curved convex anteriorly and concave posteriorly. The sides are strongly bowed. If sliced laterally, the middle of the body has a triangularly shaped perimeter, whereas the ends are circular.

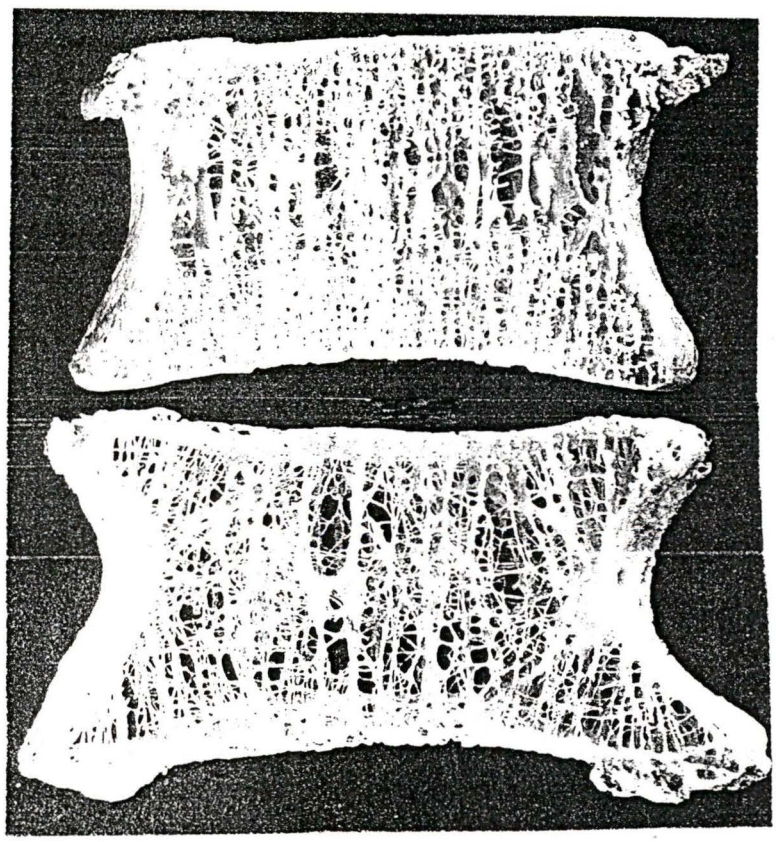

Figure A-6: (Top) Human Vertebral Bodies from a Young and (Bottom) from an Elderly Individual (from [15])

The body is composed almost entirely of spongy or trabecular bone, but has a thin shell of cortical bone on its outer surface (Figure A-6). Permeating throughout its interior are large canals for the reception of veins, which converge towards large apertures on the dorsal part of the body. Separating the disk and vertebrae is hyaline cartilage, called the end-plate. Above and below the centrally located nucleus pulposus, the end-plate acts as a barrier, while at the outer ends of the end-plate, the annulus fibers of the disk attach to the end-plate and directly into the bone tissue (called Sharpey's fibers).

A.6 Trabecular Bone

Trabecular bone is a scaffolding type of structure composed of bony beams, struts, and plates (see Figure A-7); it is also called cancellous, or spongy bone. Trabeculae refer to the individual beams. The pore cavities are quite variable in both size and shape, and since most of the cavities do communicate, the general arrangement may be approximated as an open-cell two-phase composite. One phase is bone, while the other phase consists of blood, red and yellow marrow, nerve tissue, interstitial fluid, and blood vessels.

The simplest trabecular bone consists of randomly oriented cylindrical struts, about 0.1 mm in diameter, each extending for about 1 mm before making a connection. The arrangement in the center of the vertebral body is more complex. As the major force is axial compression, the beams form an anisotropic structure with large diameter beams in the human superior/ inferior direction and with small cross bracing laterally. The trabeculae near the end-plates are tightly packed and form a more isotropic mesh.

Bone grows and recedes only at the surface. As an individual ages more trabecular bone is absorbed than is deposited. Consequently, smaller trabeculae (with high surface to

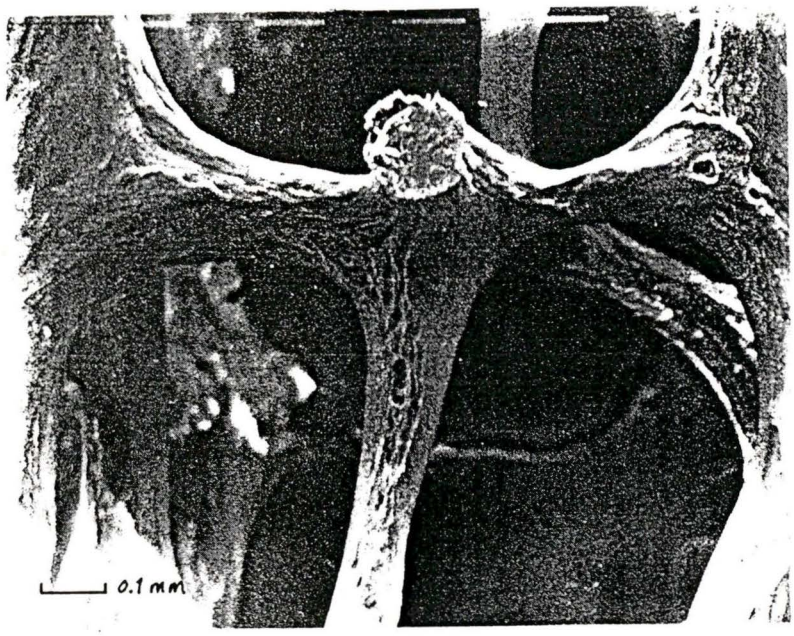

Figure A-7: Scanning Election Micrograph of Human Vertebral Trabecular Bone (from [16])

volume ratio) are preferentially absorbed to larger trabeculae, and the tightly packed trabeculae near the end-plates are removed [15].

A.7 Bone

Bone consists of a layered mineralized bone matrix surrounded by blood vessels. Bone can exist in different arrangements: poorly organized (woven bone), or flat sheet layers (lamellar), or layers around canals (haversian). During fracture repair, woven bone is deposited quickly around the fracture site (forming a callus). Mature undamaged human bones, contain haversian bone where vascular capillaries form canals for blood supply. Bone in cattle is a lamellar type (flat layers) called plexiform bone. Laminar bone tends to have greater strength and is slightly more stiff compared to haversian bone.

Haversian and lamellar bone are basically different configurations of the same material. In both configurations, no point in the tissue is more than 100 μm away from

blood supply. In lamellar bone, the sheets of deposited bone matrix (lamina) are layered parallel to a sheet of blood canals, whereas in haversian systems the lamina lie concentrically around the blood canals [7].

The bone material forming the individual trabeculae in trabecular bone is primarily lamellar but, due to the trabeculae's small size, pits and surface roughness may affect its properties. Some haversian bone which has been eroded away into fragments can have the appearance of trabecular bone, but will have a substantially lower strength.

The cortical shell of the vertebral body is not a definitive form of haversian or lamellar bone. As the thickness of the shell is about 1 mm, less than 5 layers of lamina and blood vessels can exit. The small number of layers may cause a more disorganized structure especially at the transition zone between cortical and trabecular bone.

A.8 Bone Cells

The interfaces between the laminae of both haversian and laminar bone contain an array of roughly ellipsoidal cavities containing bone cells (osteocytes) from which extend numerous fine canals (canaliculi). Other cells, which are not trapped within the structure (matrix), deposit new bone (osteoblasts) or absorb it (osteoclasts) on the exposed surfaces.

A.9 Bone Matrix

The calcified part of bone, or matrix, is roughly one-third mineral, one-third collagen, and one-third water. The matrix is a composite material with a ground substance of long-stranded protein collagen stiffened by a dense filling of calcium phosphate mineral crystals. The function of water in the matrix remains obscure. The sheets in the laminae are composed of wrapped collagen fibers impregnated at regularly spaced sites with

hydroxyapatite (a version of calcium phosphate) and other minerals. The minerals are 20 to 40 nm long [18].

Appendix B: Data Processing of L5 Vertebral Body's Digitized Surface

The surface was digitized using four different coordinate systems to allow the touch probe to measure all surfaces on the vertebral body. Figure B-1 shows the two origins used during the digitizing. The supporting structure consists of an 11-cm-long vise with wooden vertical supports. The wooden supports have bolts to hold the vertebral body. Once all the points reachable with the touch probe in one alignment were digitized, the touch probe was re-aligned, referenced to the other origin, and more data points taken. To

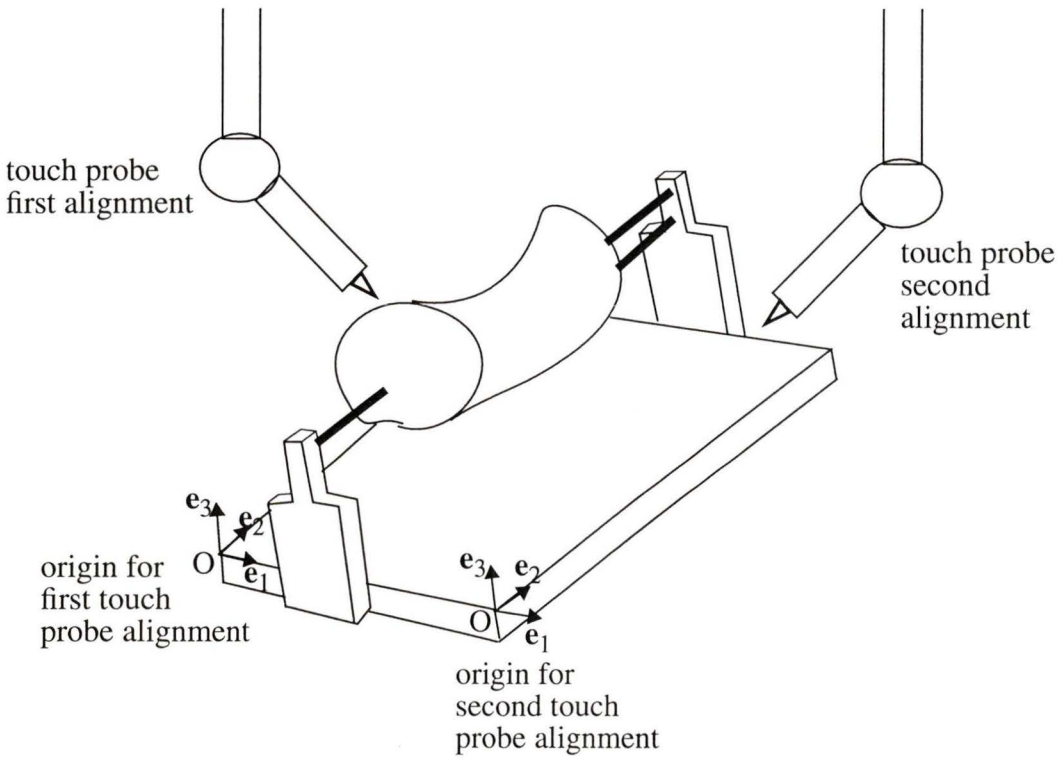

Figure B-1: Surface Digitizing of the L5 Vertebral Body

expose all the surfaces, the vertebral body was reoriented, and the two touch probe alignments were used again to complete the digitizing.

The coordinate measuring machine produced a print-out of three dimensional data points which were then inputted into a Sun Sparcworkstation. Data sets which had the same vertebral body orientation were referenced to a common origin easily, as the two origins only differed by an 11 cm translation along the $\mathbf{e}_1$ base vector. After applying these translations, the data was combined into two sets relating to the two orientations of the vertebral body. Four points on the surface of the body were measured in both orientations so that one data set could be transformed into the other's orientation. The transformation is shown graphically below in Figure B-2 with a triangle representing three points referenced by the primed and un-primed coordinate systems (three points are the minimum required to form a consistent system of equations).

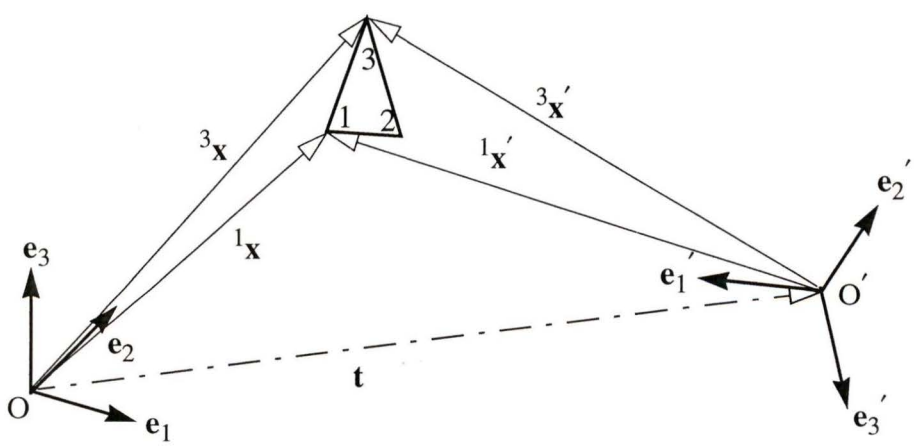

Figure B-2: Point Transformation Between the Two Orientations of the Vertebral Body

Both a translation and a rotation must be applied to the vectors ${}^{k}\mathbf{x}'$ which specify the location of the points in one orientation, or coordinate system, to find the vectors ${}^{k}\mathbf{x}$ which specify the location in the original orientation. Mathematically, using tensor notation with the summation convention:

$$ {}^{k}x_i = a_{ji}\,{}^{k}x_j' + t_i \qquad \text{(B-1)} $$

where a_{ji} is the cosine of the angle between $\mathbf{e}_j'$ and $\mathbf{e}_i$ base vectors when the origins of the coordinate systems are coincident ($i,j \in \{1,2,3\}$); t_i is the $\mathbf{e}_i$ component of the translation vector; and ${}^{k}x_i'$ is the position coordinate along $\mathbf{e}_i'$ for one of the k points ($k \in \{1,2,3,4\}$).

As the above transformation is orthogonal (each basis $\mathbf{e}_i$ and $\mathbf{e}_j'$ are composed of mutually orthogonal unit vectors), it follows that a_{ji} must also satisfy:

$$ a_{ij}a_{pj} = \delta_{pi} \qquad i, j, or\ p \ \in (1, 2, 3) \qquad \text{(B-2)} $$

where δ_{pi} is the Kronecker delta function [152]. Equation B-2 is composed of nine scalar equations of which six are independent. These constraint equations reduce the degrees of freedom in a_{ij} to three. Furthermore, the problem could be formulated with only six unknowns (three Euler angles for the rotations, and three scalars for the translation) compared to the nine unknowns a_{ji} and t_i. Though this approach may be simpler, the goal was not to find the optimum method of solution but just a solution.

At least three vector positions ${}^{k}\mathbf{x}$ (or nine scalar equations) are required for a solution as there is the added constraint that the relative position of the points with respect to each other do not change. The extra fourth point was used to improve accuracy and give an

indication of error. Equation B-1 and Equation B-2 make a system of nonlinear equations that can be solved for the nine unknowns.

Matlab™ software from The MathWorks Inc. was used to solve the system. Matlab finds the roots of a function of several variables ($F(a_{ji},t_i) = 0$) using the Gauss-Newton method. This method is based on the Newton (or Newton-Raphson) method for one variable, but when used for several variables, it requires the inversion of the Jacobian matrix. As implied by the name, Guass (or Guass-Jordan) matrix inversion is used. An initial guess for the roots is used to find a better approximation for the next iteration. These approximations will converge to the actual roots, provided that the initial guess was near. The guess used here was based on plotting the four vector positions in both coordinate systems and visualizing a possible rotation and translation to align the points. The results, with all vectors in units of mm, are listed on the following page.

After applying the transformation of Equation B-1 to all the points measured in the primed coordinate system, a total of a 327 surface points described the L5 vertebral body in the un-primed system. The four points which were measured in both systems gave an indication of the error in measurement of these points. As is shown below, there is a small difference (less than 0.13 mm) between the vector points measured in the un-primed system, and the points transformed into the un-primed system.

Initial guess:

$$a_{ji} = \begin{bmatrix} -1 & 0 & 0 \\ 0 & 1 & 0 \\ 0 & 0 & -1 \end{bmatrix}$$

$$t_i = \begin{bmatrix} -61.524 & 0.243 & -6.221 \end{bmatrix}$$

Vector positions:

$${}^1x_i = \begin{bmatrix} 66.126 & 51.000 & 87.468 \end{bmatrix} \quad {}^1x_i' = \begin{bmatrix} 124.715 & 51.306 & 90.876 \end{bmatrix}$$

$${}^2x_i = \begin{bmatrix} 130.209 & 30.457 & 100.216 \end{bmatrix} \quad {}^2x_i' = \begin{bmatrix} 62.690 & 40.409 & 70.768 \end{bmatrix}$$

$${}^3x_i = \begin{bmatrix} 64.167 & 30.336 & 82.160 \end{bmatrix} \quad {}^3x_i' = \begin{bmatrix} 125.691 & 30.093 & 88.381 \end{bmatrix}$$

$${}^4x_i = \begin{bmatrix} 131.410 & 46.443 & 111.475 \end{bmatrix} \quad {}^4x_i' = \begin{bmatrix} 62.153 & 59.440 & 67.323 \end{bmatrix}$$

Solution:

$$a_{ji} = \begin{bmatrix} -1.0437 & 0.0312 & 0.0694 \\ 0.0399 & 0.9222 & 0.3885 \\ 0.0155 & 0.4258 & -1.0594 \end{bmatrix}$$

$$t_i = \begin{bmatrix} 193.1771 & -38.9367 & 155.2708 \end{bmatrix}$$

Vector position measured in the primed coordinate system evaluated in the un-primed system through Equation B-1:

$${}^1x_i' \rightarrow {}^1x_i = \begin{bmatrix} 66.095 & 50.965 & 87.578 \end{bmatrix}$$

$${}^2x_i' \rightarrow {}^2x_i = \begin{bmatrix} 130.168 & 30.417 & 100.344 \end{bmatrix}$$

$${}^3x_i' \rightarrow {}^3x_i = \begin{bmatrix} 64.201 & 30.371 & 82.048 \end{bmatrix}$$

$${}^4x_i' \rightarrow {}^4x_i = \begin{bmatrix} 131.448 & 46.483 & 111.349 \end{bmatrix}$$

Appendix C: Comparison of Bovine Experimental Results to Human Experiments

C.1 Geometry

Figure C-1 depicts the range of end-plate areas measured in humans. The bars represent the range measured by the various researchers listed below, except the filled bar which represents the bovine cross-sectional areas measured in this work. The bovine areas are not substantially greater than the human areas.

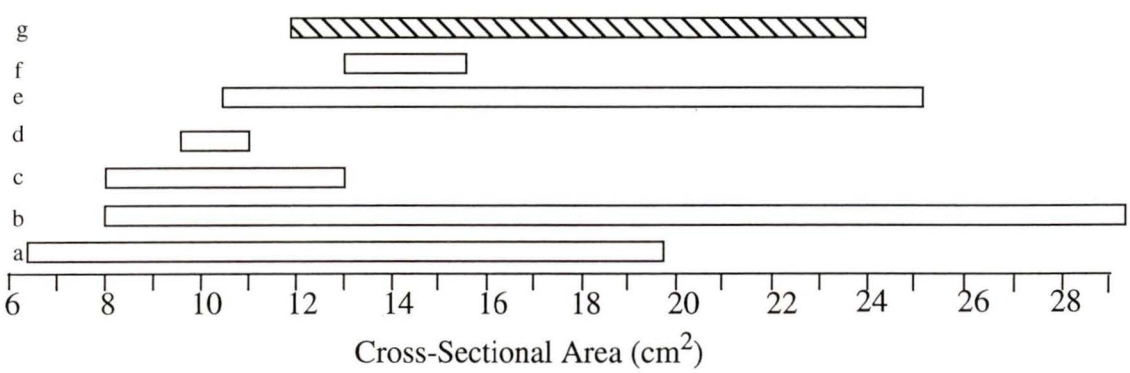

a: 60 T1 to T12 vertebrae, Kazarian and Graves [59]
b: 81 L1 to L5 vertebrae, Perey [56]
c: 12 L1 to L5 vertebrae, Messerer [61]
d: 22 persons lumbar vertebrae middles, Yamada [57]
e: 109 L1 to L4 vertebrae, Hansson et al. [138]
f: L1 to L5 disk area from 65 yr male, Breau et al. [21]
g: BOVINE L2,L3,L5 from this study

Figure C-1: Range of Cross-Sectional Area for Human Vertebral Bodies

As was illustrated in Appendix A, the bovine vertebral bodies have a more complex shape with greater variation in cross-section throughout the body. Bovine vertebral bodies are also longer than human: Alici et al. [51] have shown L3 vertebrae to have a height between 27-50 mm, and Yamada quoted an average vertebral body height of 26.2 mm [57]. The maximum bovine heights are above 70 mm.

C.2 Trabecular Density and Modulus

Regional variation in trabecular density has been seen in human specimens [121] and has been thought to be distributed due to stress concentration in the vertebra [111], just as was observed in the bovine specimens.

Table C-1: Human Vertebral Trabecular Apparent Density and Modulus from Previous Works

Apparent Density ($g\ cm^{-3}$)		Compressive Young's Modulus (MPa)			Sample Size	Number of donors, and age	References
Mean and Standard Deviation	Range	Mean and Standard Deviation	Range	Strain rate s^{-1}			
0.22 ± 0.02 0.19 ± 0.01[a]	0.1-0.4				17		[73]
0.47 ± 0.19[a]		152 ± 117		~0.0001[b]	288	32, 1 month - 89 yrs	[74]
~0.27[a]	0.07-0.76[a]	55.6 ± 0.7 35.1 ± 0.6	1.1 - 139 5.2 - 104	~0.0001[c]	32 32	4 males, 4 females, 14 - 89 yrs	[85] & [86]
			10-428		400	23 - 83 yrs	[145]
0.15 ± 0.06[a]	0.07-0.24[a]	23 ± 15	1-90	0.009 ± 0.001	231	3, 71-84 yrs	[100]
		452 ± 134 346 ± 138		0.012	15, L3 15, L4	3, 20-36 yrs 3, 20-36 yrs	[146]

a. Measured using dry bone specimens.
b. 0.01 inch per min displacement rate over the whole vertebral body compressed to 1/4 inch.
c. 0.05 mm/min displacement rate over a 1 cm long specimen.

Table C-1 lists density and modulus values for trabecular bone in human vertebral bodies. When these values are compared to those determined in this work, it becomes clear that bovine trabecular bone in vertebral bodies is denser and stiffer than that in humans. Lindahl and Lindgren [86] found one human cube specimen with a similar

density to the bovine, yet they make a qualification that the specimen came from a "powerfully built 22-year old man".

The higher apparent density of bovine specimens can be easily explained: bovine vertebrae undergo larger forces. The vertebral bodies require a stiffer and stronger structure considering the large bending moments induced on the spine of a quadruped. In comparison, the human upright posture requires some flexibility in the vertebrae so that the soft intervertebral disk is not overly stressed during dynamic movements. Also, the fact that the animals have different relative weights and yet have similar vertebral body cross-sectional areas is worth some consideration. Currey [7] has accounted for the compression forces in the quadruped spine with the following model:

> *... when a mammal, or any other tetrapod, is standing still, the vertebral column between the limb girdles will be loaded so as to sag, that is, it will tend to be convex downward. It might be possible to counteract this tendency, without making use of muscles attached to the column itself, by curving the vertebral column into an arch. The column would then be loaded in compression, with the viscera slung from it, and the tendency of the ends of the column to splay apart could be counteracted by the body wall musculature...*
> *In the trunk, between the fore and hind legs, muscles running from the rib cage to the pelvis act as tension members and the curved spine as the compression member of the system bearing the weight of the viscera.*
> *This description is greatly idealized, because real animals run around, twisting their spine to a greater or lesser amount, and most of the time do not bear much resemblance to the architectural model.*

Yet for a cow, this model may be quite fitting. One final point: domestic cattle have, on average, a far shorter relative lifetime than humans. The bone loss associated with aging will not be seen in a typical domestic animal as it is too young. Bovine bones are then denser and stiffer on average.

C.3 Stiffness

As expected from the higher modulus of bovine trabecular bone, the stiffness of bovine vertebral bodies is higher than for humans. Human vertebral bodies typically have a stiffness below 8 kN/mm as shown in Figure C-2. The lines on the plot connect the average measured values. The vertical error bars indicate the standard deviation for that

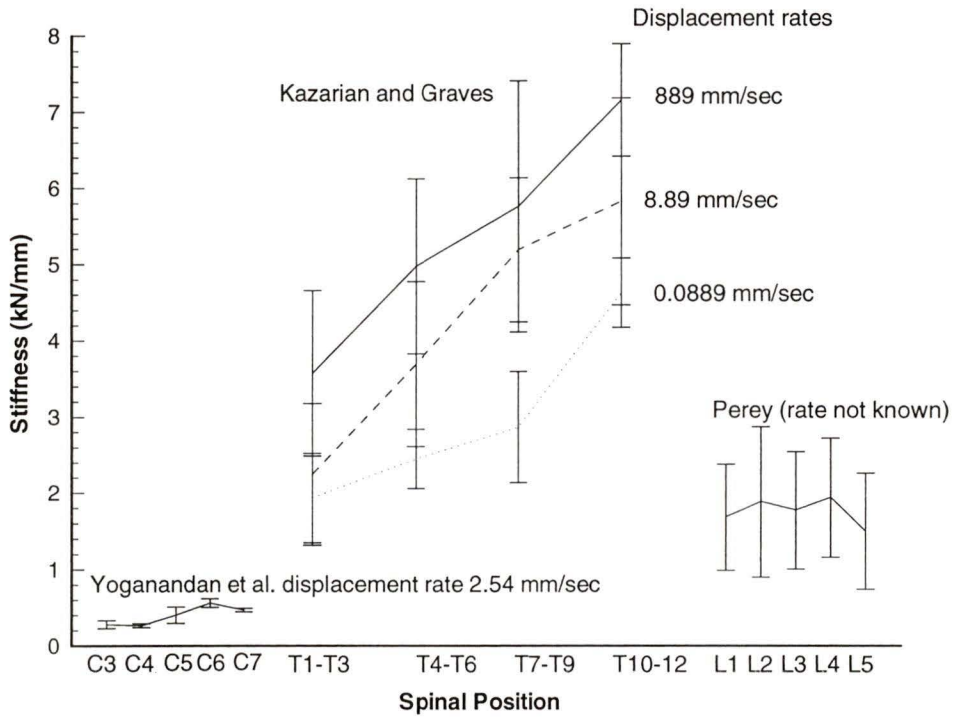

Figure C-2: Stiffness of Human Vertebral Bodies

data set. Some of the error bars overlap. The ends of a particular bar can be determined since they are spaced equally from the average value. The data for this plot were taken from three papers. Yoganandan et al. [58] used cervical specimens from elderly females and measured very low stiffness. Perey [56] used lumbar specimens (average age between 40-60 years). The standard deviations for a particular vertebral body type were high and no increased stiffness was seen with spinal position. In contrast, Kazarian and Graves [59]

did show a trend of increased stiffness with increased spinal position. Their study used thoracic specimens from a young population (26-38 years range) and measured a very high stiffness. Also, in their tests they used three displacement rates and found an increased displacement rate increased the measured stiffness. But the range of the data was large and standard deviations between the various groups overlapped. Though human vertebral bodies have a wide range of stiffness, the bovine stiffness is significantly higher as all values were above 20 kN/mm.

Kazarian and Graves [59] used techniques similar to this present study employing an aluminum test fixture with dental acrylic resin as a fixing agent. Though the other two data sets did not include explicit methods, it appears that the vertebrae were tested directly on the surface of a metal force plate. Whether these differences in technique caused a higher stiffness to be measured is not known.

The relaxation behavior observed during the compression tests also occurs in human specimens. Yamada [57] measured the following creep properties:

> *The creep limit corresponds to 30% of the ultimate strength for cervical and upper thoracic vertebrae, 35% for the lower thoracic vertebrae, and 50% for the lumbar vertebrae. The maximum creeping time is 24 hours for cervical and thoracic vertebrae and 48 hours for lumbar vertebrae. The contraction at creeping rupture is greater than the ultimate contraction in a normal test.*

C.4 Ultimate Load and Ultimate Strength

Numerous studies have considered the ultimate strength and load of human lumbar vertebra. For ergonomic and prosthetic design considerations, these are clearly important material properties. Though no review can be all encompassing, as much raw data as possible was compiled from various sources in this section.

What is evident in most of the following figures is large scatter in the data. But even with this uncertainty, the bovine vertebral bodies in this study are markedly stronger than human bodies. The strength of the bodies seen here may be attributed to the bones exposure to larger forces (as discussed in Section C.2). Figure C-3 shows the ultimate load determined for human vertebral bodies. As human and bovine cross-sections are about the same, and ultimate strength results for humans are also much lower.

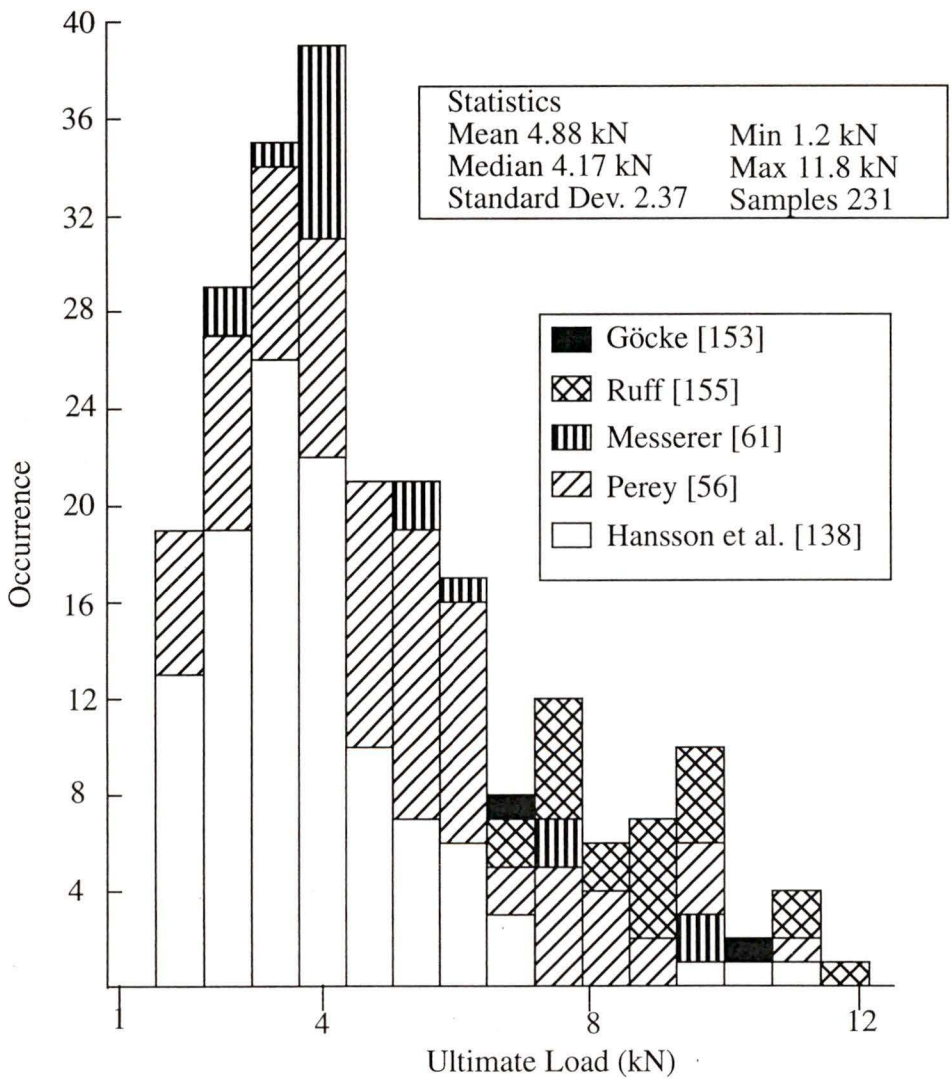

Figure C-3: Histogram of Ultimate Load for Human Lumbar Vertebrae

The data used in Figure C-3 can be compared to average values quoted in other research using specimens from the entire spine (shown graphically in Figure 1-1). Yamada [57] quoted a Japanese study involving 22 persons with an average lumbar vertebral strength of 4.95 kN which is markedly close to the above result. Yet the results of Gozulov et al. [60] for samples from 19-40 yr males (n= 6-16) were between 10.7 and 12.6 kN as quoted by Kazarian and Graves [59].

Figure 1-1 indicated that vertebral ultimate load increases with the position of the body in the spine as in the bovine results. The same trend is seen in this data compilation yet there is substantial spread in the data (Figure C-4).

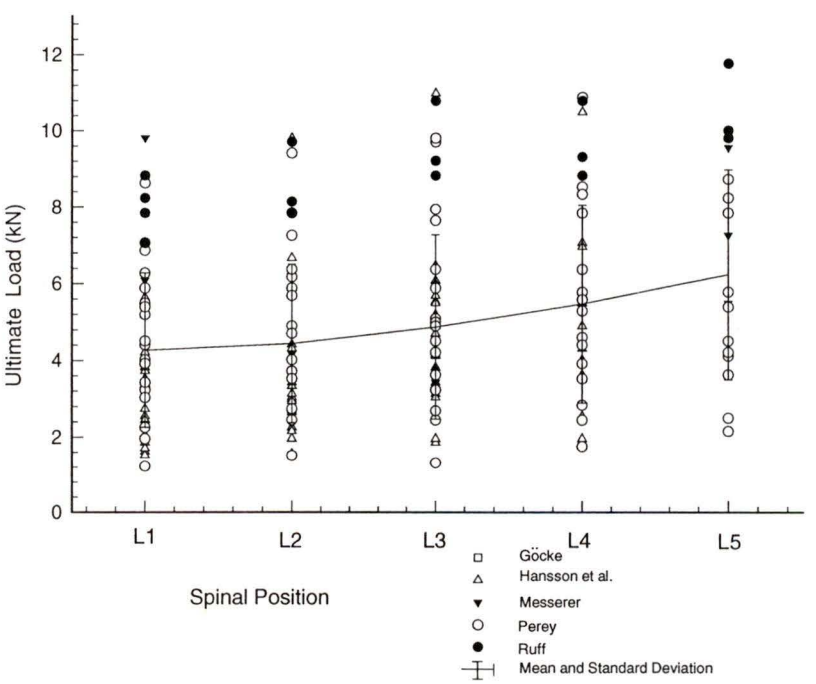

Figure C-4: Human Lumbar Vertebral Body Ultimate Load as a Function of Spinal Position (sources referenced in Figure C-3)

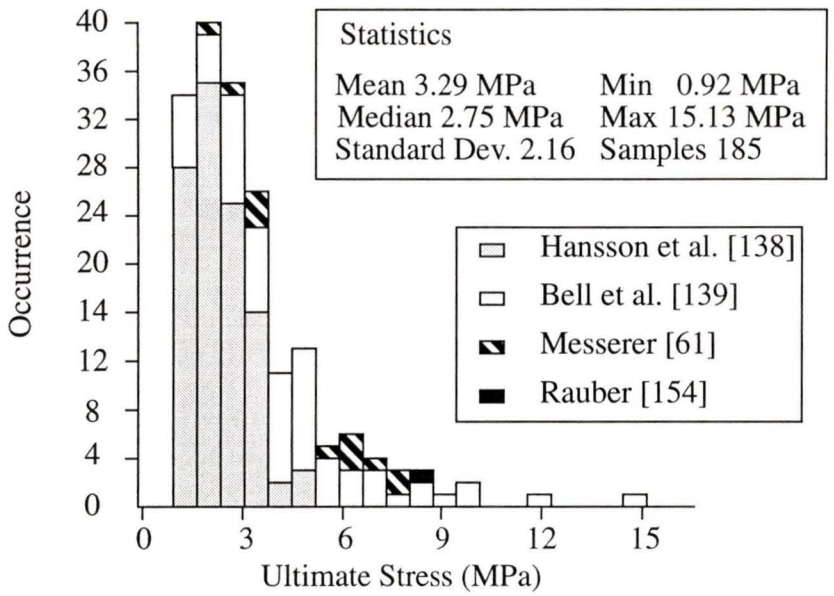

Figure C-5: Histogram of Ultimate Strength for Human Lumbar Vertebrae

Ultimate stress values were also compiled from various sources. The distribution is shown in Figure C-5. By including the cross-sectional area, part of the variation due to specimen size is taken into consideration. Unfortunately, the variation in the data is still high. Results from Hansson et al. [138] are lower than Bell's [139] and Messerer's [61]. Other studies have quoted higher average values than this compilation; these are listed in

Table C-2: Published Ultimate Strength Values for Human Lumbar Vertebrae

Reference	Ultimate Stress (MPa)
Yamada [57] age group 20-39 years for lumbar spine	6.3 ± 0.1
Yamada age group 40-59 years for lumbar spine	4.4 ± 0.2
Yamada age group 60-79 years for lumbar spine	3.0 ± 0.1
Göcke [153] for lumbar spine	5.6 - 6.9 (range)

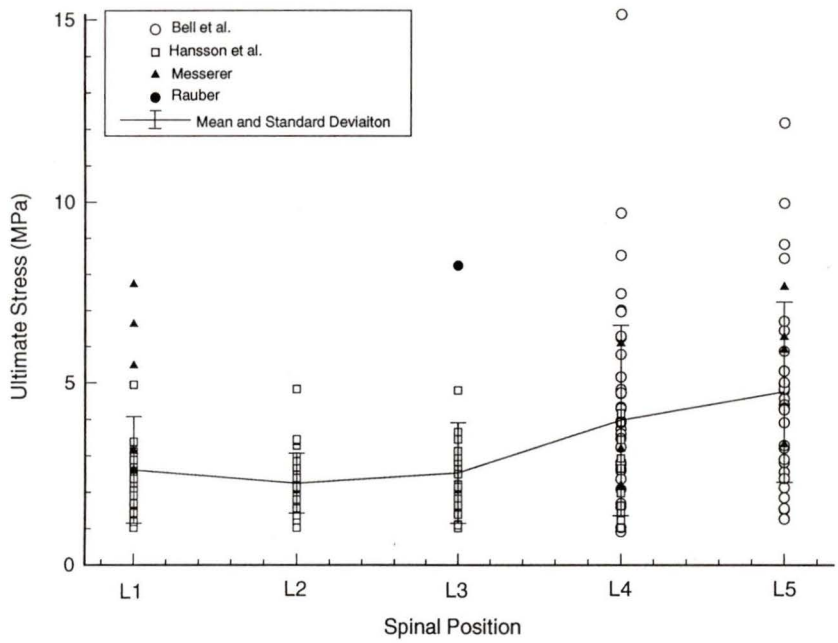

Figure C-6: Ultimate Stress as a Function of Spinal Position for Human Lumbar Vertebral Bodies (sources referenced in Figure C-5)

Table C-2. As trabecular and cortical bone are strain rate dependent, part of the variation in the ultimate load is due to different strain rates used in the studies above.

Increase in ultimate load with spinal position can be partly explained by Figure C-6 which does not show a linear increase in ultimate stress with spinal position. Clearly, a portion of the ultimate load increase is due to an increase of cross-section with spinal position. But there is an increase in ultimate stress between the upper and lower lumbar spine. A reasonable explanation of this increase is due to greater apparent density, though other factors such as strain rate, specimen preparation, and specimen age may have affected the results between different studies.

VITA

Surname: Sanders Given Names: Michael Morrison

Place of Birth: Abbotsford, B.C. Date of Birth: 12 July 1969

Educational Institutions Attended:

University of Victoria 1987 to 1994

Degrees Awarded:

B.Sc. University of Victoria 1992

Honors and Awards:

Since 1992:

NSERC Postgraduate Scholarship 1992-94

B.C. Advanced Systems Institute Graduate Entrance Scholarship 1992-93

Presidents's Research Scholarship 1992-93

Petch Research Scholarship 1993-94

The Charles S. Humphrey Graduate Student Award 1994-95

PARTIAL COPYRIGHT LICENSE

I hereby grant the right to lend my thesis to users of the University of Victoria Library, and to make single copies only for such users or in response to a request from the Library of any other university, or similar institution, on its behalf or for one of its users. I further agree that permission for extensive copying of this thesis for scholarly purposes may be granted by me or a member of the University designated by me. It is understood that copying or publication of this thesis for financial gain shall not be allowed without my written permission.

Title of Thesis: An Investigation of Bovine Lumbar Vertebral Body Stiffness with Experimental Measurement and Finite Element Modelling.

Author 

Michael Morrison Sanders

10 November 1994